Regulation of Inflammation and Glucose Homeostasis by Poly(ADP-ribose) Polymerase 1 (PARP1)

Dissertation

zur

Erlangung der naturwissenschaftlichen Doktorwürde

(Dr. sc. nat.)

vorgelegt der

Mathematisch-naturwissenschaftlichen Fakultät

der

Universität Zürich

von

Süheda Erener

aus der

Türkei

Promotionskomitee

Prof. Dr. Dr. Michael O. Hottiger
(Vorsitz und Leitung der Dissertation)
Prof. Dr. Annette Oxenius
Prof. Dr. Michael Hengartner
Prof. Dr. Jürg Tschopp

Zürich, 2010

Overview of submitted and published articles

Article 1: Inflammasome activated caspase 7 cleaves PARP1 to enhance NF-κB dependent transcription

Article 2: PARP1 knockout mice develop obesity through deteriorated glucose homeostasis

Article 3: SIRT2 regulates NF-κB-dependent gene expression through deacetylation of lysine 310

Article 4: PARP1 regulates tumor progression by co-activating HIF-1 dependent gene expression

Inflammasome Activated Caspase 7 Cleaves PARP1 to Enhance NF-κB Dependent Transcription

Süheda Erener[1,2], Virginie Petrilli[3,4], Ingrid Kassner[1,2], Paul O. Hassa[1], Rosa Castillo[3], Jürg Tschopp[3] and Michael O. Hottiger[1,*]

[1]Institute of Veterinary Biochemistry and Molecular Biology
University of Zurich, Winterthurerstrasse 190,
8057 Zurich, Switzerland
Phone: +41-44-635 54 74, Fax: +41-44-635 68 40
Email: hottiger@vetbio.uzh.ch

[2]Life Science Zurich Graduate School, Molecular Life Science Program,
University of Zurich

[3]Department of Biochemistry, University of Lausanne
Chemin des Boveresses 155, 1066 Epalinges, Switzerland

[4]Centre Léon Bérard, Génétique moléculaire, signalisation et cancer UMR5201,
28 rue Laennec 69008 Lyon, France

*Corresponding author

SUMMARY

Poly(ADP-ribose) polymerase 1 (PARP1) cleavage is the hallmark of apoptosis. Yet PARP1 cleavage is not necessary for apoptosis, suggesting that it has another physiological role. Here we show that caspase 7 is a target of the NALP3 inflammasome-activated caspase 1 in LPS stimulated macrophages. Active caspase 7 in turn translocates to the nucleus and cleaves PARP1 to regulate NF-κB target gene expression. Mutation of the aspartic acid residue at the PARP1 cleavage site (D214) abolishes caspase 7-mediated PARP1 cleavage and release of PARP1 from chromatin, thus maintaining chromatin compaction and restraining gene induction necessary for the host response. These findings propose a non-apoptotic regulatory role for caspase 7 in PARP1-dependent transcription and provide novel mechanistic insights into how the inflammasomes can relay inflammatory signals to transcription.

Keywords: PARP-1; caspase 7; inflammasome; transcription; chromatin; NF-κB

Short title: Inflammasome-regulated gene expression

HIGHLIGHTS

- **Caspase 7 mediates non-apoptotic PARP1 cleavage upon inflammatory stimulus**
- **NALP3 inflammasome regulates transcription via caspase 1 and 7**
- **PARP1 cleavage at D214 enhances NF-κB target gene expression**
- **PARP1 cleavage increases chromatin accessibility**

GRAPHICAL ABSTRACT

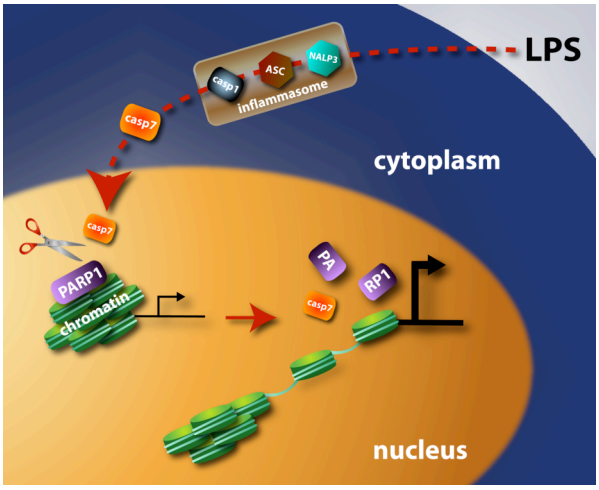

INTRODUCTION

Induction of Nuclear factor kappaB (NF-κB) signal transduction pathways occurs in response to a wide range of stimuli and results in nuclear accumulation of NF-κB transcription factors and expression of a large number of target genes (Mankan et al., 2009). Appropriate regulation of NF-κB is critical for the function and survival of the cell and aberrant NF-κB activity has been implicated in the pathogenesis of several diseases (Ghosh and Hayden, 2008). There is an increased understanding of the importance of nuclear events in regulating NF-κB's activities as a transcription factor, including reversible post-translational modification of the transcription factor itself (e.g. acetylation), recruitment of cofactors (e.g. CBP/p300) or the role of chromatin structure (Lomvardas and Thanos, 2002; Natoli, 2006; Ramirez-Carrozzi et al., 2009).

Poly(ADP-ribose) polymerase 1 (PARP1) is a nuclear chromatin-associated multifunctional enzyme found in most eukaryotes apart from yeast (Hassa et al., 2006). PARP1 is able to catalyze polymerization of ADP-ribose units from donor NAD^+ molecules (Hassa et al., 2006; Kim et al., 2005). The enzyme has only low basal activity but is activated by damaged DNA *in vivo* or by stem/loop boundaries of cruciform hairpins of undamaged genomic DNA (Woodhouse and Dianov, 2008). The targets of PARP1's enzymatic activity include a variety of nuclear proteins, including PARP1 itself and histones (Quénet et al., 2009). Recent studies have suggested a role for PARP1 in the regulation of chromatin structure and transcription, including NF-κB-dependent gene expression (Hassa et al., 2006; Hassa and Hottiger, 1999; Kraus, 2008). During apoptosis, PARP1 is cleaved by caspases, a hallmark of cell death (Nicholson et al., 1995; Tewari et al., 1995). Caspase 3 and 7 are responsible *in vivo* to process PARP1 to its apoptotic 24- and 89-kDa fragments (Nicholson and Thornberry, 1997; Salvesen and Dixit, 1997). The p24 fragment, which contains a part of the DNA binding domain (DBD) is thought to recognize altered structures in DNA rather than particular sequences and has also been reported to be involved in protein–protein interactions (Hassa et al., 2006; Pion et al., 2005). Without the 24kDa amino-terminal domain, the 89kDa fragment cannot be activated by DNA (Altmeyer et al., 2009).

Caspases belong to a family of highly conserved cysteine-dependent aspartate-specific proteases (Alnemri et al., 1996). The human caspase gene family consists of

12 mammalian members that are grouped into two major sub-families, namely inflammatory and apoptotic caspases (Chowdhury et al., 2008). Caspase 1 is the prototypical member of the inflammatory caspases and following its recruitment and activation within large cytoplasmic complexes, called inflammasomes, mediates the maturation of inflammatory cytokines like pro-IL-1β and pro-IL-18 (Ghayur et al., 1997; Martinon et al., 2004; Thornberry et al., 1992). Genetic studies in mice suggest at least four inflammasomes, with distinct components and activating stimuli. The identity of the inflammasome depends on the nature of the nucleotide binding and oligomerization domain (NOD)-like receptor (NLR) members. The interaction between NLR proteins and inflammatory caspases is mediated by the bipartite adaptor protein ASC. Deletion of ASC abolishes inflammasome activation in response to a wide range of triggers (Mariathasan et al., 2004). Inflammasome formation can be induced by a variety of PAMPs (pathogen-associated molecular patterns). For example, NALP3 inflammasome formation can be triggered by LPS, bacterial toxins, double stranded RNA or whole pathogens like *Candida albicans*, whereas IPAF inflammasome is activated by gram-negative bacteria like *Salmonella typhimurium* (Schroder and Tschopp, 2010). The activation mechanisms for NALP1b and AIM2 inflammasomes are less clear but *Bacillus anthracis* lethal toxin or vaccinia virus have been reported to require the NALP1b and AIM2 inflammasome for caspase 1 processing, respectively (Fink et al., 2008; Hornung et al., 2009).

On the other hand, caspase 3 and 7 were identified as key mediators of apoptosis (Nicholson et al., 1995; Tewari et al., 1995). Activation of caspases requires proteolytical removal of the linker region between large and small catalytic subunits (Boatright et al., 2003). In turn, active caspase 3 and 7 cleave a large set of substrates that ultimately results in apoptosis. (Kuida et al., 1996). Whereas caspase 3 and caspase 7 knock-out mice show no phenotypic abnormalities, caspase3/7 double knock-out mice suffer from early perinatal lethality, indicating the redundant roles caspase 3 and 7 play during embryonic development (Lakhani et al., 2006). However, accumulating evidence suggests also non-redundant roles and non-apoptotic functions for caspase 3 and caspase 7 in different cellular processes such as cell proliferation, cell-cycle regulation, and cell differentiation and inflammation (Algeciras-Schimnich et al., 2002; Denis et al., 1998; Lamkanfi et al., 2008).

Interestingly, PARP1 knock-in mice (D214N), which harbor a mutated caspase cleavage site of PARP1, $DEVD_{214}$, develop normally, indicating that cleavage

of PARP1 is not required during apoptosis (Pétrilli et al., 2004). This observation raises a fundamental question why there should be such an elaborate mechanism for selective degradation of a subset of cellular proteins, when eventually all the cellular components need to be destroyed An obvious answer would be that the targeted cleavage is important for regulatory functions other than apoptosis. Intriguingly, PARP1 knock-in mice (D214N) are highly resistant to endotoxic shock and to intestinal and renal ischemia-reperfusions (Pétrilli et al., 2004). Target tissues and cells show reduced inflammatory responses due to the compromised production of specific inflammatory mediators, suggesting that cleavage of PARP1 is functionally relevant for inflammation dependent gene expression.

Here we have examined the role of PARP1 cleavage at the molecular level under inflammatory conditions. We found that PARP1 is cleaved at D214 by caspase 7 after stimulation of macrophages with LPS. LPS activated caspase 7 is a target of the NALP3 inflammasome and its absence compromised NF-κB target gene induction. LPS activated, proteolytic PARP1 cleavage releases PARP1 from chromatin, reduces chromatin compaction and enhances NF-κB-dependent gene expression suggesting a regulatory non-apoptotic role of caspase 7 and linking caspase 7 to inflammation and transcription.

RESULTS

Induction of a Subset of NF-κB Target Genes is Compromised in Peritoneal Macrophages Isolated from D214N PARP1 Mice.

We first asked whether PARP1 cleavage is induced with an inflammatory stimulus like LPS. Peritoneal macrophages from C57Bl/6 mice expressing either WT or non-cleavable D214N PARP1 were isolated, stimulated with LPS and subjected to western blotting. With an antibody recognizing cleaved C-terminal PARP1 fragment, we observed that PARP1 cleavage (p89) was rapid and detected as early as 1 hour (Fig 1A). To investigate a potential regulatory role of PARP1 cleavage in NF-κB dependent gene expression, intraperitoneal macrophages (IP cells) were stimulated with LPS and pro-inflammatory gene expression was analysed. Real-time RT-PCR revealed that LPS dependent induction of *CSF2*, *IL-6* and *LIF* was dependent on PARP1 cleavage in these cells, but not the one of *IP-10* (Fig. 1B). To investigate if the reduced gene induction in D214N PARP1 cells was due to inefficient p65-PARP1 complex formation or hampered recruitment of p65 to DNA, immunoprecipitation and ChIP experiments were performed in IP cells, respectively. LPS induced complex formation between p65 and PARP1 was not affected by the D214N mutation (Fig. S1A). Likewise, p65 recruitment to target promoters such as *CSF2*, *IL-6* and *IP-10* occurred as soon as 30 minutes and was comparable in WT and D214N IP cells (Fig. 1C). These results suggest that PARP1 cleavage might regulate the induction of a subset of NF-κB dependent genes and that the moderate gene induction in D214N IP cells is not due to reduced complex formation with p65 nor deficient NF-κB signaling.

LPS Induced PARP1 Cleavage Regulates the Expression of *IL-6* in THP1 Cells.

Next, we tested whether the above-mentioned observations could be extended to human THP1 monocyte/macrophage like cells. THP1 monocyte-like cells can be differentiated to macrophage-like cells by treatment with PMA. We first tested whether LPS would induce PARP1 cleavage in PMA primed human THP1 cells. Indeed, after stimulation of THP1 cells with LPS for different time periods ranging from 2 to 6 hours, PARP1 cleavage was detected by western blot using an antibody detecting the C-terminal large PARP1 fragment (p89) resulting from cleavage at

D214 (Fig. 2A). Similar results were obtained with unprimed THP1 cells (Fig. S1B). Since PARP1 cleavage is a hallmark of apoptosis, we next investigated whether LPS treatment of THP1 cells induces cell death under the tested conditions. Stimulated THP1 cells were stained with ethidium homodimer and calcein for dying and viable cells, respectively. While treatment of cells with camptothecin induced significant increase in the amount of dead cells, LPS stimulation did not induce any detectable increase in cell death for the indicated time period (Fig. 2B).

To further investigate the physiological relevance of LPS-induced PARP1 cleavage in these cells, THP1 cells were transduced with a lentivirus containing shRNA against PARP1 or a scrambled control RNA (Fig. 2C). Clones efficiently depleted of PARP1 were subsequently complemented by retroviral transduction with an empty vector (PRRL), the myc-tagged full-length WT or the D214N non-cleavable mutant PARP1 (Fig. 2D). Complemented THP1 cells confirmed that PARP1 was not cleaved when mutated (D214N, Fig. S1C). Stimulation of these cells for 1 hour with LPS, and subsequent expression analysis of pro-inflammatory genes by real-time RT-PCR revealed that *IP-10* and *COX-2* expression increased to the same extent in WT and D214N PARP1 THP1 cells (Fig. 2E). Interestingly, the gene induction of *IL-6* was significantly reduced in cells complemented with non-cleavable PARP1, suggesting that PARP1 cleavage is also important for the transcriptional activation of a subset of NF-κB target genes in human THP1 cells.

Caspase 7 Cleaves PARP1 at D214N *in vitro* and Enhances NF-κB Dependent Gene Induction *in vivo.*

PARP1 cleavage at D214 is mediated by caspases (Lazebnik et al., 1994). To investigate whether caspases are also responsible for the LPS induced PARP1 cleavage, peritoneal macrophages were stimulated with LPS for different times in the absence or presence of pan caspase inhibitor Z-VAD-fmk. Western blot analysis showed that LPS dependent PARP1 cleavage was abrogated in the presence of Z-VAD-fmk (Fig. 3A). This effect was specific to Z-VAD-fmk and was not observed with another inhibitor, cycloheximide (CHX) which inhibits protein synthesis (Fig. S1D). These results suggest that caspases are responsible for LPS induced PARP1 cleavage, yet which caspase cleaves PARP1 upon LPS stimulation is unknown. We thus examined *in vitro* the caspases that efficiently cleave PARP1 at D214. WT and

D214N mutant PARP1 were both *in vitro* translated and subsequently incubated with different purified active human caspases (caspase 1-10). Caspases 3 and 7 were found to cleave PARP1 most efficiently, while caspases 1, 8 as well as 6 and 10 also processed PARP1 under the tested conditions, although to a different extent (Fig. 3B, upper blot). In most of the observed cases, cleavage took place at D214, since the corresponding D214N PARP1 mutant was not cleaved under the tested conditions. To exclude that other proteases from the reticulo-lysate were responsible for the observed cleavage, experiments were repeated with recombinant wild type and D214N PARP1 mutant proteins expressed in the baculo system. Western blot analysis with an antibody directed against the catalytic domain of PARP1 confirmed that PARP1 is predominantly cleaved at D214 by caspase 3 and 7 and to a lesser extent by caspases 6, 8 and 10 (Fig. 3B, lower blot).

To investigate whether caspase 7 or its close relative caspase 3 have a functional role in LPS-dependent NF-κB gene induction, we next transiently transfected IP cells with siRNA oligos targeting caspase 3 or 7 and stimulated them with LPS for one hour. Real-time RT-PCR analysis revealed that induction of a subset of NF-κB target genes was reduced in cells transfected with caspase 7 siRNA (Fig. 3C). In contrast, caspase 3 knock-down had either beneficial or no effect on NF-κB gene activation implicating that caspase 3 and 7 have distinct functions in mediating pro-inflammatory gene expression. Similar results were obtained in PMA primed THP1 cells (Fig. S2A). Interestingly, genes that showed reduced induction upon caspase 7 knock-down overlapped with the genes that showed dependency on PARP1 cleavage, suggesting that the observed effect of caspase 7 on NF-κB might be mediated by PARP1 cleavage. To confirm that the LPS dependent role of caspase 7 on NF-κB is linked to PARP1 cleavage, THP1 cells expressing WT or D214N PARP1 (Fig. 2D) were PMA primed, transiently transfected with mock or caspase 7 siRNA oligos and stimulated one hour with LPS. Indeed, real-time RT-PCR analysis revealed that caspase 7 knock-down led to 50% reduction in *IL-6* gene induction in WT PARP1 expressing THP1 cells, whereas no significant effect was observed upon caspase 7 knock-down in D214N PARP1 expressing THP1 cells (Fig. 3D and S2B). To investigate whether caspase 7 would translocate to the nucleus upon LPS induction where PARP1 is localized, THP1 monocytes were stimulated with LPS for 1.5 or 3.5 hours and cytoplasmic and nuclear fractions were prepared. Western blot analysis

with an antibody that detects only the activated caspase 7 resulting from cleavage at Asp198 (p19) revealed that active caspase 7 was absent from the nucleus in the unstimulated state but translocated to nucleus as soon as 1.5 hours after stimulation. Full-length (F.L) caspase 7 levels, on the other hand, did not change upon LPS stimulation and it was mainly localized to cytoplasm, suggesting that the cleaved caspase 7 is a very minor portion of the total caspase 7 pool. In accordance with the above-proposed role for caspase 7 in PARP1 cleavage, kinetics of PARP1 cleavage paralleled active caspase appearance in the nucleus. PARP1 and tubulin blots showed the pureness of the nuclear and cytoplasmic fractions, respectively. Taken together, we conclude that caspase 7 has a pro-inflammatory role in NF-κB mediated gene induction and this effect is mainly mediated by PARP1 cleavage.

Caspase 7 Is a Target of NALP3 Inflammasome.

Next, we investigated the molecular pathways that lead to caspase 7 activation under inflammatory conditions. Pro-inflammatory effects seen for caspase 7 encouraged us to test the link between PARP1 cleavage, inflammatory caspase 1 and caspase 7. Peritoneal macrophages from WT, *caspase 1* -/- and *caspase 7* -/- mice were stimulated with LPS for different times ranging from 1 hour to 16 hours and PARP1 cleavage was monitored by western blotting. In WT cells, PARP1 cleavage was visible as early as one hour after stimulation but not in *caspase 7* -/- cells, confirming the above proposed role for caspase 7 in cleaving PARP1 upon LPS stimulation *in vivo* (Fig. 4A). Interestingly, also in *caspase 1* -/- cells no PARP1 cleavage was detected. Furthermore, activation of caspase 1 and caspase 7 upon LPS stimulation correlated with PARP1 cleavage, suggesting an interplay between caspase 1, caspase 7 and PARP1 cleavage under inflammatory conditions. In *caspase 1* -/- cells, caspase 7 activation was absent whereas in *caspase 7* -/- cells, LPS dependent caspase 1 activation was not effected, providing evidence that caspase 1 is upstream of caspase 7 activation, not *vice versa*. Furthermore, caspase 7 was not required for the inflammasome formation that was activated upon various other stimuli (Fig. S3A and S3B). Caspase 1 is the best characterized inflammatory caspase and its catalytic activity is tightly regulated by signal dependent autoactivation of inflammasomes (Martinon et al., 2002). NALP3 inflammasome can be activated by exposure to bacterial products like LPS (Mariathasan et al., 2004). We thus tested whether LPS dependent caspase 7 activation requires the NALP3 inflammasome components. LPS

dependent caspase 1 activation but also caspase 7 activation was abolished in bone marrow derived macrophages (BMDMs) lacking NALP3 (Fig. 4B). Similarly, in intraperitoneal macrophages lacking the essential inflammasome adaptor ASC, LPS dependent caspase 1 activation, caspase 7 activation and PARP1 cleavage was abolished indicating that LPS dependent caspase 7 activation is mediated by caspase 1 containing NALP3 inflammasome (Fig. 4B and 4C). To investigate whether the signaling pathway leading to caspase 7 activation was functional in D214N PARP1 cells, intraperitoneal macrophages from WT and D214N PARP1 mice were stimulated with LPS for different times and total proteins were analyzed by western blot. Western blot analysis revealed that LPS induction led to comparable caspase 1 and 7 activation in both of the cell lines (Fig. 4D).

PARP1 Dissociates from *IL-6* Transcription Start Site upon LPS Induction.

PARP1 cleavage by caspase 7 generates 24- and 89kDa fragments of which the smaller one contains a part of PARP1's DBD (Altmeyer et al., 2009; Hassa and Hottiger, 2008). We recently reported that PARP1 is acetylated in a stimuli dependent manner and that this acetylation is reversible by type I HDACs (Hassa et al., 2005). To investigate whether HDACs are able to interact with the cleaved PARP1 fragments *in vivo*, we performed immunoprecipitation experiments with p24 and p89 together with HDAC1 and 2. HDAC1 and 2 interacted with full-length PARP1 and p24 but not with p89 *in vivo* (Fig. 5A and 5B). Since HDAC activities are described to condense chromatin structure and thereby inhibit transcription, we hypothesized that PARP1 cleavage could be a means of removing the inhibitory HDACs from the chromatin upon LPS stimulation. ChIP experiments using anti-myc antibody to immunoprecipitate amino-terminally tagged PARP1 in THP1 cells (see Fig. 2D) revealed that p24 association was reduced at the transcriptional start site (TSS) of *IL-6* upon LPS stimulation in cells complemented with WT PARP1. In contrast, the myc-tagged amino-terminal part of PARP1 was still detectable in cells complemented with non-cleavable PARP1 (D214N) (Fig. 5C). Interestingly, PARP1 seemed even to be enriched at the *IL-6* TSS in these cells upon LPS stimulation. This was not observed for the TSS of *H2B*, which served as control gene. These results suggest that lack of PARP1 cleavage does not allow dissociation of full-length PARP1 from chromatin and this correlates with reduced gene induction upon LPS treatment. The observed dissociation of WT PARP1 rather depended on the cleavage at D214 than on the

ADP-ribosylation activity of PARP1, since both, WT and D214N PARP1 proteins were comparably enzymatically active (Fig. 5D). In addition, LPS treatment did not lead to any detectable poly-ADP-ribose formation as analyzed by immunofluorescence microscopy (data not shown). We earlier reported that full-length PARP1 is required for pre-initiation complex (PIC) formation of NF-κB (Hassa and Hottiger, 1999). Therefore, we tested whether the cleaved PARP1 fragments would still be able to interact with p65 and potentially contribute to NF-κB-dependent gene expression. Interaction of recombinant PARP1 proteins with full-length GST-p65 was analyzed by pull-down experiments. Both full-length proteins (WT and D214N) interacted with p65 to a comparable extent (Fig. 5E, left panel). However, the cleaved PARP1 p89 fragment did not bind p65 under the tested conditions. Similar experiments with PARP1 p24 suggested that also the smaller fragment of PARP1 is not able to interact with p65 (Fig. 5E, right panel). Together, both experiments revealed that while full-length PARP1 binds to p65, cleaved PARP1 fragments do not interact with p65 implicating that once PARP1 is cleaved by caspase 7, the cleaved PARP1 fragments most probably are not any longer required for p65 dependent gene expression and thus not the cause for the compromised gene induction in D214N PARP1 cells.

PARP1 Cleavage by LPS Enhances Chromatin Accessibility around the TSS.
Next, we isolated BMDMs from WT or D214N PARP1 mice and analyzed pro-inflammatory gene expression in these cell lines. In agreement with previous results, stimulation of these primary cells with LPS for one hour and subsequent real-time RT-PCR analysis revealed also in primary BMDMs a subset of LPS-induced NF-κB target genes to be dependent on PARP1 cleavage. While the induction of *CSF2* and *NOS-2* were strongly reduced in BMDM isolated from D214N PARP1 knock-in mice, the expression of *IP-10* or *MIP-2* was not affected (Fig. 6A).

We sought to gain more mechanistic insights into LPS activated PARP1 cleavage and enhancement of gene activation. PARP1 is reported to compact chromatin *in vitro* (Wacker et al., 2007) and we observed HDAC1and 2 to interact with PARP1 and p24 (Fig. 5A and 5B). Therefore, we asked whether cleavage of PARP1 and the release of these fragments from chromatin would lead to more accessible chromatin and enhanced transcription. To address this question, chromatin

accessibility assay was performed in primary BMDMs isolated from mice. Nuclei from unstimulated or one hour LPS stimulated cells were isolated and digested with MNase and subsequently analyzed by CHART-PCR. Chromatin at the TSS of NF-κB target genes like *CSF2 or NOS-2* became more accessible upon LPS stimulation (Fig. 6B, upper panel, grey bars), correlating with chromatin release of PARP1 and the increase in gene expression. This effect was much more pronounced around the TSS than 1kB upstream of this site. Interestingly, analysis of the corresponding site in cells isolated from D214N PARP1 mice revealed that the extent of chromatin decompaction was significantly reduced upon LPS stimulation (Fig. 6B, lower panel, grey bars), providing strong evidence that PARP1 cleavage and release are decreasing chromatin compaction at the TSS *in vivo* and thereby enhance gene activation. Similar results were obtained for the chromatin around *CSF2* TSS in IP cells (Fig. S4).

DISCUSSION

In this study we have characterized the activation of caspase 7 by NALP3 inflammasome and determined its role in the activation of NF-κB-dependent gene expression through PARP1 cleavage. We provide evidence that the observed cleavage of PARP1 is not a consequence of induced apoptosis, but represents rather a novel non-apoptotic function of caspase 7. We show that activated caspase 7 cleaves PARP1 at the TSS of certain genes to release PARP1 from the chromatin and allow productive NF-κB dependent gene expression. Our conclusions are based on several observations: (i) on differential gene expression in mouse primary cells and in human THP1 cells genetically complemented with WT or non-cleavable D214N PARP1, (ii) on different mouse models lacking individual components of NALP3 inflammasome (iii) on ChIP experiments for PARP1, (iv) on differential chromatin accessibilities based on MNase experiments.

Caspase 7 knock-down in THP1 cells expressing uncleavable PARP1 did not affect the NF-κB response to LPS whereas THP1 cells expressing WT PARP1 did. Active caspase 7 also translocated to the nucleus upon LPS stimulation. This suggests that PARP1 is a main nuclear target of caspase 7 for the observed LPS induced transcriptional response. We can currently not exclude that active caspase 7 is cleaving additional proteins important for other cellular processes during LPS stimulation. Only a very small fraction of cellular caspase 7 was activated and translocated into the nucleus to cleave a very minor fraction of the cellular PARP1 pool at the TSS (Fig. 4A, 4D and S1B). This points at a very tight regulation, which makes sense in terms of not initiating a detrimental response for the cell under inflammatory conditions. It might be achieved by LPS-induced activation of a very distinct cytoplasmic complex containing caspase 7 and/or the induction of a post-translational modification, which would allow caspase 7 to translocate to the nucleus. Alternatively, the activity of caspase 7 might be regulated by xIAP, which is a natural and potent inhibitor of caspase 7 (Deveraux et al., 1997).

A recent proteomic study revealed that caspase 7 (but not caspase 3) is a downstream target of caspase 1 which provides evidence for the existence of distinct activation mechanisms for caspase 3 and 7 in response to microbial stimuli and bacterial infection (Lamkanfi et al., 2008). Our results are in agreement with this

study. However, Lamkanfi et al. have used pure LPS and ATP to activate caspase 1 whereas we used throughout our study crude LPS without ATP (Lamkanfi et al., 2008). This discrepancy can be explained by our previous reports that highly concentrated crude LPS is able to trigger inflammasome formation whereas high purity LPS cannot and needs ATP for caspase 1 activation (Martinon et al., 2004). Indeed with the crude LPS we used, we could activate caspase 1 formation (Fig. 4A,B,C).

Whether all PARP1-dependent NF-κB target genes are regulated by cleavage of PARP1 or whether additional aspects are important, such as structural or epigenetic changes, needs to be determined. It was earlier suggested, that PARP1 is unequally distributed throughout the chromatin (Jump et al., 1979; Mullins et al., 1977). The mechanism by which PARP1 is recruited to gene promoters remains unknown. Enrichment of PARP1 at the TSS of different genes under non-stimulated conditions has been reported before (Krishnakumar et al., 2008). It is currently not clear whether certain histone variants or the positioning of histones is responsible for the enrichment of PARP1 at these sites. We have observed in ChIP experiments that PARP1 recruitment to the *IL-6* TSS requires cleavage for full transcriptional activation upon LPS stimulation. These results suggest that promoters with PARP1 recruitment might also depend on PARP1 cleavage since accumulated PARP1 binding might affect chromatin compaction and thereby accessibility for other cofactors.

The selection of genes dependent on PARP1 cleavage seems not to be same for all tested cell types suggesting that the observed regulatory mechanism is dependent on cell type and stimulus. We cannot currently exclude that other caspases are also able to cleave PARP1 upon LPS stimulation or another stimulus (e.g. caspase 6, 7, 8 or 10, Fig. 3B). Therefore, caspase 7 might be activated in combination with other caspases (e.g. caspase 6, 8, or 9) to regulate different cellular processes. Interestingly, PARP1 cleavage was also observed in extracts of differentiating cells, providing additional evidence that PARP1 cleavage is physiologically relevant (Fujita et al., 2008). Intriguingly, upon exposure of cells to some bacterial toxins we observed PARP1 cleavage (data not shown). It will be interesting to see whether activation of other inflammasomes than NALP3 can also lead to PARP1 cleavage and link inflammasome activity to transcription.

Compaction of chromatin was decreased upon cleavage and dissociation of PARP1 from the chromatin (Fig. 5C and 6B). PARP1 was reported to promote the

localized compaction of chromatin into supra-nucleosomal structures (Wacker et al., 2007). The DBD (aa1-373) of PARP1 was necessary and sufficient for binding to nucleosomes, yet alone was unable to promote chromatin compaction and could only partially repress the chromatin templates. The catalytic domain of PARP1 cooperated with the DBD to promote chromatin compaction and efficient transcriptional repression in a manner independent of its enzymatic activity. Thus, cleavage of PARP1 by caspase 7 might be the physiological link for the observed structural changes. Alternatively, cleavage of PARP1 and subsequent release from chromatin might not only remove PARP1, but also proteins associated with PARP1. A previously identified PARP1 corepressor complex containing nucleolin, nucleophosmin, and Hsp70 as well as the N-CoR and HDAC3 corepressors are associated with the repressed promoter (Ju et al., 2004). Indeed, we observed protein complex formation of PARP1 with HDACs through p24. Caspase 7-mediated PARP1 cleavage would release p24 and HDACs from the TSS.

Whether the enzymatic activity of PARP1 is involved in the caspase 7-dependent regulation of transcription needs to be further investigated. In our studies, DNA stimulated WT and D214N PARP1 to the same extent, excluding that the observed difference in gene expression is due to a reduced ADP-ribosylation activation of the D214N PARP1 (Figure 5D).

In summary, we provide evidence that NALP3 inflammasome activated caspase 7 mediates PARP1 cleavage which in turn regulates NF-κB target gene expression by altering the chromatin accessibility under sustained inflammatory conditions.

EXPERIMENTAL PROCEDURES

Mice And Cell Isolation

C57BL/6, WT and transgenic mice were maintained in a specific pathogen-free facility. For the isolation of bone marrow macrophages, 6-8 weeks old mice were sacrificed and the cells were isolated as described elsewhere (Pétrilli et al., 2007). Cells were plated in 10 cm uncharged plastic plates (`Petri dish`) and incubated for full differentiation in RPMI medium supplemented with 10% FCS, 100 units/ml penicillin/streptomycin (Gibco), 1x non-essential amino acids (Gibco), 1mM sodium pyruvate (Gibco), 50 μM β-mercaptoethanol (Gibco) and 20% L929 conditioned medium for 6 days in a humidified incubator (with 5% CO2 at 37°C). At the end of 6 days, cells were counted and seeded in 6-well tissue culture plates. After 16 hours, cells were stimulated with 10 μg/ml LPS for 1 hour and harvested for RNA extraction.

For the isolation of intraperitoneal cells (IP cells), 6-8 weeks old mice were i.p injected with 1mL of 5% thioglycollate brewer medium for four days. Mice were sacrificed and cells were collected like described previously (Pétrilli et al., 2004). Briefly, cells were collected in RPMI medium by abdominal lavage, washed with PBS and seeded at a cell density of $1x10^6$ cells/ml in tissue culture plates in full-RPMI medium containing 10% FCS, 100 units/ml penicillin/streptomycin (Gibco), 1x non-essential amino acids (Gibco) and 1mM sodium pyruvate (Gibco), 50 μM β-mercaptoethanol (Gibco). Cells were cultured in full-RPMI medium. Animal experiments were performed according to the regulations of the cantonal veterinary office.

RNA Extraction And Gene Expression Analysis By Real-Time RT-PCR

Sub-confluent (50%) cells were stimulated with 10 μg/ml LPS for one hour. Total RNA was isolated using 'Total RNA isolation mini kit' (Macherey-Nagel), except from total RNA from primary bone derived macrophages, which was isolated using Ambion RNAqueous®-Micro Kit. RNA was subsequently reverse-transcribed using the 'High-capacity cDNA reverse transcription kit' (Applied Biosystems). Real-time PCR was performed using the Rotor-Gene 3000 (Corbett Life Science, now Qiagen) and TaqMan assays or SYBR Green using the primers listed in Table S1 and S2.

Mean value ± SE was calculated and blotted into graphs with GraphPad Prism (GraphPad Software).

Transient Transfections

THP1 cells were primed with PMA (10ng/mL) for 24 hours and were transfected with 30 pmol siRNA oligos (Qiagen) with 4 µl Lipofectamine RNAimax reagent (Invitrogen) according to manufacturer`s protocol for two days. Transfection into HEK293 cells was described elsewhere (Hassa et al., 2005).

Stable PARP1 Knockdown And Complementation In THP1 Cells

Generation of viruses and transduction of cells was done as described earlier (Ariumi et al., 2005). Briefly, pRDI vector containg PARP1 shRNA (#5) was used to transduce THP1 cells. The short hairpin RNA was against 5`UTR region of PARP1 mRNA. Transduced cells were selected through puromycin resistance gene. Complementation of cells was done with pRRL-myc-PARP1 vectors containing a blasticidin resistance marker and complemented cells were subsequently selected for three weeks with 2 µg/ml blasticidin.

Chromatin Immunoprecipitation

Cells were crosslinked with either 1% formaldehyde (Calbiochem) or with formaldehyde and the protein crosslinking agent dimethyl 3,3`-DTBP (Kurdistani and Grunstein, 2003). Chromatin fragmentation was achieved with the Bioruptor (Diagenode). Antibodies were incubated with crosslinked chromatin overnight at 4°C and collected with Protein A Agarose/salmon sperm DNA (Milipore) for 3 hours. After reversal of the crosslink and digestion with proteinase K, DNA was extracted and measured by real-time PCR using SYBR Green and the Rotor-Gene 3000 (Corbett Life Science, now Qiagen). Primers used for ChIP RT-PCR analysis are listed in table S3.

Chromatin Accessibility By Real-Time PCR

Accessibility of DNA to MNase was analyzed using chromatin accessibility by real-time PCR (CHART-PCR) as described elsewhere (Rao et al., 2001). The genomic DNA was isolated using a `Mammalian Genomic DNA miniprep kit` (Sigma). Primers used in real-time PCR analysis are listed in table S3.

SUPPLEMENTAL DATA

Supplemental data include 4 figures, 3 tables and Supplemental Experimental Procedures.

ACKNOWLEDGEMENTS

We thank Zhao-Qi Wang for PARP1 D214N mice. We are grateful to all the members of the Institute of Veterinary Biochemistry and Molecular Biology (University of Zurich, Switzerland) and group Tschopp for helpful advice and discussions. This work was supported by the Marie Curie Fellowship to VT and in part by Swiss National Science Foundation Grant 31-122421 (S.E.) and the Kanton of Zurich (M.O.H.).

AUTHOR CONTRUBUTIONS

SE and VP designed the experiments; SE, VP, IK and POH performed experiments; JT and MOH designed and supervised the study. SE and MOH wrote the manuscript. All the authors read and corrected the manuscript.

The authors declare that they have no conflict of interest.

FIGURE LEGENDS

Fig. 1. Induction of a Subset of NF-κB Genes is Compromised in D214N PARP1 IP Cells

(A) PARP1 cleavage is induced by LPS stimulation. Peritoneal macrophages from wild-type and D214N mice were stimulated for the indicated times with 10 μg/ml LPS. Total cell extracts were analyzed by western blot **(B)** Gene expression profile of *CSF2, IL-6*, *LIF, IP-10* in intraperitoneal cells (IP cells) isolated from WT and D214N PARP1 mice. Cells were stimulated with LPS for one hour and mRNA levels were determined by real-time RT-PCR analysis. Samples were normalized to *Rps12* expression levels and expressed as fold increase relative to unstimulated mRNA levels. Data are means of ±SEM at least four independent experiments. **(C)** Analysis of p65 recruitment to target promoters by chromatin immunoprecipitation. IP cells were stimulated with LPS 30 or 60 minutes. Recruitment to indicated promoters was analyzed by real-time RT-PCR. Results were expressed as fold increase relative to unstimulated p65 occupancy levels. Prolactin promoter served as a negative control. Data are means of ±SEM of at least three independent experiments.

Fig. 2. LPS Induced PARP1 Cleavage Regulates the Expression of *IL-6 in* THP1 Cells

(A) PARP1 cleavage profile in LPS treated THP1 macrophages. Total cell extracts were prepared and analyzed by western blot using indicated antibodies. **(B)** LPS stimulation does not affect cell viability. THP1 macrophages were stimulated with LPS for the indicated times and stained with calcein and ethidium homodimer. Cells were analyzed by immunofluorescent microscopy. **(C)** Stable knockdown of PARP1 in THP1 monocytes using a lentiviral system. shRNA against PARP1 targets the 5` untranslated region of PARP1 mRNA. **(D)** Stable complementation of THP1 PARP1 knockdown cells either with PRRL-empty vector, myc-tagged WT PARP1 or uncleavable PARP1 D214N mutant. Total cell extracts were prepared and proteins were immunoprecipitated with a myc antibody and analyzed by western blot using PARP1 antibody. Gapdh was used as loading control. **(E)** Gene expression profile of *IL-6, IP-10* and *COX-2* in stably complemented THP1 cells. Cells were stimulated with LPS for one hour and mRNA levels were determined by real-time RT-PCR

analysis. Samples were normalized to *Rpl28* expression levels and expressed as fold increase relative to unstimulated mRNA levels. Data are means of ± SD, n=2. Ctrl* is the sample treated with Etoposide for 16 hours.

Fig. 3. Caspase 7 Knock-down Reduces LPS Dependent NF-κB Target Gene Response

(A) Pan caspase inhibitor Z-VAD-fmk blocks PARP-1 cleavage. Bone-marrow derived macrophages from wild-type mice were stimulated with LPS for different times in the absence or presence of Z-VAD-fmk (50 μM). Total cell extracts were prepared and PARP1 cleavage was analyzed by western blot. **(B)** Screening caspase family (one-ten) for PARP1 cleavage at D214 *in vitro***.** Either *in vitro* translated and ^{35}S labeled PARP1 WT or D214N mutant plasmids (upper blot) or recombinant PARP1 WT or D214N mutant recombinant proteins (lower blot) were incubated with active caspases (1-10) for 20 minutes at 30°C in a caspase cleavage buffer. Reaction products were analyzed by SDS gel followed by autoradiography (upper blot) or western blot using PARP1 antibody (lower blot**). (C and D)** Effect of caspase knock-down on LPS dependent NF-κB target gene response. IP cells (C) or complemented THP1 cells (D) were transiently transfected with the indicated siRNA oligos and gene expression was analyzed by real-time RT-PCR. (C) Samples were normalized to *Rps12* and expressed as fold increase relative to unstimulated mRNA levels. Data are means of ± SD, n=2. (D) Samples were normalized to *Rpl28* expression levels and increase in gene expression to LPS was expressed as fold response. Fold response was set arbitrarily as 100% in simock transfected cells. Data are means of ± SD, n=2. **(E)** THP1 cells were stimulated with LPS (10μg/ml) for the indicated times. Cells were then fractionated and cytoplasmic and nuclear extracts were subjected to western blotting with antibodies directed against Caspase-7 (full-length and cleaved form), PARP1 and tubulin. ► shows the cleaved p89 PARP1 fragment.

Fig. 4. Caspase 7 Is Target of NALP3 Inflammasome

(A) PARP1 cleavage upon LPS stimulation is mediated by caspase 1 and caspase 7. Peritoneal macrophages from wild-type, *caspase 1* -/- and *caspase 7* -/- mice were stimulated for the indicated times with LPS, total cell extracts were prepared and PARP1 cleavage, caspase 1 and caspase 7 activation was analyzed by western blot.

(B) Caspase 7 activation upon LPS stimulation is impaired in the absence of NALP3. Bone-marrow derived macrophages from wild-type and *NALP3* -/- mice were stimulated for the indicated times with LPS, total cell extracts were prepared and caspase 1 and caspase 7 activation was analyzed by western blot.. **(C)** PARP1 cleavage upon LPS stimulation is impaired in the absence of ASC. Peritoneal macrophages from wild-type and *ASC* -/- mice were stimulated for the indicated times with LPS, total cell extracts were prepared and PARP1 cleavage, caspase 1 and caspase 7 activation was analyzed by western blot. **(D)** Uncleavable PARP1 (D214N) does not interfere with caspase activation by LPS. Peritoneal macrophages from wild-type and D214N PARP1 mice were stimulated for the indicated time with LPS, total cell extracts were prepared and PARP1 cleavage, caspase 1 and caspase 7 activation was analyzed by western blot.

Fig. 5. PARP1 Dissociates from the Promoters of Target Genes

(A and B) PARP1 interacts with HDAC1 and 2 through its ZF domain *in vivo*. FLAG-tagged HDACs and Myc-tagged PARP1 full-length (FL), PARP1 (p89) or PARP1 (p24) fragments were co-expressed in HEK 293 cells. PARP1 complexes were co-immunoprecipitated (IP) from nuclear extracts of untreated HEK 293 cells using an anti-Myc antibody and subsequently tested for Myc-tagged PARP1 and FLAG-tagged HDAC-1 (A) and HDAC-2 (B) by western blot analysis using anti-Myc and anti-FLAG antibodies. **(C)** Chromatin immunoprecipitation analysis of PARP1 occupancy upon LPS stimulation on the target promoters. WT and D214N *PARP1* complemented THP1 cells were stimulated with LPS for 60 minutes. PARP1 was immunoprecipitated with a myc antibody and the occupancy on the indicated promoters was measured by qRT-PCR. Results are corrected for the input controls and expressed as relative occupancy, unstimulated levels being set arbitrarily as 1. H2B promoter was assessed as negative control. Data are means of ± SD, n=2. **(D)** Enzymatic activity of recombinant PARP1 proteins. WT, D214N, E988K PARP1 baculo virus generated proteins were incubated with DNA for 5 minutes and ribosylation was analyzed by autoradiography. **(E)** Interaction of PARP1 fragments with GST-p65**.** GST-p65 recombinant protein purified from insect cells was incubated with cleaved (p24, p89) and full-length WT and D214N PARP1 proteins. Interaction was analyzed by western blot.

Fig. 6. PARP1 Cleavage by LPS enhances Chromatin Accessibility around TSS

(**A**) Gene expression profile of *CSF2*, *NOS-2*, *IP-10* and *MIP-2* in bone marrow derived macrophages (BMDM) isolated from WT and D214N PARP1 mice. Cells were stimulated with LPS for one hour and mRNA levels were determined by real-time RT-PCR analysis. Samples were normalized to *Rps12* expression levels and expressed as fold increase relative to unstimulated mRNA levels. Data are means of ±SEM three independent mice groups where each group contains two mice, n=6. (**B**) Chromatin accessibility by real-time PCR (CHART-PCR) in BMDMs. Nuclei from unstimulated and LPS stimulated BMDMs were incubated with MNase. (-1) kb upstream promoter and TSS of *CSF2, NOS-2* was analyzed by qRT-PCR. Results were expressed as uncut over cut genomic DNA and normalized to unstimulated levels. Unstimulated uncut / cut genomic DNA levels around TSS was arbitrarily set as 100. Data are from a pool of 6 mice and means of ± SD, n=2.

REFERENCES

Algeciras-Schimnich, A., Barnhart, B.C., and Peter, M.E. (2002). Apoptosis-independent functions of killer caspases. Curr Opin Cell Biol *14*, 721-726.

Alnemri, E.S., Livingston, D.J., Nicholson, D.W., Salvesen, G., Thornberry, N.A., Wong, W.W., and Yuan, J. (1996). Human ICE/CED-3 protease nomenclature. Cell *87*, 171.

Altmeyer, M., Messner, S., Hassa, P.O., Fey, M., and Hottiger, M.O. (2009). Molecular mechanism of poly(ADP-ribosyl)ation by PARP1 and identification of lysine residues as ADP-ribose acceptor sites. Nucleic Acids Research *37*, 3723-3738.

Ariumi, Y., Turelli, P., Masutani, M., and Trono, D. (2005). DNA damage sensors ATM, ATR, DNA-PKcs, and PARP-1 are dispensable for human immunodeficiency virus type 1 integration. J Virol *79*, 2973-2978.

Boatright, K.M., Renatus, M., Scott, F.L., Sperandio, S., Shin, H., Pedersen, I.M., Ricci, J.E., Edris, W.A., Sutherlin, D.P., Green, D.R., and Salvesen, G.S. (2003). A unified model for apical caspase activation. Molecular Cell *11*, 529-541.

Chowdhury, I., Tharakan, B., and Bhat, G.K. (2008). Caspases - an update. Comp Biochem Physiol B, Biochem Mol Biol *151*, 10-27.

Denis, F., Rhéaume, E., Aouad, S.M., Alam, A., Sékaly, R.P., and Cohen, L.Y. (1998). The role of caspases in T cell development and the control of immune responses. Cell Mol Life Sci *54*, 1005-1019.

Deveraux, Q.L., Takahashi, R., Salvesen, G.S., and Reed, J.C. (1997). X-linked IAP is a direct inhibitor of cell-death proteases. Nature *388*, 300-304.

Fink, S.L., Bergsbaken, T., and Cookson, B.T. (2008). Anthrax lethal toxin and Salmonella elicit the common cell death pathway of caspase-1-dependent pyroptosis via distinct mechanisms. Proc Natl Acad Sci USA *105*, 4312-4317.

Fujita, J., Crane, A.M., Souza, M.K., Dejosez, M., Kyba, M., Flavell, R.A., Thomson, J.A., and Zwaka, T.P. (2008). Caspase activity mediates the differentiation of embryonic stem cells. Cell Stem Cell *2*, 595-601.

Ghayur, T., Banerjee, S., Hugunin, M., Butler, D., Herzog, L., Carter, A., Quintal, L., Sekut, L., Talanian, R., Paskind, M*., et al.* (1997). Caspase-1 processes IFN-gamma-inducing factor and regulates LPS-induced IFN-gamma production. Nature *386*, 619-623.

Ghosh, S., and Hayden, M.S. (2008). New regulators of NF-kappaB in inflammation. Nat Rev Immunol *8*, 837-848.

Hassa, P.O., Haenni, S.S., Buerki, C., Meier, N.I., Lane, W.S., Owen, H., Gersbach, M., Imhof, R., and Hottiger, M.O. (2005). Acetylation of poly(ADP-ribose) polymerase-1 by p300/CREB-binding protein regulates coactivation of NF-kappaB-dependent transcription. J Biol Chem *280*, 40450-40464.

Hassa, P.O., Haenni, S.S., Elser, M., and Hottiger, M.O. (2006). Nuclear ADP-ribosylation reactions in mammalian cells: where are we today and where are we going? Microbiol Mol Biol Rev *70*, 789-829.

Hassa, P.O., and Hottiger, M.O. (1999). A role of poly (ADP-ribose) polymerase in NF-kappaB transcriptional activation. Biol Chem *380*, 953-959.

Hassa, P.O., and Hottiger, M.O. (2008). The diverse biological roles of mammalian PARPS, a small but powerful family of poly-ADP-ribose polymerases. Front Biosci *13*, 3046-3082.

Hornung, V., Ablasser, A., Charrel-Dennis, M., Bauernfeind, F., Horvath, G., Caffrey, D.R., Latz, E., and Fitzgerald, K.A. (2009). AIM2 recognizes cytosolic dsDNA and forms a caspase-1-activating inflammasome with ASC. Nature *458*, 514-518.

Ju, B.-G., Solum, D., Song, E.J., Lee, K.-J., Rose, D.W., Glass, C.K., and Rosenfeld, M.G. (2004). Activating the PARP-1 sensor component of the groucho/ TLE1 corepressor complex mediates a CaMKinase IIdelta-dependent neurogenic gene activation pathway. Cell *119*, 815-829.

Jump, D.B., Butt, T.R., and Smulson, M. (1979). Nuclear protein modification and chromatin substructure. 3. Relationship between poly(adenosine diphosphate) ribosylation and different functional forms of chromatin. Biochemistry *18*, 983-990.

Kim, M.Y., Zhang, T., and Kraus, W.L. (2005). Poly(ADP-ribosyl)ation by PARP-1: 'PAR-laying' NAD+ into a nuclear signal. Genes & Development *19*, 1951-1967.

Kraus, W.L. (2008). Transcriptional control by PARP-1: chromatin modulation, enhancer-binding, coregulation, and insulation. Curr Opin Cell Biol *20*, 294-302.

Krishnakumar, R., Gamble, M.J., Frizzell, K.M., Berrocal, J.G., Kininis, M., and Kraus, W.L. (2008). Reciprocal binding of PARP-1 and histone H1 at promoters specifies transcriptional outcomes. Science *319*, 819-821.

Kuida, K., Zheng, T.S., Na, S., Kuan, C., Yang, D., Karasuyama, H., Rakic, P., and Flavell, R.A. (1996). Decreased apoptosis in the brain and premature lethality in CPP32-deficient mice. Nature *384*, 368-372.

Kurdistani, S.K., and Grunstein, M. (2003). In vivo protein-protein and protein-DNA crosslinking for genomewide binding microarray. Methods *31*, 90-95.

Lakhani, S.A., Masud, A., Kuida, K., Porter, G.A., Booth, C.J., Mehal, W.Z., Inayat, I., and Flavell, R.A. (2006). Caspases 3 and 7: key mediators of mitochondrial events of apoptosis. Science *311*, 847-851.

Lamkanfi, M., Kanneganti, T.-D., Van Damme, P., Vanden Berghe, T., Vanoverberghe, I., Vandekerckhove, J., Vandenabeele, P., Gevaert, K., and Núñez, G. (2008). Targeted peptidecentric proteomics reveals caspase-7 as a substrate of the caspase-1 inflammasomes. Mol Cell Proteomics *7*, 2350-2363.

Lazebnik, Y.A., Kaufmann, S.H., Desnoyers, S., Poirier, G.G., and Earnshaw, W.C. (1994). Cleavage of poly(ADP-ribose) polymerase by a proteinase with properties like ICE. Nature *371*, 346-347.

Lomvardas, S., and Thanos, D. (2002). Modifying gene expression programs by altering core promoter chromatin architecture. Cell *110*, 261-271.

Mankan, A.K., Lawless, M.W., Gray, S.G., Kelleher, D., and McManus, R. (2009). NF-kappaB regulation: the nuclear response. J Cell Mol Med *13*, 631-643.

Mariathasan, S., Newton, K., Monack, D.M., Vucic, D., French, D.M., Lee, W.P., Roose-Girma, M., Erickson, S., and Dixit, V.M. (2004). Differential activation of the inflammasome by caspase-1 adaptors ASC and Ipaf. Nature *430*, 213-218.

Martinon, F., Agostini, L., Meylan, E., and Tschopp, J. (2004). Identification of bacterial muramyl dipeptide as activator of the NALP3/cryopyrin inflammasome. Curr Biol *14*, 1929-1934.

Martinon, F., Burns, K., and Tschopp, J. (2002). The inflammasome: a molecular platform triggering activation of inflammatory caspases and processing of proIL-beta. Molecular Cell *10*, 417-426.

Mullins, D.W., Giri, C.P., and Smulson, M. (1977). Poly(adenosine diphosphate-ribose) polymerase: the distribution of a chromosome-associated enzyme within the chromatin substructure. Biochemistry *16*, 506-513.

Natoli, G. (2006). Tuning up inflammation: how DNA sequence and chromatin organization control the induction of inflammatory genes by NF-kappaB. FEBS Lett *580*, 2843-2849.

Nicholson, D.W., Ali, A., Thornberry, N.A., Vaillancourt, J.P., Ding, C.K., Gallant, M., Gareau, Y., Griffin, P.R., Labelle, M., and Lazebnik, Y.A. (1995). Identification and inhibition of the ICE/CED-3 protease necessary for mammalian apoptosis. Nature *376*, 37-43.

Nicholson, D.W., and Thornberry, N.A. (1997). Caspases: killer proteases. Trends Biochem Sci *22*, 299-306.

Pétrilli, V., Herceg, Z., Hassa, P.O., Patel, N.S.A., Di Paola, R., Cortes, U., Dugo, L., Filipe, H.-M., Thiemermann, C., Hottiger, M.O*., et al.* (2004). Noncleavable poly(ADP-ribose) polymerase-1 regulates the inflammation response in mice. J Clin Invest *114*, 1072-1081.

Pétrilli, V., Papin, S., Dostert, C., Mayor, A., Martinon, F., and Tschopp, J. (2007). Activation of the NALP3 inflammasome is triggered by low intracellular potassium concentration. Cell Death Differ *14*, 1583-1589.

Pion, E., Ullmann, G.M., Amé, J.-C., Gérard, D., de Murcia, G., and Bombarda, E. (2005). DNA-induced dimerization of poly(ADP-ribose) polymerase-1 triggers its activation. Biochemistry *44*, 14670-14681.

Quénet, D., El Ramy, R., Schreiber, V., and Dantzer, F. (2009). The role of poly(ADP-ribosyl)ation in epigenetic events. Int J Biochem Cell Biol *41*, 60-65.

Ramirez-Carrozzi, V.R., Braas, D., Bhatt, D.M., Cheng, C.S., Hong, C., Doty, K.R., Black, J.C., Hoffmann, A., Carey, M., and Smale, S.T. (2009). A unifying model for the selective regulation of inducible transcription by CpG islands and nucleosome remodeling. Cell *138*, 114-128.

Rao, S., Procko, E., and Shannon, M.F. (2001). Chromatin remodeling, measured by a novel real-time polymerase chain reaction assay, across the proximal promoter region of the IL-2 gene. J Immunol *167*, 4494-4503.

Salvesen, G.S., and Dixit, V.M. (1997). Caspases: intracellular signaling by proteolysis. Cell *91*, 443-446.

Schroder, K., and Tschopp, J. (2010). The inflammasomes. Cell *140*, 821-832.

Tewari, M., Quan, L.T., O'Rourke, K., Desnoyers, S., Zeng, Z., Beidler, D.R., Poirier, G.G., Salvesen, G.S., and Dixit, V.M. (1995). Yama/CPP32 beta, a mammalian homolog of CED-3, is a CrmA-inhibitable protease that cleaves the death substrate poly(ADP-ribose) polymerase. Cell *81*, 801-809.

Thornberry, N.A., Bull, H.G., Calaycay, J.R., Chapman, K.T., Howard, A.D., Kostura, M.J., Miller, D.K., Molineaux, S.M., Weidner, J.R., and Aunins, J. (1992). A novel heterodimeric cysteine protease is required for interleukin-1 beta processing in monocytes. Nature *356*, 768-774.

Wacker, D.A., Ruhl, D.D., Balagamwala, E.H., Hope, K.M., Zhang, T., and Kraus, W.L. (2007). The DNA binding and catalytic domains of poly(ADP-ribose) polymerase 1 cooperate in the regulation of chromatin structure and transcription. Molecular and Cellular Biology *27*, 7475-7485.

Woodhouse, B.C., and Dianov, G.L. (2008). Poly ADP-ribose polymerase-1: an international molecule of mystery. DNA Repair (Amst) *7*, 1077-1086.

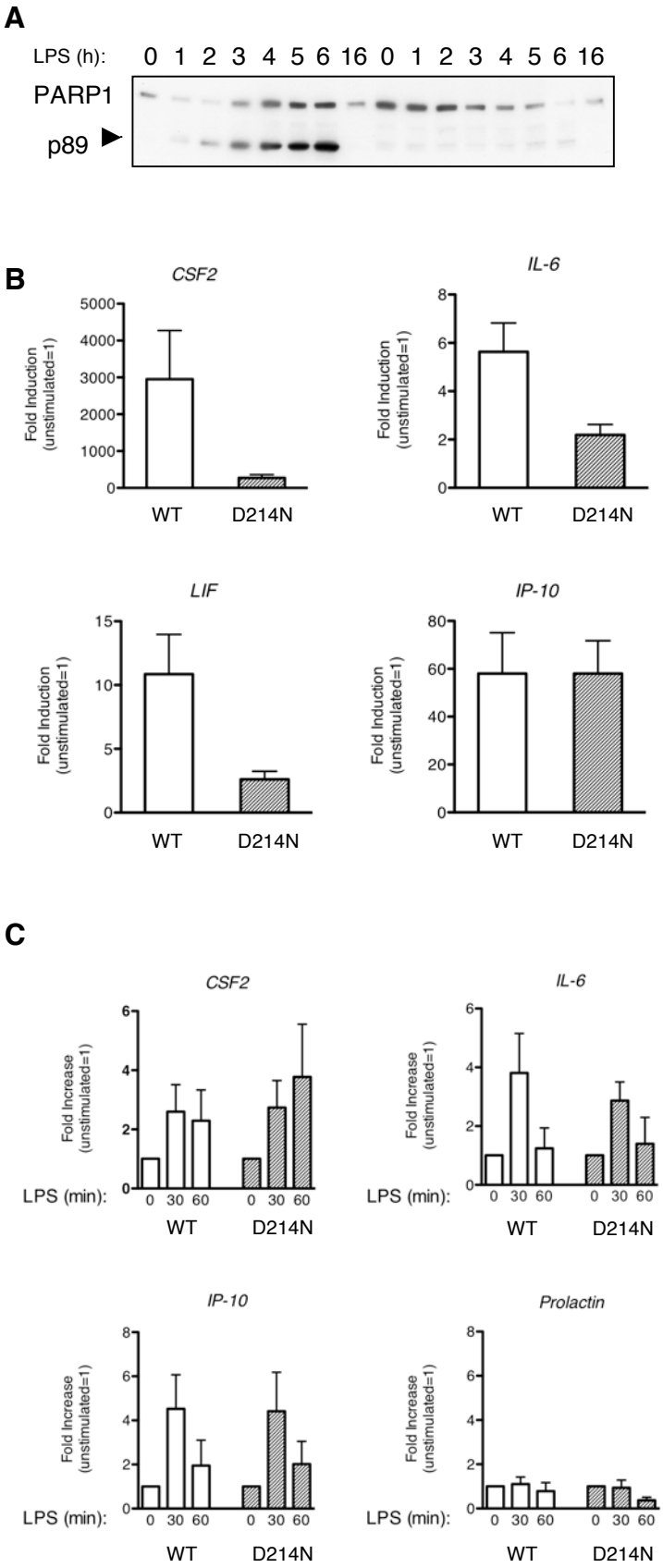
A
LPS (h): 0 1 2 3 4 5 6 16 0 1 2 3 4 5 6 16
PARP1
p89
B
CSF2
IL-6
LIF
IP-10
Fold Induction (unstimulated=1)
WT
D214N
C
CSF2
IL-6
IP-10
Prolactin
Fold Increase (unstimulated=1)
LPS (min): 0 30 60 0 30 60
WT
D214N

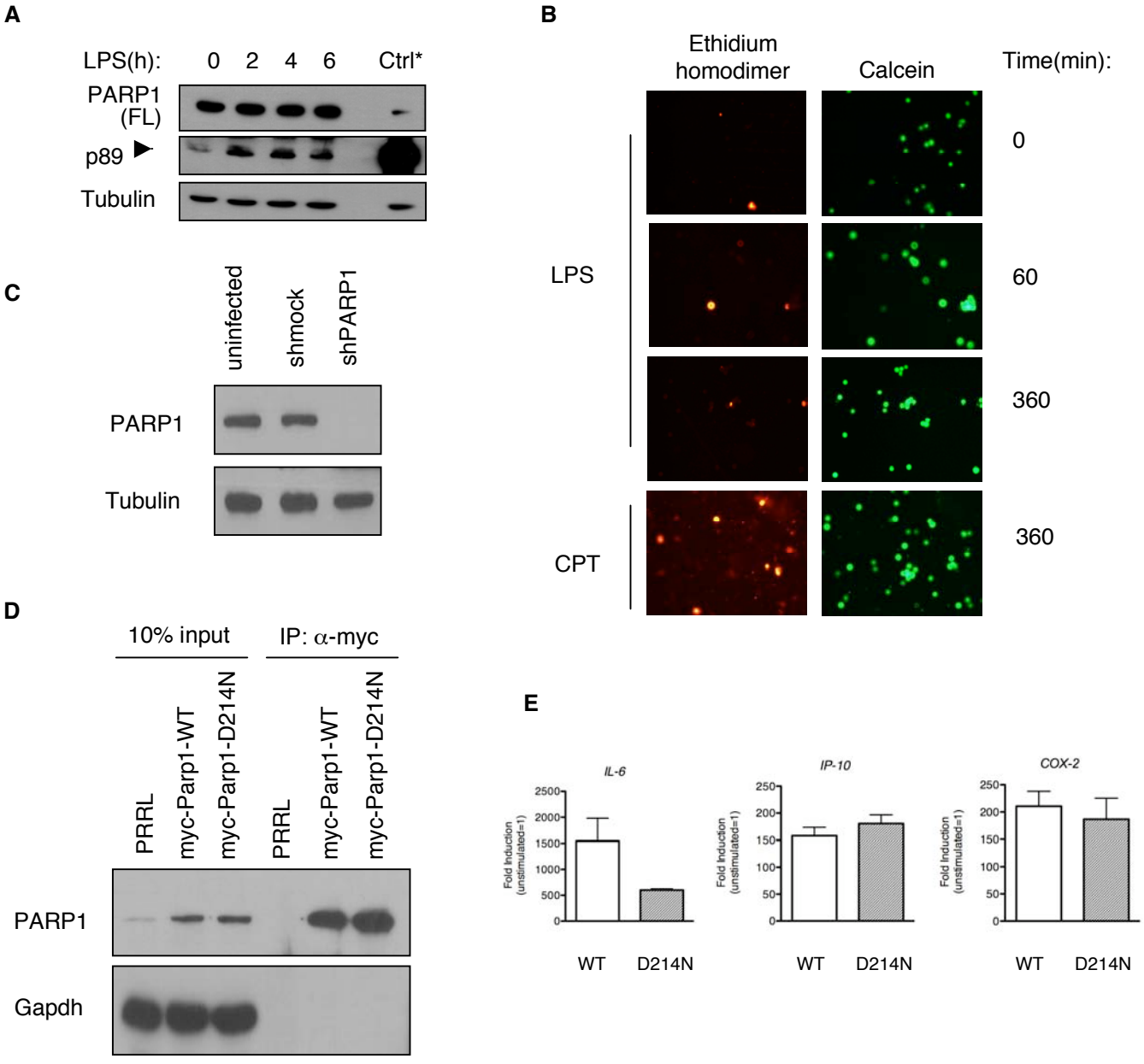
A
LPS(h): 0 2 4 6 Ctrl*
PARP1 (FL)
p89
Tubulin
B
Ethidium homodimer
Calcein
Time(min):
LPS
CPT
0
60
360
360
C
uninfected
shmock
shPARP1
PARP1
Tubulin
D
10% input
IP: α-myc
PRRL
myc-Parp1-WT
myc-Parp1-D214N
PRRL
myc-Parp1-WT
myc-Parp1-D214N
PARP1
Gapdh
E
IL-6
IP-10
COX-2
Fold Induction (unstimulated=1)
WT
D214N
WT
D214N
WT
D214N

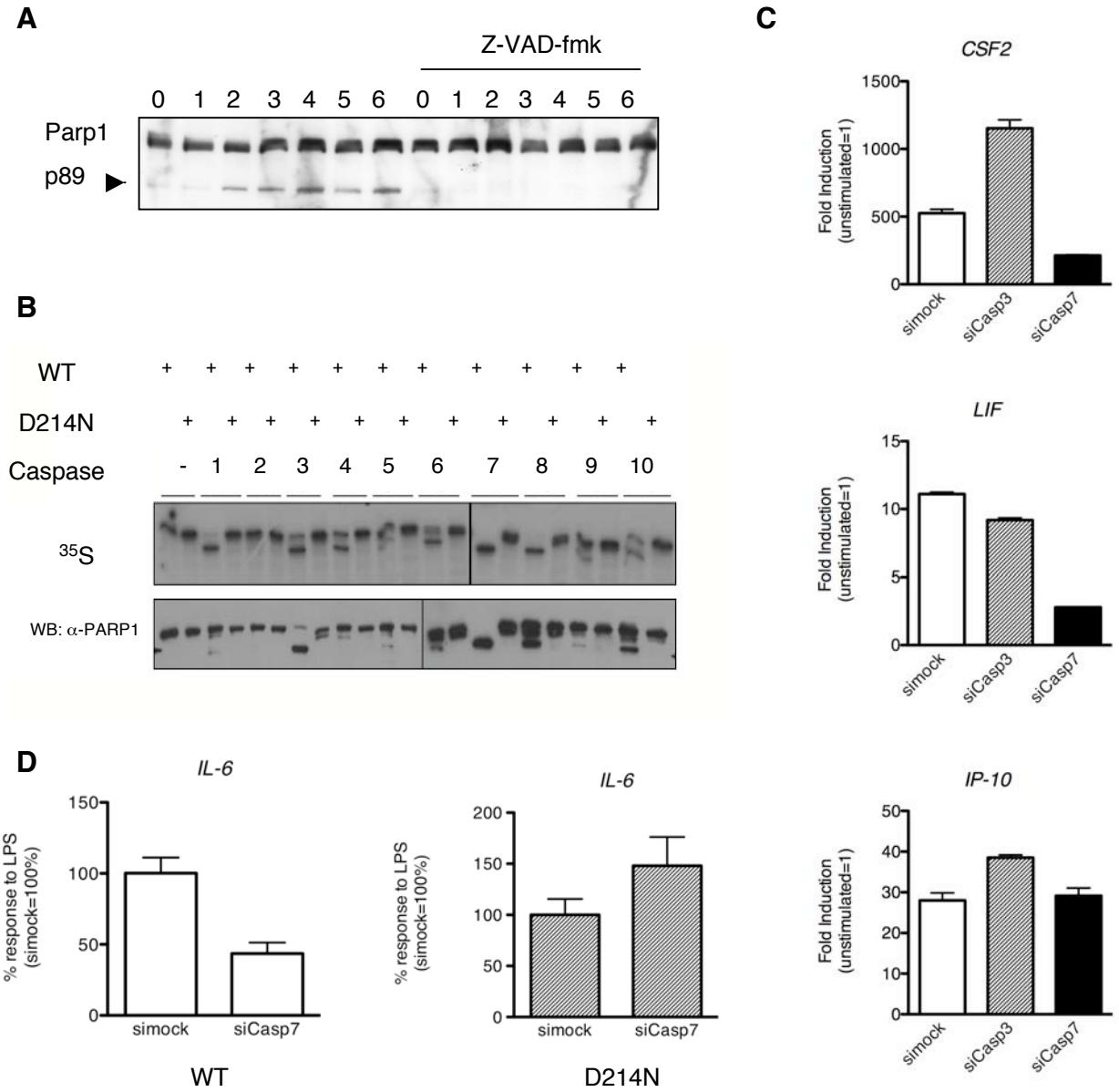
A
Z-VAD-fmk
0 1 2 3 4 5 6 0 1 2 3 4 5 6
Parp1
p89
B
WT + + + + + + + + + + +
D214N + + + + + + + + + + +
Caspase - 1 2 3 4 5 6 7 8 9 10
35S
WB: α-PARP1
C
CSF2
Fold Induction (unstimulated=1)
1500
1000
500
0
simock
siCasp3
siCasp7
LIF
15
10
5
0
IP-10
50
40
30
20
D
IL-6
% response to LPS (simock=100%)
150
100
50
simock
siCasp7
WT
200
D214N
E
Cytoplasmic
Nuclear
LPS(h): 0 1.5 3.5 0 1.5 3.5
Casp 7 (FL)
Casp7 (p19)
PARP1
Tubulin

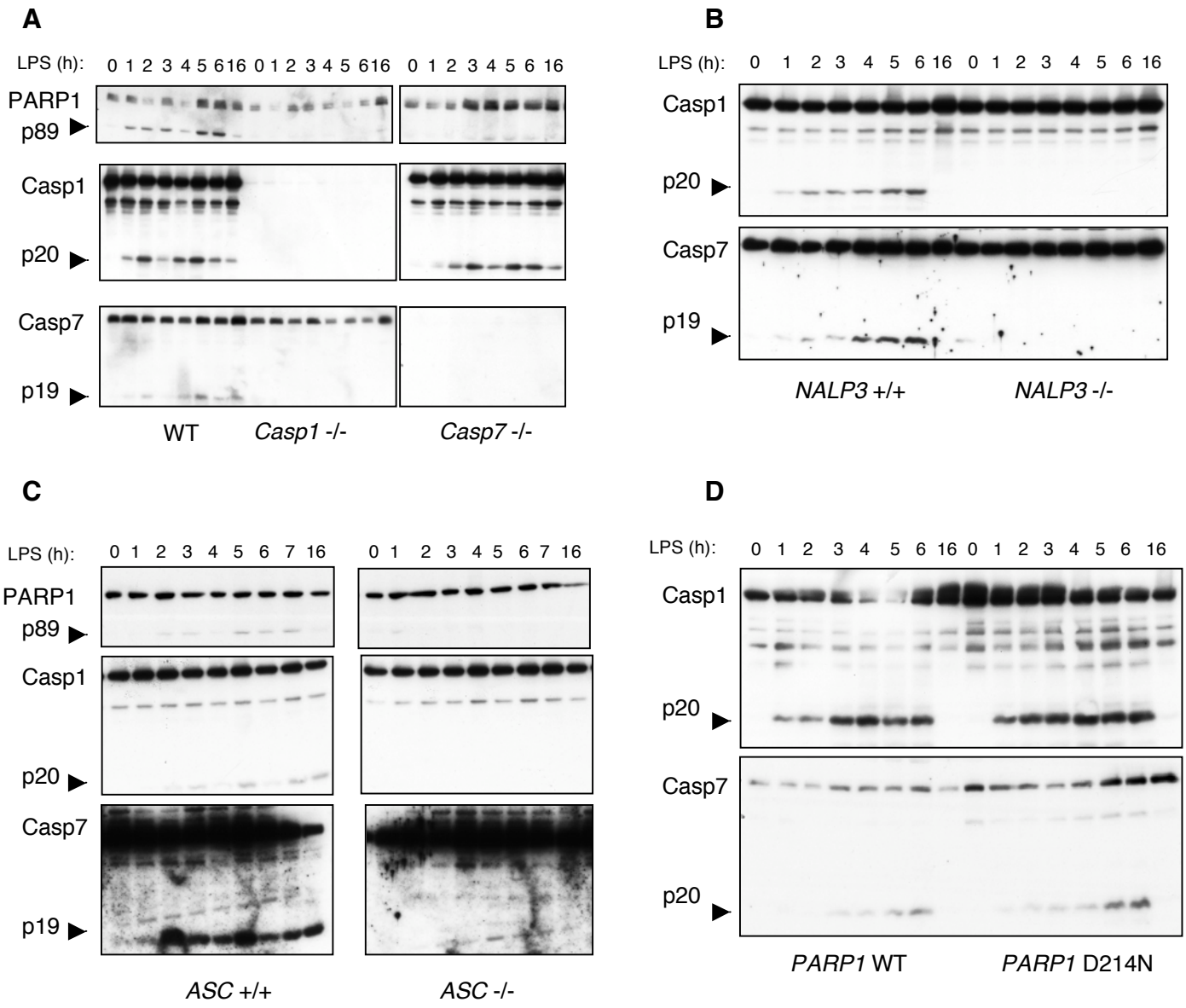
A
LPS (h): 0 1 2 3 4 5 6 16 0 1 2 3 4 5 6 16 0 1 2 3 4 5 6 16
PARP1
p89
Casp1
p20
Casp7
p19
WT
Casp1 -/-
Casp7 -/-
B
LPS (h): 0 1 2 3 4 5 6 16 0 1 2 3 4 5 6 16
Casp1
p20
Casp7
p19
NALP3 +/+
NALP3 -/-
C
LPS (h): 0 1 2 3 4 5 6 7 16 0 1 2 3 4 5 6 7 16
PARP1
p89
Casp1
p20
Casp7
p19
ASC +/+
ASC -/-
D
LPS (h): 0 1 2 3 4 5 6 16 0 1 2 3 4 5 6 16
Casp1
p20
Casp7
p20
PARP1 WT
PARP1 D214N

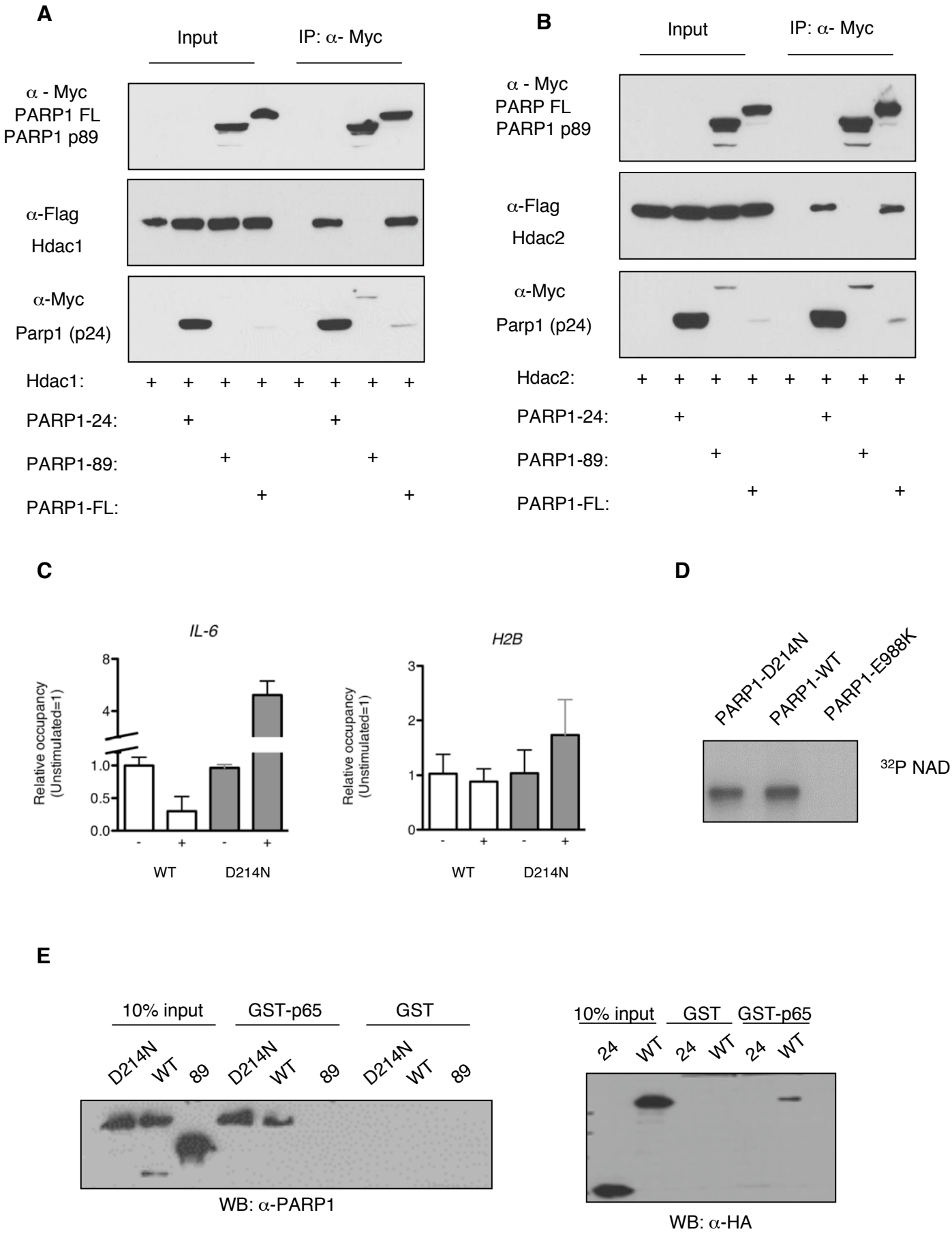
A
Input
IP: α- Myc
α - Myc
PARP1 FL
PARP1 p89
α-Flag
Hdac1
α-Myc
Parp1 (p24)
Hdac1:
PARP1-24:
PARP1-89:
PARP1-FL:
B
Input
IP: α- Myc
α - Myc
PARP FL
PARP1 p89
α-Flag
Hdac2
α-Myc
Parp1 (p24)
Hdac2:
PARP1-24:
PARP1-89:
PARP1-FL:
C
IL-6
H2B
Relative occupancy (Unstimulated=1)
WT
D214N
D
PARP1-D214N
PARP1-WT
PARP1-E988K
32P NAD
E
10% input
GST-p65
GST
D214N
WT
89
WB: α-PARP1
10% input
GST
GST-p65
24
WT
WB: α-HA

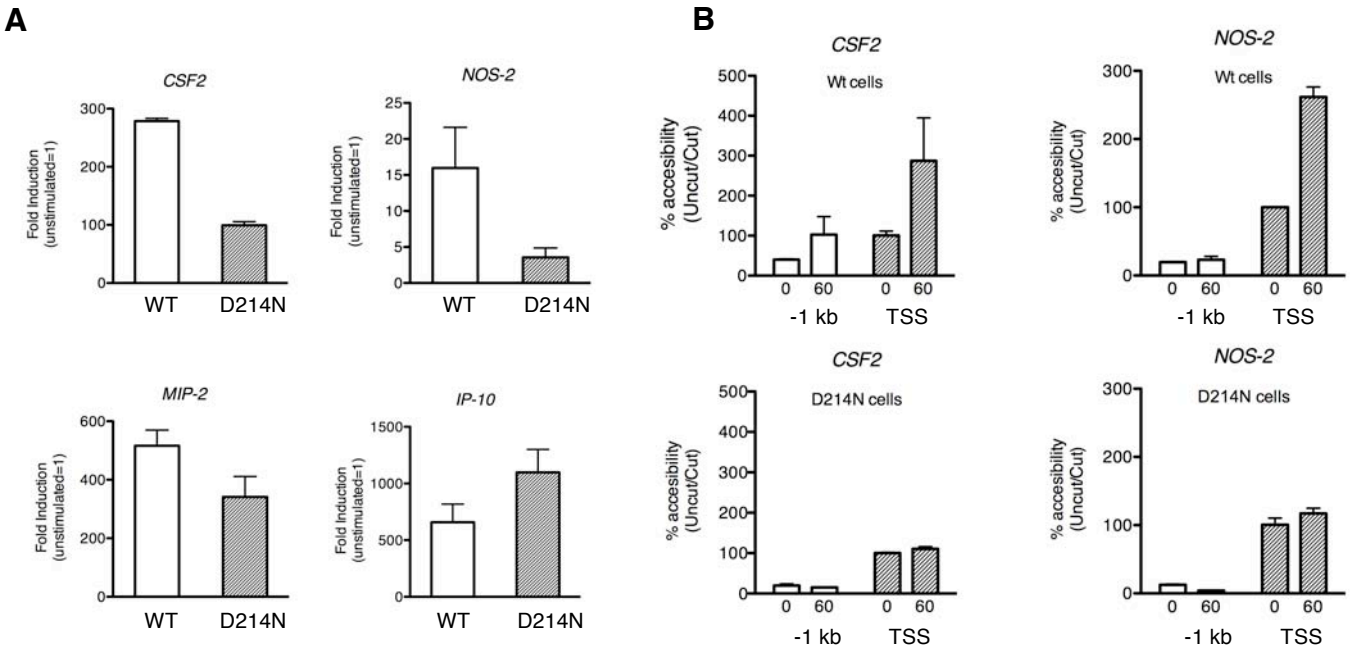
A
CSF2
Fold Induction (unstimulated=1)
300
200
100
0
WT
D214N
NOS-2
Fold Induction (unstimulated=1)
25
20
15
10
5
0
WT
D214N
MIP-2
Fold Induction (unstimulated=1)
600
400
200
0
WT
D214N
IP-10
Fold Induction (unstimulated=1)
1500
1000
500
0
WT
D214N
B
CSF2
Wt cells
% accesibility (Uncut/Cut)
500
400
300
200
100
0
0 60 0 60
-1 kb
TSS
NOS-2
Wt cells
% accesibility (Uncut/Cut)
300
200
100
0
0 60 0 60
-1 kb
TSS
CSF2
D214N cells
% accesibility (Uncut/Cut)
500
400
300
200
100
0
0 60 0 60
-1 kb
TSS
NOS-2
D214N cells
% accesibility (Uncut/Cut)
300
200
100
0
0 60 0 60
-1 kb
TSS

SUPPLEMENTAL DATA

SUPPLEMENTAL TABLES

Table S1, S2, S3: PCR primers used in this study. The sequences of forward (F) and reverse (R) primers used for PCR are given in 5`-3`direction.

TABLE S1. SyBr green primers used in real-time RT-PCR analysis

Gene	Species	Sequence (F, R; 5`-3`)
CSF2	Mus musculus	ACATGCCTGTCACGTTGAAT TTGAGTTTGGTGAAATTGCC
IP-10	Mus musculus	GCACGAACTTAACCACCATCTTCC CTACCCATTGATACATACTTGATGACAC
IL-6	Mus musculus	ACTGACAATATGAATGTTGGGACAC ACCATCTGGCTAGGTAACAGAA
MIP2	Mus musculus	ACATCCCACCCACACAGTGAAAGA TCCTTCCATGAAAGCCATCCGACT
LIF	Mus musculus	CCATAGATGCAGCAAGGAGA CAGTCCTGAGATGAGCCTGA
RPS12	Mus musculus	GAAGCTGCCAAAGCCTTAGA AACTGCAACCAACCACCTTC
RPL28	Homo Sapiens	GCAATTCCTTCCGCTACAAC TGTTCTTGCGGATCATGTGT
IL-6	Homo Sapiens	GGCACTGGCAGAAAACAACC GCAAGTCTCCTCATTGAATCC

TABLE S2. Taqman probes used in real-timer RT-PCR analysis

Gene	Species	Taqman-Number
NOS-2	Mus musculus	Mm00440485
CALNEXIN	Mus musculus	Mm00500330_m1
IP-1O	Homo Sapiens	Hs00171042_m1
CSF2	Homo Sapiens	Hs99999044_m1
COX-2	Homo Sapiens	Hs00153133_m1

TABLE S3. SyBr green primers used in ChIP and CHART RT-PCR analysis

Gene	Species	Sequence (F, R; 5`-3`)
IP-10	Mus musculus	GCAATGCCCTCGGTTTACAG GGCTGACTTTGGAGATGACTCA
IL-6	Mus musculus	CCCCACCCTCCAACAAAGATTTT CCCCAGTCTCATATTTATTAGGAGTCAAC
CSF2	Mus musculus	AATTCTGCAGCCACATCCTC GCCAGGAGATTCCACAACTC
CSF2(-1KB)	Mus musculus	CTTGAGACCATGCTGCCTTT GCTTCCCTGGCAAGTTCTC
NOS-2	Mus musculus	ATGGCCTTGCATGAGGATAC GCAGCAGCCATCAGGTATTT
NOS-2 (-1KB)	Mus musculus	GGGTGTTGCCTGGATAAAGA CACTTGCACACACACACAGC
Prolactin	Mus musculus	CCTTCATTTCTGGCCAATGT GCCTGAGAGAACCACAGCTT
IL-6	Homo Sapiens	CCTCACCCTCCAACAAAGAT GCCTCAGACATCTCCAGTCC
H2B	Homo Sapiens	TTGCATAAGCGATTCTATATAAAAGCG ATAAAGCGCCAACGAAAAGG

SUPPLEMENTAL EXPERIMENTAL PROCEDURES

Tissue Culture

THP1 monocytic cells were grown in suspension and maintained in RPMI supplemented with 10% FCS, 1mM sodium pyruvate (Gibco), 1x non-essential amino acids (Gibco) and 100units/ml penicillin/streptomycin (Gibco), 50 μM β-mercaptoethanol (Gibco) at a cell density of 0.3 to $1.0x10^6$/mL. For differentiation into macrophages, cells were plated at a density of $1x10^6$/6-cm dish in RPMI with 10 ng/ml PMA for 18 hours to become fully differentiated macrophages before use in experiments. HEK 293 cells were maintained in DMEM supplemented with 10% FCS and 100 units/ml penicillin/streptomycin. All cells were maintained at 37°C in 5% CO_2.

Plasmids

Plasmid for the mammalian expression of human PARP1 was generated by cloning human PARP1 cDNA into XhoI cloning site of pCDNA 3 with a hemagglutinin-tag at the C-terminus. Corresponding D214N PARP1 mutant was generated by site directed mutagenesis and confirmed by sequencing. Plasmids for the mammalian expression of HDAC 1-2 were described elsewhere (Hassa et al., 2005). myc-PARP1(WT), myc-PARP1 (89 kDa), myc-PARP1 (24 kDa) were cloned into pCMV vector and the latter two constructs had a nuclear localization signal at the N-terminus.

Reagents and Antibodies

Lipopolysaccharide (LPS, 055:B5) was purchased from Sigma. Active recombinant human caspase Set IV was purchased from Biovision. Etoposide was purchased from Calbiochem. Ethidium homodimer and Calcein AM were purchased from Fluka. SyBR Green was purchased from Quantace. The following antibodies were purchased from Santa Cruz Biotechnologies: anti-RelA (sc-372), anti-PARP1 (sc-7150), anti-GAPDH (FL-335), anti-caspase 7 (sc-28295). The anti-PARP1 (89) and active-caspase 7 (9491) antibodies were from Cell Signaling. Anti-mouse caspase-1 was obtained from Peter Vandernabele. The anti-myc antibodies were either purchased from Roche (11-667-149-001) or purified from hybridoma cells. The anti-Tubulin and anti-Flag (M2) antibodies were purchased from Sigma and the anti-HA was from Covance (MMS-101P).

Generation Of Recombinant Proteins

The recombinant proteins were expressed by baculovirus in Sf21 cells using either the FastBac (Invitrogen) or the BacPAK systems (Clontech). His-tagged proteins were purified over Ni^{2+}-beads (ProBond, Invitrogen) and GST-tagged proteins over L-Glutathione beads (Sigma). All purified proteins were analyzed by coomassie staining and confirmed by western blot analysis using the corresponding antibodies.

^{32}P- NAD Automodification

Experiment was performed as described elsewhere (Altmeyer et al., 2009).

In Vitro Translation

HA-tagged WT and D214N mutant PARP1 were *in vitro* translated using the `TNT couped reticulocyte lysate systems` (Promega) following the manufacturer's instructions.

In Vitro PARP1 Cleavage Assay

10 pmol recombinant or 125 ng *in vitro* translated ^{35}S labeled WT or D214N PARP1 proteins were incubated for 20 minutes at 37°C with 1U of recombinant caspases in caspase cleavage buffer (50 mM Hepes pH 7.2, 50 mM NaCl, 0.1% Chaps, 10 mM EDTA, 5% Glycerol, 10 mM DTT). Proteins were subsequently resolved by SDS-PAGE and analyzed by western blot or autoradiography.

In Vitro Interaction and GST Pull-Down Assays

GST-p65 expressed in insect cells was immobilized on glutathione-sepharose beads (Amersham Biosciences) and incubated with recombinant PARP1 proteins (WT, D214N mutant, p24 or p89 PARP1 fragments) in binding buffer (50 mM Tris pH 8, 100 mM NaCl, 0.5% NP-40, 5 mM DTT, 1 mM PMSF) for 2 h at 4°C rolling. Glutathione beads were washed three times with precission buffer (50 mM Tris-HCl pH 7.5, 150 mM NaCl, 1mM EDTA, 1 mM DTT) and incubated with precission enzyme in 50 ul precission buffer overnight. Proteins in the supernatant were boiled, resolved on SDS-PAGE and subjected to western blot using anti-PARP1 or anti-HA antibodies.

Whole Cell Extract and Immunoprecipitation for Myc-PARP1

Unless stated otherwise, whole cell extracts were prepared by lyzing the cells for 15 minutes in lysis buffer (50 mM Tris pH 8, 500 mM NaCl, 1% Triton X-100, 1μg/ml pepstatin, 1μg/ml bestatin, 1μg/ml leupeptin, 2 mM PMSF) at 4°C. One milligram of whole cell extract was incubated with anti-myc antibody for 2 hours at 4°C. Immunocomplexes were collected with Protein A agarose beads (GE Healthcare) for 1 hour at 4°C and washed three times with wash buffer containing 120 mM NaCl. Immunocomplexes were analyzed by standard western blot analysis using anti-PARP1 and anti-GAPDH antibodies.

Nuclear Extract Preparation

Cells were stimulated with 10 μg/ml LPS for the indicated times**,** washed with PBS, harvested and washed again three times in buffer A (10 mM HEPES KOH pH7.9, 1.5 mM $MgCl_2$, 10 mM KCl, 1μg/ml pepstatin, 1μg/ml bestatin, 1μg/ml leupeptin, 2 mM PMSF, 5mM DTT). Cells were lysed with A+ buffer (Buffer A+ 0.06 % NP-40) and centrifuged for 5 minutes at 5000 rpm. Supernatant corresponding to cytoplasm was saved for western blot analysis. Pellet was washed three times with buffer A and subsequently resuspended in three volumes of Buffer C (20 mM HEPES KOH pH7.9, 0.42 M NaCl, 1.5 mM $MgCl_2$, 25% v/v glycerol, 1μg/ml pepstatin, 1μg/ml bestatin, 1μg/ml leupeptin, 2 mM PMSF, 5 mM DTT) and incubated for 15 minutes at 4°C on rotating wheels. Lysate was centrifuged for 10 minutes at 4°C at 14000 rpm with the supernatant corresponding to the nuclear fraction.150 μg cytoplasmic extracts and 50 μg nuclear extracts were boiled with Laemmli buffer, resolved on 15% SDS-PAGE and subjected to western blot using different antibodies.

Cell Viability Assay

THP1 macrophages stimulated with 10 μg/ml LPS for the indicated times were incubated with 4 μM Ethidium homodimer and 2 μM Calcein mix in PBS for 30 minutes at 37°C incubator. Ethidium homodimer positive and Calcein positive cells were visualized using Olympus BX51 microscope.

***In Vitro* Inflammasome Formation**

Peritoneal macrophages were primed overnight with 100 ng/ml of ultra-pure LPS and stimulated as indicated asbestos (150 mg/ml), MSU (150 mg/ml), R837 (10 mg/ml), Nigericin (20mM) for 6hr except ATP 5mM 30' (Pétrilli et al., 2007).

SUPPLEMENTAL FIGURES

Fig. S1. LPS Stimulation Leads to PARP1 Cleavage

(A) Interaction of PARP1 with p65 in WT and D214N PARP1 IP cells**.** WT and D214N PARP1 IP cells were stimulated with LPS for 30 minutes and nuclear extracts were prepared. PARP1 complexes were co-immunoprecipitated (IP) using an anti-PARP1 antibody and subsequently tested for PARP1 and p65 by western blot analysis using anti-PARP1 and anti-p65 antibodies. **(B)** THP1 monocytes were stimulated with LPS for different times, total cell extracts were prepared from and analyzed by western blot using antibodies against the full-length and cleaved C-terminal fragment of PARP1 (p89) and Tubulin as loading control. **(C)** PARP1 cleavage in complemented THP1 cells. THP1 cells were stimulated with campothethcin (CPT), total cell extracts were prepared and proteins were analyzed by western blot using the indicated antibodies. **(D)** CHX does not interfere with PARP1 cleavage induced by LPS. Bone-marrow derived macrophages from wild-type mice were stimulated with LPS in the presence or absence of CHX for different time points. Total cell extracts were prepared and PARP1 cleavage was analyzed by western blot using PARP1 antibody that recognizes the cleaved large fragment (p89).

Fig. S2. Caspase 7 Knock-down Reduces NF-κB Response to LPS in THP1 Cells

(A) THP1 cells were transiently transfected with mock, caspase 3 or caspase 7 siRNA oligos for two days. Cells were stimulated with LPS for one hour and mRNA levels were determined by real-time RT-PCR analysis. Samples were normalized to *Rpl28* expression levels and increase in gene expression to LPS was expressed as fold induction. Data are means of ± SD, n=2. **(B)** Caspase 7 knock-down in THP1 cells. THP1cells complemented with WT or D214N PARP1 were PMA primed, transfected with mock or caspase 7 siRNA oligos for two days, total cell extracts were prepared and subjected to western blotting using the indicated antibodies.

Fig. S3. Absence of Caspase 7 Does Not Effect Inflammasome Activation

(A) Peritoneal macrophages from WT and *caspase 7* -/- mice were activated with different inflammasome activators, cell supernatants and cell extracts were prepared, IL-1β secretion and caspase 1 activation was analyzed by western blot.

Fig. S4. PARP1 Cleavage by LPS Enhances Chromatin Accessibility around TSS in IP Cells

Chromatin accessibility by real-time PCR (CHART-PCR) in IP cells. Nuclei from unstimulated and LPS stimulated BMDMs were incubated with MNase. (-1) kb upstream promoter and TSS of *CSF2* was analyzed by qRT-PCR. Results were expressed as uncut over cut genomic DNA and normalized to unstimulated levels. Unstimulated uncut / cut genomic DNA levels around TSS was arbitrarily set as 100. Data ± SE are from three independent experiments.

REFERENCES

Altmeyer, M., Messner, S., Hassa, P.O., Fey, M., and Hottiger, M.O. (2009). Molecular mechanism of poly(ADP-ribosyl)ation by PARP1 and identification of lysine residues as ADP-ribose acceptor sites. Nucleic Acids Research *37*, 3723-3738.

Hassa, P.O., Haenni, S.S., Buerki, C., Meier, N.I., Lane, W.S., Owen, H., Gersbach, M., Imhof, R., and Hottiger, M.O. (2005). Acetylation of poly(ADP-ribose) polymerase-1 by p300/CREB-binding protein regulates coactivation of NF-kappaB-dependent transcription. J Biol Chem *280*, 40450-40464.

Pétrilli, V., Papin, S., Dostert, C., Mayor, A., Martinon, F., and Tschopp, J. (2007). Activation of the NALP3 inflammasome is triggered by low intracellular potassium concentration. Cell Death Differ *14*, 1583-1589.

A

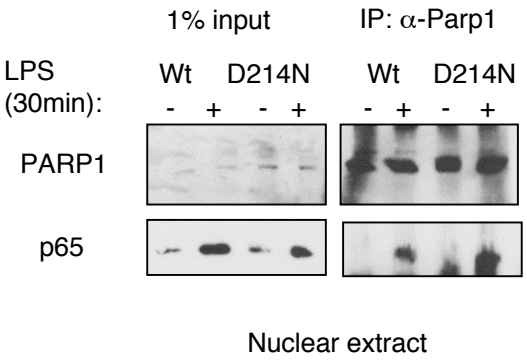
1% input
IP: α-Parp1
LPS
(30min):
Wt
D214N
Wt
D214N
- + - + - + - +
PARP1
p65
Nuclear extract

B

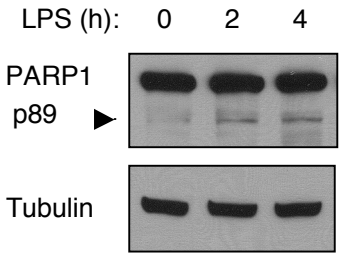
LPS (h): 0 2 4
PARP1
p89
Tubulin

C

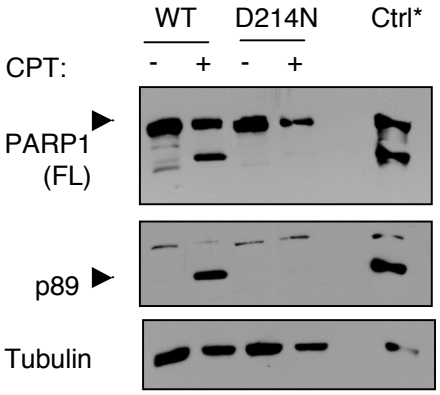
WT
D214N
Ctrl*
CPT:
- + - +
PARP1
(FL)
p89
Tubulin

D

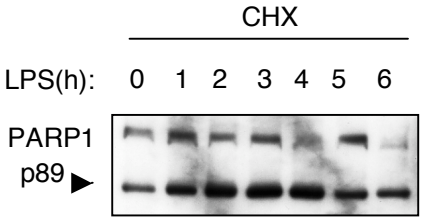
CHX
LPS(h): 0 1 2 3 4 5 6
PARP1
p89

A

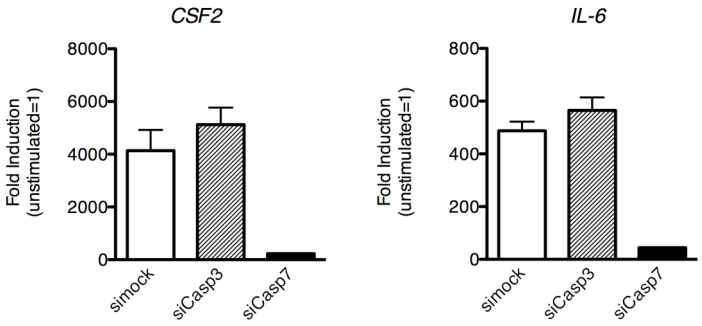
CSF2
IL-6
Fold Induction (unstimulated=1)
8000
6000
4000
2000
0
800
600
400
200
0
simock
siCasp3
siCasp7

B

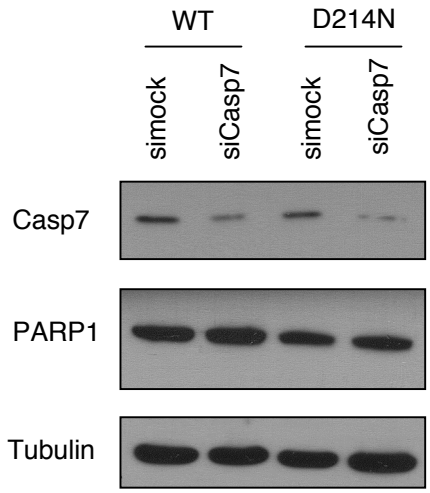
WT
D214N
simock
siCasp7
simock
siCasp7
Casp7
PARP1
Tubulin

Supernatants

A

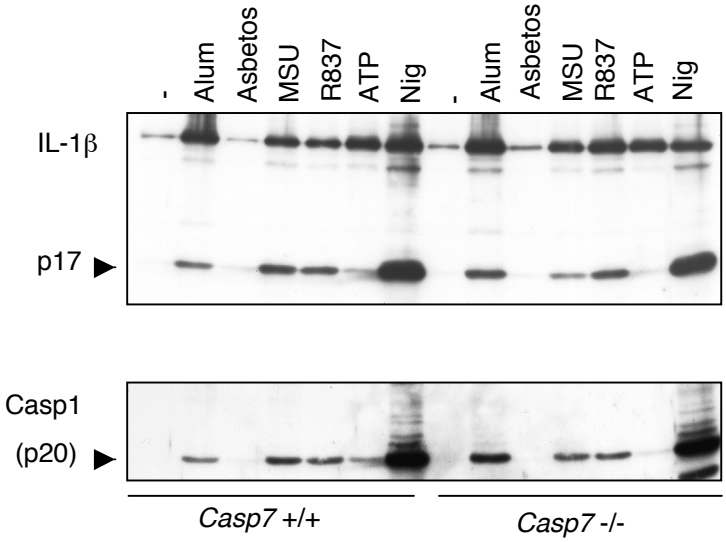

Cell extracts

B

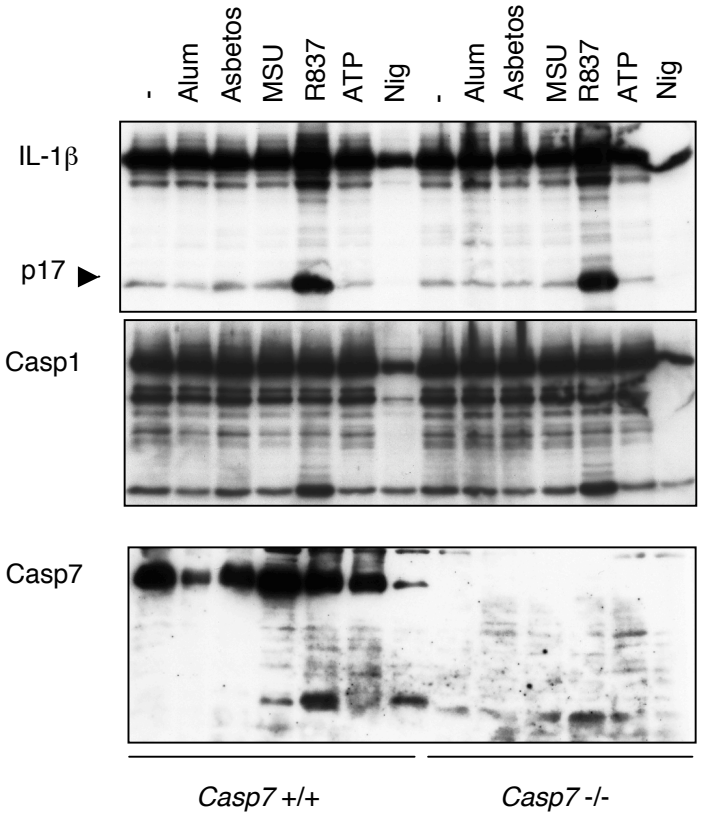

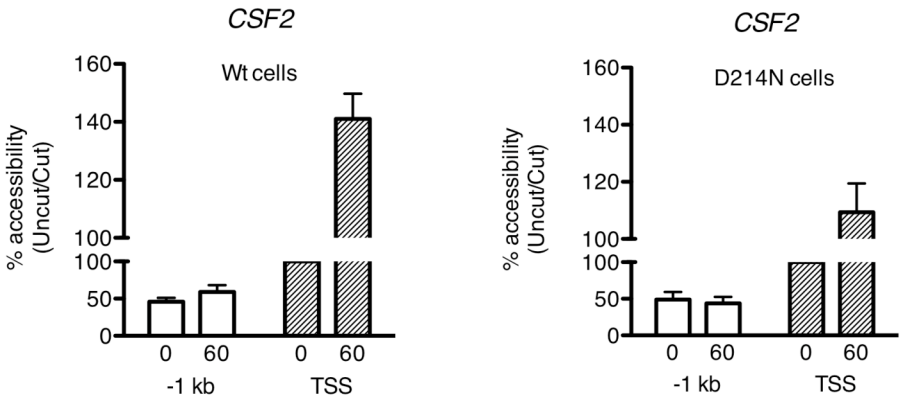
CSF2
Wt cells
% accessibility (Uncut/Cut)
160
140
120
100
100
50
0
0
60
0
60
-1 kb
TSS
CSF2
D214N cells
% accessibility (Uncut/Cut)
160
140
120
100
100
50
0
0
60
0
60
-1 kb
TSS

Manuscript in preparation

PARP1 Knockout Mice Develop Obesity through Deteriorated Glucose Homeostasis

Suheda Erener[1,2], Helga Ellingsgaard[3], Christina Boyle-Neuner[4], Thomas A. Lutz[4] Marc Y. Donath[3] and Michael O. Hottiger[1,*]

[1]Institute of Veterinary Biochemistry and Molecular Biology
University of Zurich, Winterthurerstrasse 190,
8057 Zurich, Switzerland
Phone: +41-44-635 54 74, Fax: +41-44-635 68 40
Email: hottiger@vetbio.uzh.ch

[2]Life Science Zurich Graduate School, Molecular Life Science Program,
University of Zurich

[3]Division of Endocrinology and Diabetes and Center for Integrated Human Physiology, University Hospital of Zurich, Zurich, Switzerland

[4]Institute of Veterinary Physiology and Center of Integrative Human Physiology,
University of Zurich, Zurich, Switzerland

*Corresponding author

SUMMARY

Deregulated glucose homeostasis leads to obesity, which is associated with chronic low-grade inflammation that negatively impacts insulin sensitivity. Here, we show that PARP1 knockout mice in the C57BL/6 background develop obesity and display decreased energy expenditure on normal diet when compared to their wild type littermates. Obese *PARP1-/-* mice show elevated expression of proinflammatory cytokines like *IL-6*, *IP-10*, *MCP1* and *TNFα* in adipose tissues and develop insulin resistance. In liver, *PDK4* and *G6Pase* two important genes involved in glucose homeostasis are upregulated in *PARP1-/-* mice. Interestingly young *PARP1-/-* mice preserve insulin signaling, but have already increased glucose levels, suggesting a regulatory role of PARP1 in the transcriptional regulation of genes involved in gluconeogenesis and glucose homeostasis.

Introduction

The liver is a central regulator of glucose homeostasis and stores or releases glucose according to metabolic demands. In insulin resistant states or diabetes the dysregulation of hepatic glucose release contributes significantly to the pathophysiology of these conditions. Type 2 diabetes mellitus is characterized by both insulin resistance as manifested by reduced insulin-stimulated glucose uptake in skeletal muscle and adipose tissue, inappropriately high hepatic glucose output and reduced insulin secretion by pancreatic β-cells [1-3]. Although the specific molecular pathophysiology remains unclear, many risk factors have been identified for Type 2 diabetes mellitus, including family history of diabetes and prominent environmental factors such as excessive food intake leading to obesity, alterations in early life development, decreased physical activity and aging [1, 3, 4].

At the cellular level, multiple regulatory mechanisms and metabolic pathways may contribute to the pathogenesis of insulin resistance, potentially mediated by alterations in insulin receptor signaling [5], mitochondrial oxidative metabolism and ATP production [6-8], fatty acid oxidation [9], or proinflammatory signaling [10]. Insulin drives the global anabolic response to nutrient ingestion, regulating both carbohydrate and lipid metabolism. Insulin binds to insulin receptor to activate a cascade of intracellular signaling events [11], including the MAPK pathway, which mediates various cellular effects, such as growth and mitogenesis; the PI3K–Akt pathway, which controls gluconeogenesis, glycogen and protein synthesis via regulation of mammalian target of rapamycin (mTOR), forkhead box O1 (FOXO-1) and others; and the c-Cbl-associated protein (CAP)/Cbl and small G protein TC10 pathway that regulates glucose transporter 4 (GLUT-4) and uptake of glucose into adipocytes and muscle [12]. The prevalent model of hepatic insulin signaling is that activated Akt phosphorylates and inhibits the transcription factor FoxO, peroxisome proliferator-activated receptor-coactivator-1a (PGC-1a), and others, thereby terminating expression of the rate-controlling enzymes of gluconeogenesis [13, 14]. Another important aspect of the control of hepatic glucose metabolism is neuronal insulin signaling. Insulin's effect on the liver seem to depend largely on a primary insulin action in the brain. Neuron-specific insulin receptor disrupted (NIRKO) mice were found to develop mild insulin resistance and elevated plasma insulin levels in association with obesity (Brüning and Kahn 2000).

Poly(ADP-ribose) polymerase-1 (PARP1) is an abundant and ubiquitous nuclear enzyme that catalyzes the nicotinamide adenine dinucleotide (NAD^+)-dependent addition of ADP-ribose polymers on a variety of target proteins [15]. It has been implicated in diverse biological processes, including transcriptional regulation, chromatin remodeling, DNA repair, cell proliferation, and apoptosis [15, 16]. In transcription, PARP1 acts as transcriptional cofactor (either a coactivator or a corepressor) for a variety of transcription factors. The enzymatic activity of PARP1 was described to be required for some transcription factors (e.g., HES1, NFAT, and p53) [17-19], while for others it is not required (e.g., NF-κB, B-Myb, and retinoic acid receptor) [20-22]. Loss of PARP1 is shown to affect gene expression profile in a genome-wide manner [23]. Although young *PARP1-/-* mice display no phenotypic abnormalities, older mice originating from a mixed genetic background (129/Sv×C57BL/6) were susceptible to epidermal hyperplasia and obesity, suggesting an important role for PARP1 in general metabolism [24]. This study is supported by data demonstrating that *PARP1-/-* female mice on 129 back-ground older than 21 months gained body weight more than their wild-type litter mates when fed a normal diet [25] and that *PARP1-/-* on the 129 back ground mice are highly susceptible to diet-induced obesity, accumulate more fat tissue and develop hyperleptinemia and insulin resistance and glucose intolerance compared to their wild type counterparts [26].

Here, we present an *in vivo* model that PARP1 is regulating glucose homeostasis through the regulation of the expression of genes involved in gluconeogenesis in the C57BL/6 background on normal diet, which with age leads to obesity and obesity induced inflammation.

RESULTS

PARP1 Knockout Mice Display Increased Weight Gain and Decreased Energy Expenditure on Chow Diet Compared to Their Wild Type Counterparts

PARP1 was described to regulate gene expression and cellular NAD^+, the substrate of PARP1, was described to alter upon diet. We sought to investigate whether PARP1 plays a role in energy metabolism. Wild type (WT) and *PARP1* knock-out (-/-) mice, at the age of 6-8 weeks were either fed with normal chow diet (ND) or high-fat diet (HFD) [24]. 6 weeks after the start of experiments, *PARP1-/-* mice on ND weighed significantly more than WT on the same ND (Fig. 1A,B). However, at the end of the experiments WT mice on HFD weighed 20g more than the WT on ND whereas *PARP1-/-* mice on HFD weighed only 11g more than the *PARP1-/-* mice on ND. These results suggest that PARP1 under normal physiological conditions helps to maintain energy metabolism but its absence might protect from obesity under HFD. Surprisingly, 6 weeks after the start of experiments, body weight, circulating levels of glucose differed significantly *PARP1-/-* mice and their wild-type littermates on ND but not in HFD (Fig. 1C). Although mice on HFD gained more weight and had higher glucose levels compared to mice on ND, no significant difference was observed between the genotypes after 6 weeks (Fig. 1C).

Body weight represents a net balance of food intake and energy expenditure. Leptin is an important player involved in regulating energy intake and energy expenditure [27]. HFD after 13 weeks increased serum leptin levels by 80 fold in wild-type mice (Fig. 2A). No difference was detected between WT and *PARP1-/-* mice on HFD. Interestingly, *PARP1-/-* mice on ND had higher leptin levels than WT. At this age (19 weeks), the body weight of WT and *PARP1-/-* mice on ND differed statistically, even more than 12 weeks old mice (see Fig. 1A). Paradoxically, *PARP1-/-* on ND showed lower daily food intake per body weight compared to wild-type mice, perhaps due to higher circulating leptin serum levels (Fig. 2B). Energy expenditure (EE) was similar in WT and *PARP1-/-* mice on HFD whereas on ND *PARP1-/-* mice tended to have lower EE than WT mice (Fig. 2C). This difference was significant in dark phase. We also compared the respiratory quotient (RQ = VCO_2/VO_2), as a measure of fuel-partitioning patterns. RQ fluctuated between 0.85 and 1.0 in mice on a ND, and fluctuated between 0.8 and 0.9 in mice on HFD for both genotypes (Fig. 2D). No effect for genotype was observed neither under ND nor

HFD, suggesting that there was no difference in fuel selection between carbohydrates and lipids for WT and *PARP1-/-* mice.

PARP1 Knock-Out Mice Display Deteriorated Glucose Homeostasis

Differences in glucose homeostasis between *PARP1-/-* and WT mice were most pronounced under ND. This effect seemed to vanish when mice were fed with HFD. Since *PARP1-/-* had increased glucose levels, we investigated whether PARP1 might play a role in glucose homeostasis. We performed intraperitoneal (IP) glucose and insulin tolerance tests after 3 months of exposure of mice to ND or HFD. Chronic exposure to HFD increased fasting glucose levels (Fig. 3A compare right-left panel, 0 min). Interestingly, *PARP1-/-* mice on ND were glucose intolerant compared to WT. A similar trend was also observed in mice under HFD although the difference between WT and *PARP1-/-* mice was less marked. Intolerance to glucose in *PARP1-/-* mice was not due to reduced insulin levels, since *PARP1-/-* mice had even higher insulin levels (Fig. 3B). Furthermore, *PARP1-/-* mice on ND but also on HFD had a lower sensitivity to IP insulin compared to WT mice (Fig.3C).

PARP1-/- mice had comparable fed free fatty acid and cholesterol serum levels on HFD and ND (Fig. 3D), which were similar to wild-types, suggesting that the lipid homeostasis was not affected by the lack of PARP1.

Old *PARP1-/-* Mice Are Prone to Obesity-Induced Inflammation

At the age of 19 weeks *PARP1-/-* mice on chow diet weighed significantly more than WT (Fig. 1A,B). Obesity leads to an increase in tissue inflammation, particularly within adipose tissue [28, 29]. Large numbers of macrophages accumulate in fat depots in obese mice and human [30, 31]. Tissue macrophages recruited to adipose tissue in obese animals exhibit increased expression of proinflammatory genes including *TNF-α* and *IL-6*. Blocking the functions of these macrophages result in a more glucose tolerant, insulin sensitive state [28, 32]. We investigated whether obese mice had increased inflammatory gene expression in white adipose tissue (WAT). As expected, HFD elevated the mRNA expression of proinflammatory cytokines like *IL-6*, *IP-10*, *MCP1* and *TNF-α* but no effect for genotype was observed on HFD except for *IL-6* (Fig. 4A). Because body weight matched controls were not included, we speculate that this might reflect the small difference in body weight between WT and

PARP1-/- under HFD. However, *PARP1-/-* on ND had significantly increased proinflammatory gene expression in comparison to WT, supporting the conclusion that these mice are obese and prone to inflammation. We have previously reported that PARP1 activates NF-κB gene expression [20]. The increased inflammatory gene response in older *PARP1-/-* mice on ND is therefore more likely to be secondary to the developed obesity. Next, we analysed PPARγ target gene expression in WAT. While the overall expression levels of PPARγ were not altered under the tested diets, we observed that HFD increased the expression of *CD36* and decreased *Glut4* expression levels in both genotypes (WT and *PARP1-/-*) (Fig. 4B). Genotypic expression differences were only observed for *PARP1-/-* mice fed with ND. These results indicated that gene expression profiles WAT of obese *PARP1-/-* mice also displayed differential expression of PPARγ target genes.

Insulin Regulated Gene Expression Is Affected in Liver

Next we examined the expression profiles in liver from ND and HFD mice. No significant difference was observed for liver weights when normalized to body weight (Fig. 5A). In addition, PARP1 protein level was not dependent on the diet (Fig. 5B).

We analysed hepatic gene expression by real-time RT-PCR. Hepatic *PPARγ* and target gene *CD36* was greatly induced in *PARP1-/-* mice on ND in comparison to WT controls (Fig. 5C). In contrast, *Glut4* levels were decreased in *PARP1-/-* mice on ND and for both genotypes on HFD, indicating that the expression levels for *Glut4* might be additionally regulated by the obesity. In addition, while genes involved in β-oxidation such as *PPAR-α*, *ACOX*, *CPT1*, *MCAD* were slightly reduced in mice on HFD, were unchanged when compared between the two genotypes (Fig. 5D). Interestingly, two genes involved in glucose homeostasis, pyruvate dehydrogenase kinase isoform 4 (*PDK4*) and glucose-6-phosphatase (*G6Pase*) were strongly upregulated in *PARP1-/-* mice on ND, but not on HFD, whereas insulin receptor (*IR*) expression was comparable in both genotypes (Fig. 5E). *PDK4* and *G6Pase* expression was reported to be inhibited by the insulin signaling under physiological conditions. Despite the elevated levels of insulin in *PARP1-/-* mice on ND, *PDK4* and *G6Pase* levels were not reduced, suggested an increase gluconeogenesis and glucose serum levels in this genotype. Together, these results indicate that PARP1 might

regulate glucose homeostasis by regulating expression of enzymes involved in glucogeonesis.

Young *PARP1-/-* Mice Preserve Insulin Signaling

To investigate the mechanisms by which the targeted *PARP1* gene disruption affects glucose homeostasis which would, under chronic conditions, lead to obesity in mice on ND, we performed glucose and insulin tolerance in young mice (6 weeks old) on ND. At this age body weight and fasting glucose levels were comparable. GTT indicated that the overall uptake of glucose serum levels is only slightly reduced in *PARP1-/-* mice (Fig.6A). ITT experiments revealed that fed glucose levels were increased in *PARP1-/-* mice, but that the insulin induced uptake was comparable between the two tested genotypes (Fig. 6B). To further strengthen the observation that the insulin signaling is not altered and not the cause for the observed obesity in *PARP1-/-* mice on ND, liver extract from both wild-type and *PARP1-/-* mice fed on ND, was generated 10 minutes after injection of insulin. Liver extracts were subsequently analyzed by immunoblot for Akt phosphorylation. *PARP1-/-* mice exhibited normal insulin-stimulated Akt phosphorylation compared to WT mice (Fix. 6D). Comparable insulin signaling through Akt phosphorylation could also been confirmed in WAT or muscle tissues of *PARP1-/-* and WT mice (Fig.6C and E). In addition Glut4 levels were comparable in WT and *PARP1-/-* muscle extracts, suggesting that Glut4 levels is less likely to be the cause for the observed impaired glucose homeostasis in *PARP1-/-* mice. Together, these experiments confirmed, that the insulin signaling and Glut4 levels per se are not affected in young *PARP1-/-* and WT mice, but that the glucose serum levels are already elevated in *PARP1-/-* mice at this age.

DISCUSSION

Here we show that mice lacking PARP1 have an impaired glucose homeostasis, which develops a mature-onset obesity phenotype with insulin resistance which is not due to increased caloric intake. Our conclusions are based on several observations: (i) body weight and energy expenditure measurements of WT and *PARP1*-/- on chow or high-fat diet, (ii) ITT and GTT measurements of these mice after 13 weeks of diet, and, finally (iii) gene expression profiling in liver and adipose tissue of these mice. Interestingly, young *PARP1-/-* mice preserve insulin signaling, strongly indicating that the insulin resistance observed in older mice is a consequence of obesity, rather than the cause of the observed phenotype.

Obesity is a multifactorial disorder and inter- and intrapopulation genetic variations exist in susceptibility to diet-induced obesity among various inbred strains of mice [33]. Both mono- and polygenic variations contribute to the development of obesity phenotype in mice. Spontaneous mutations or variations in the expression levels of selective genes can induce obesity when fed a high fat (HF) diet, but little or no effect on a low-fat diet [34]. Some inbred strains of mice vary in their susceptibility to diet-induced obesity indicating that obesity is a complex trait and modifications of multiple genes may be necessary for its etiology [34, 35]. C57Bl/6 mice were described to be readily susceptible to diet-induced obesity and associated type-2 diabetes, while the 129 mouse strain is shown to be resistant to diet-induced obesity and insulin resistance [35-37].

Insulin resistance is the inability of the peripheral tissues to respond properly to insulin. During insulin resistance, this process is blunted, and the persistence of hepatic glucose output following a meal compounds diminished glucose uptake into muscle, resulting in postprandial hyperglycemia [38]. The observed GTT and ITT data strongly indicate at an insulin resistance at the periphery, rather than a pathophysiological process in the pancreas.

Central insulin sensitivity is recognized as of high relevance for hepatic glucose metabolism controlled by insulin. Currently we cannot exclude that the potential genotypic differences in the brain of WT and *PARP1-/-* mice might contribute the development of T2D in *PARP1-/-* mice.

A mechanism connecting adipose tissue to insulin resistance is the increased release of free fatty acids into the circulation that in turn may induce insulin resistance in the muscle and possibly in the liver [39]. Adipose tissue produces several

hormones that regulate energy homeostasis, lipid and glucose metabolism such as leptin, adiponectin, TNFα and others [40, 41]. Disturbances in the production of these factors may contribute to the development of insulin resistance or impaired insulin secretion in patients with type 2 diabetes. Type 2 diabetes mellitus with insulin resistance is accompanied by abnormal accumulation of triglyceride in the liver, high serum triglycerides and low HDL cholesterol [42, 43]. Interestingly the FFA and triglyceride levels in WT and *PARP1-/-* mice were not significantly altered indicating that the metabolic disorder was mainly affecting the glucose metabolism in the liver. The comparable levels for FFA and triglycerides in both genotypes, might be a consequence of increased CD36 levels in *PARP1-/-* cells. Interestingly, total cholesterol levels were increased in *PARP1*-/- *ApoE*-/- compared with *PARP1*+/+*ApoE*-/- mice [44]. The elevated levels were however not considered to be relevant for atherogenesis as *PARP1*-/- *ApoE*-/- mice exhibited less atherosclerosis [44].

White adipose tissue (WAT) has been recognized as an important endocrine organ secreting different hormone-like factors (adipokines) and cytokines, thereby regulating metabolism locally and systemically [45]. In obesity, excess adipose tissue accumulation is accompanied by local inflammation, characterized by infiltration of inflammatory cells [46] and by elevated production of proinflammatory cytokines, jointly activating inflammatory pathways in adipocytes. It is proposed that the consequent alteration in the composition of secreted products from adipocytes contributes to both local and systemic insulin resistance [47][48]. Particularly, liver insulin sensitivity can be impaired by obesity-induced alterations in adipokine secretion and by elevation in fat tissue–derived cytokines. Messenger RNA (mRNA) expression of proinflammatory cytokines including IL-6, TNFα, and IL-1 increases with increasing adiposity [49, 50]. While it is clear that obesity can induce inflammation in adipose tissue, it is possible that inflammation occurs in liver as well [51, 52]. Interestingly, we observed the increased expression of proinflammatory cytokines in WAT of *PARP1*-/- cells on ND, which was comparable to these mice on HFD. The increased cytokine expression very likely contributes to the insulin resistance observed in the liver of these mice.

NAD^+ is a potent activator and substrate of PARP1. Liver NAD^+ levels were increased by 33% by fasting and returned to control levels after refeeding [62]. These data suggest that increased NAD^+ concentration might contribute to the PARP1

activity under certain conditions. However NAD^+ levels were comparable in the tissues (e.g pancreas and spleen) isolated from WT and *PARP1-/-* mice suggesting that NAD^+ levels are rather unlikely to be the cause for T2D in *PARP1-/-* mice (personal communication).

Hepatic glucose production is tightly controlled *in vivo*. Upon binding of insulin to its receptor, tyrosine phosphorylation of IRS1 and 2 results in the recruitment of phosphatidylinositol-3-kinase (PI3K), which phosphorylates phosphatidylinositol biphosphate into phosphatidylinositol triphosphate (PIP3) [53-57]. PIP3 recruits to the membrane and activates the serine/threonine kinases PKD1 and PKB/Akt. The activation of this pathway mediates glycogen synthesis, via PKB/Akt inhibitory phosphorylation of glycogen synthase kinase 3 (GSK3), a kinase that negatively regulates glycogen synthase. It inhibits, via PKB/Akt-activation of Forkhead transcription factors, the transcription of key enzymes for gluconeogenesis: phosphoenolpyruvate carboxy-kinase (*PEPCK*) and glucose-6-phosphatase (*G6P*). Thus through activation of PI3K and PKB/Akt, and subsequent inactivation of GSK3 and activation of Forkhead transcription factors, insulin promotes storage of glucose as glycogen and inhibits glucose synthesis and glucose output.

The Forkhead box A2 transcription factor (Foxa2/HNF-3β) has been shown to be a key regulator of genes involved in the maintenance of glucose and lipid homeostasis in the liver [58]. It is constitutively inactivated in several hyperinsulinemic/obese mouse models, thereby enhancing their metabolic phenotypes. Foxa2 is activated under fasting conditions but is inhibited by insulin signaling via phosphatidylinositol 3-kinase/AKT in a phosphorylation-dependent manner, which results in its nuclear exclusion. The negative regulation of Forkhead transcription factors by nutritional or stress signals is not unique to Foxa2. In mammals, this regulation has also been described for Forkhead transcription Foxo1, 2 and 3 [59]. Recently, evidence was provided that PARP1 functions as a negative regulator of Foxo1 [60]. PARP1 interacts with and poly(ADP-ribosyl)ates Foxo1 protein. PARP1 represses Foxo1-mediated expression of cell cycle inhibitor p27Kip1 gene in an enzymatic independent manner. Furthermore, knockdown of PARP1 led to a decrease in cell proliferation in a manner dependent on Foxo1 function. Chromatin immunoprecipitation experiments confirmed that PARP-1 is recruited to the p27Kip1 gene promoter through a binding to Foxo1. These results suggest that PARP1 acts as a corepressor for Foxo1, which could play an important role in proper cell proliferation

by regulating p27Kip1 gene expression. Whether other Foxo1 target genes involved in metabolism are affected by PARP1 is currently not known. Genome-wide analyses of genes expressed in liver of *PARP1-/-* mice revealed the number of down-regulated genes was higher than that of the up-regulated genes [23]. The genes with altered expression in the livers were also ascribed to the metabolism. Recent transcriptomics studies related to type 2 diabetes mellitus have revealed changes in expression of a large number of metabolic genes in a variety of tissues. Interestingly, NAD^+ was also among the novel metabolites that they identified to change with altered glucose homeostasis. An algorithm based on the analysis of the promoter regions of the genes associated with reporter metabolites revealed a transcription factor regulatory network connecting several parts of metabolism. The identified transcription factors include members of the CREB, NRF1 and PPAR family, among others, and represent regulatory targets for further experimental analysis [61].

Taken together, the presented work sheds new light on the transcriptional control of gene involved in gluconeogenesis by PARP1.

Experimental Procedures

Animals and Animal Care

Wild type or *PARP1-/-* male C57BL/6 mice were fed a high fat diet consisting of 60% of calories from fat (S3282 Bioserv) starting at 6-8 weeks of age for 14weeks. Control mice were fed a standard diet consisting of 4.5% fat. Animals were housed in a specific pathogen-free facility with a 12-hour light/12-hour dark cycle and given free access to food and water. Animal experiments were performed according to the regulations of the Cantonal Veterinary Office (Zurich, Switzerland).

Serum Measurements

Serum insulin concentrations were measured by insulin ELISA kit (Mercodia Inc.). Blood glucose was measured by FreeStyle Lite glucometer (Abbott). Leptin concentration was measured by Milliplex Mouse Adipokine kit purchased from Millipore.

Glucose and Insulin Tolerance Tests

For glucose tolerance test, mice were fasted overnight (14 hours); glucose (2g/kg body weight) was injected intraperitoneally. For the insulin tolerance test mice were fasted for 3 hours. and then received human recombinant insulin (0.75U/kg, 1.2U/kg or 1.4U/kg body weight) intraperitoneally. Blood glucose concentrations were determined from tail using FreeStyle Lite glucometer (Abbott).

Insulin Signaling Analysis

Muscle, liver and WAT tissues were collected from mice in the basal state or 10 min or 20 min after an IP injection of insulin (0.75U/BW), and quickly frozen in liquid nitrogen. Frozen tissues were homogenized on ice in RIPA lysis buffer, grinded and rocked for 1 hr in cold room. 40 μg proteins were resolved by a 10% SDS-polyacrylamide gel electrophoresis and transferred to nitrocellulose membranes and analyzed by immunoblotting.

RNA Extraction and Real-time PCR Analysis

Mouse tissues were isolated, rinsed in Phosphate Buffered Saline (PBS), frozen in

liquid nitrogen and stored at –80° C until extraction. Total RNA was extracted from WAT using the RNeasy Lipid Tissue Kit (Qiagen) according to the manufacturer's instructions with the inclusion of a DNase digestion step. Total RNA from liver and muscle was extracted using the 'Total RNA isolation mini kit' (Macherey Nagel) with a DNase step. Equal amount of RNA from 5-8 mice were pooled and reverse-transcribed using the 'High-capacity cDNA reverse transcription kit' (Applied Biosystems). Real-time PCR was performed using the Rotor-Gene 3000 (Corbett Life Science, now Qiagen) and SYBR Green using the primers listed in table S1. Sequences of all primers were taken from [63]. *Cyclophilin* was chosen as the internal control for normalization after screening several candidate genes. Mean value ± SD from two technical replicates was calculated and blotted into graphs with GraphPad Prism (GraphPad Software Inc., San Diego, CA, USA). For qPCR with tissue samples, WT fed with ND was set as 1.

Indirect Calorimetry

For the assessment of energy expenditure (EE) and respiratory quotient (RQ), WT and *PARP1-/-* mice, fed either chow or high-fat diet (HF) were individually housed in plexiglas air-tight cages designed for open circuit calorimetry (AccuScan Inc., Columbus, OH, USA). Group sizes were: WT/chow (n=7), WT/HF (n=9), KO/chow (n=6), KO/HF (n=8). Using Integra ME 2.21 software (AccuScan, Inc.), oxygen and carbon dioxide levels in each chamber were measured for 30 seconds every 5 minutes. Based on these values, EE and RQ were calculated according to [64], and used to determine average hourly and light- and dark-phase EE and RQ. Data were collected for three 23-hour periods. Data from each animal was averaged over the three days to calculate representative values for each mouse used for statistical analysis. Two animals that lost significant amounts of body weight (more than 10% of initial weight) in the metabolic chambers were not included in the analysis.

All data are represented as mean ± SEM. Statistical significance of differences in EE and RQ measurements were tested using two-way ANOVA and Bonferroni's post-hoc test for individual comparisons. A p-value < 0.5 was considered statistically significant. The software in use was Prism Version 5.0a for Mac OS X (GraphPad Software Inc., San Diego, CA, USA).

ACKNOWLEDGEMENTS

We are grateful to Ines Mittner for FFA measurements (University of Zurich, Switzerland). This work was supported in part by Swiss National Science Foundation Grant 31-122421 (to S.E.) and the Kanton of Zurich (to M.O.H.).

FIGURE LEGENDS

Fig. 1. *PARP1*-/- Mice Develop Mature-Onset Obesity

(A) Body weight measured for WT and *PARP1-/-* mice fed with chow or HF diet during 14 weeks-period (n=7-9 in each group; t=0, mice 6-8 weeks old). **(B)** Representative images of mice from WT and *PARP1-/-* mice fed with chow or high fat (HF) diet. **(C)** Blood glucose levels of 12-14 weeks old mice were measured after 14 hr fasting. WT (black bar) and KO (white bar) mice fed with chow or HF diet as indicated. n = 7-9 mice per group.

Fig. 2. *PARP1*-/- Mice Display Increased Weight Gain and Decreased Energy Expenditure nn Chow Diet

(A) Leptin levels in serum from WT and *PARP1-/-* (KO) mice fed with chow or HF diet as indicated. n=7-9 mice per group. *, *p*-value<0.05. **(B)** Food intake was measured every day for 3 days for WT and *PARP1-/-* (KO) mice fed with chow or HF diet. n = 7-9 mice. **(C)** Energy expenditure was measured for three days as indicated**.** 23-hr Energy expenditure (left) and dark- and light-phase energy expenditure (middle,right) are shown. Energy expenditure was averaged over the light and dark phases and assessed using two-way ANOVA (factors: genotype x diet). Bonferroni's test detected an individual difference between WT and *PARP1-/-* (KO) in 23-hr Energy expenditure analysis (t= 3.49; *, *p*-value<0.05). **(D)** Respiratory quotient (RQ) measured for three days as indicated**.** 23-hr Respiratory quotient (left) and dark- and light-phase respiratory quotient (middle, right) are shown. Respiratory quotient was averaged over the light and dark phases and assessed using two-way ANOVA (factors: genotype x diet). No significant main effect of genotype on RQ for chow- or HF-fed mice (p = 0.46 and 0.62, respectively).

Fig. 3. *PARP1-/-* Mice Display Deteriorated Glucose Homeostasis

(A) Glucose tolerance test (GTT) measured after14 hr-fasting WT and *PARP1-/-* mice fed with chow (left panel) or HFD (right panel). Mice on chow diet were injected 2g glucose per body weight (BW), mice on HFD were injected 1.2g glucose per body weight. n = 7-9 mice per group, mean ±SE. **(B)** Serum insulin levels measured for mice during GTT shown in (A) at time points 0, 15 and 30 after injection. . n = 7-9 mice per group, mean ±SE. **(C)** Insulin tolerance test (ITT)

measured after 3 hr fasting WT and *PARP1-/-* mice fed with chow or HFD. Mice on chow diet were injected 1.2 U insulin per body weight, mice on HFD were injected 1.4U insulin per body weight n = 7-9 mice per group, mean ±SE. **(D)** Fed serum FFA and triglyceride levels from WT (black bar) and KO (white bar) mice fed with ND or HFD as indicated. n = 4-5 mice per group, mean ±SE.

Fig. 4. Obesity-Induced Inflammation Is Enhanced in *PARP1-/-* Mice on Chow

(A) qPCR analysis of expression of genes encoding IL-6, IP-10, MCP-1, TNF-α in WAT of WT (black bar) and KO (white bar) mice fed with chow or HFD as indicated. n = 5-6 mice, mean ±SD. **(B)** qPCR analysis of expression of the indicated genes in WAT of WT (black bar) and KO (white bar) mice fed with chow or HFD as indicated. n = 5-6 mice, mean ±SD.

Fig. 5. Insulin Regulated Gene Expression Is Affected in Liver

(A) Liver weight normalized with body weight was measured from WT and *PARP1-/-* mice fed with chow or HF diet as indicated. n = 6-8 for each group. **(B)** Immunoblot analysis from the liver extracts of WT and *PARP1-/-* mice fed with chow diet (c) or with HFD. 2 mice per group. **(C-E)** qPCR analysis of expression of the indicated genes in the liver of WT (black bar) and KO (white bar) mice fed with chow or HFD as indicated. n = 5-6 mice, mean ±SD.

Fig. 6. Young *PARP1-/-* Mice Preserve Insulin Signaling

(A) Glucose tolerance test (GTT) measured after 14 hr-fasting of 6 weeks old WT and KO mice fed with chow. Mice were IP-injected 2g glucose per BW. n = 5 mice per group, mean ±SE. **(B)** Insulin tolerance test (ITT) measured after 3 hr fasting of 9 weeks old WT and KO mice fed with chow. Mice were IP-injected with 0.75U insulin per BW. n = 5 mice per group, mean ±SE. **(C-E)** Mice fasted for 14 hr were IP-injected with 0.75U insulin per body weight. Lysates from muscle (C) liver (D) WAT (E) of WT or KO mice fed with chow were immunoblotted with indicated antibodies.

REFERENCES

1. Shulman, G.I., *Cellular mechanisms of insulin resistance.* J Clin Invest, 2000. **106**(2): p. 171-6.
2. Pehling, G., et al., *Abnormal meal carbohydrate disposition in insulin-dependent diabetes. Relative contributions of endogenous glucose production and initial splanchnic uptake and effect of intensive insulin therapy.* J Clin Invest, 1984. **74**(3): p. 985-91.
3. Muoio, D.M. and C.B. Newgard, *Mechanisms of disease: molecular and metabolic mechanisms of insulin resistance and beta-cell failure in type 2 diabetes.* Nat Rev Mol Cell Biol, 2008. **9**(3): p. 193-205.
4. Simpson, R.W., J.E. Shaw, and P.Z. Zimmet, *The prevention of type 2 diabetes--lifestyle change or pharmacotherapy? A challenge for the 21st century.* Diabetes Res Clin Pract, 2003. **59**(3): p. 165-80.
5. Saltiel, A.R. and C.R. Kahn, *Insulin signalling and the regulation of glucose and lipid metabolism.* Nature, 2001. **414**(6865): p. 799-806.
6. Kelley, D.E., et al., *Dysfunction of mitochondria in human skeletal muscle in type 2 diabetes.* Diabetes, 2002. **51**(10): p. 2944-50.
7. Mootha, V.K., et al., *PGC-1alpha-responsive genes involved in oxidative phosphorylation are coordinately downregulated in human diabetes.* Nat Genet, 2003. **34**(3): p. 267-73.
8. Patti, M.E., et al., *Coordinated reduction of genes of oxidative metabolism in humans with insulin resistance and diabetes: Potential role of PGC1 and NRF1.* Proc Natl Acad Sci USA, 2003. **100**(14): p. 8466-71.
9. Boden, G., *Fatty acids and insulin resistance.* Diabetes Care, 1996. **19**(4): p. 394-5.
10. Ueki, K., et al., *Central role of suppressors of cytokine signaling proteins in hepatic steatosis, insulin resistance, and the metabolic syndrome in the mouse.* Proc Natl Acad Sci USA, 2004. **101**(28): p. 10422-7.
11. Leclercq, I.A., et al., *Insulin resistance in hepatocytes and sinusoidal liver cells: mechanisms and consequences.* J Hepatol, 2007. **47**(1): p. 142-56.
12. Biddinger, S.B. and C.R. Kahn, *From* mice *to men: insights into the insulin resistance syndromes.* Annu Rev Physiol, 2006. **68**: p. 123-58.
13. Gross, D.N., A.P.J. van den Heuvel, and M.J. Birnbaum, *The role of FoxO in the regulation of metabolism.* Oncogene, 2008. **27**(16): p. 2320-36.
14. Li, X., et al., *Akt/PKB regulates hepatic metabolism by directly inhibiting PGC-1alpha transcription coactivator.* Nature, 2007. **447**(7147): p. 1012-6.
15. Hassa, P.O., et al., *Nuclear ADP-ribosylation reactions in mammalian cells: where are we today and where are we going?* Microbiol Mol Biol Rev, 2006. **70**(3): p. 789-829.
16. Hassa, P.O. and M.O. Hottiger, *The diverse biological roles of mammalian PARPS, a small but powerful family of poly-ADP-ribose polymerases.* Front Biosci, 2008. **13**: p. 3046-82.
17. Ju, B.-G., et al., *Activating the PARP-1 sensor component of the groucho/ TLE1 corepressor complex mediates a CaMKinase IIdelta-dependent neurogenic gene activation pathway.* Cell, 2004. **119**(6): p. 815-29.
18. Olabisi, O.A., et al., *Regulation of transcription factor NFAT by ADP-ribosylation.* Molecular and Cellular Biology, 2008. **28**(9): p. 2860-71.
19. Kanai, M., et al., *Inhibition of Crm1-p53 interaction and nuclear export of p53 by poly(ADP-ribosyl)ation.* Nat Cell Biol, 2007. **9**(10): p. 1175-83.

20. Hassa, P.O., et al., *The enzymatic and DNA binding activity of PARP-1 are not required for NF-kappa B coactivator function.* J Biol Chem, 2001. **276**(49): p. 45588-97.
21. Santilli, G., et al., *PARP co-activates B-MYB through enhanced phosphorylation at cyclin/cdk2 sites.* Oncogene, 2001. **20**(57): p. 8167-74.
22. Pavri, R., et al., *PARP-1 determines specificity in a retinoid signaling pathway via direct modulation of mediator.* Molecular Cell, 2005. **18**(1): p. 83-96.
23. Ogino, H., et al., *Loss of Parp-1 affects gene expression profile in a genome-wide manner in ES cells and liver cells.* BMC Genomics, 2007. **8**: p. 41.
24. Wang, Z.Q., et al., *Mice lacking ADPRT and poly(ADP-ribosyl)ation develop normally but are susceptible to skin disease.* Genes & Development, 1995. **9**(5): p. 509-20.
25. Piskunova, T.S., et al., *Deficiency in Poly(ADP-ribose) Polymerase-1 (PARP-1) Accelerates Aging and Spontaneous Carcinogenesis in Mice.* Curr Gerontol Geriatr Res, 2008: p. 754190.
26. Devalaraja-Narashimha, K. and B. Padanilam, *PARP-1 DEFICIENCY EXACERBATES DIET-INDUCED OBESITY IN MICE.* J Endocrinol, 2010.
27. Trayhurn, P., et al., *Hormonal and neuroendocrine regulation of energy balance--the role of leptin.* Arch Tierernahr, 1998. **51**(2-3): p. 177-85.
28. Schenk, S., M. Saberi, and J.M. Olefsky, *Insulin sensitivity: modulation by nutrients and inflammation.* J Clin Invest, 2008. **118**(9): p. 2992-3002.
29. Hotamisligil, G.S. and E. Erbay, *Nutrient sensing and inflammation in metabolic diseases.* Nat Rev Immunol, 2008. **8**(12): p. 923-34.
30. Xu, H., et al., *Chronic inflammation in fat plays a crucial role in the development of obesity-related insulin resistance.* J Clin Invest, 2003. **112**(12): p. 1821-30.
31. Weisberg, S.P., et al., *Obesity is associated with macrophage accumulation in adipose tissue.* J Clin Invest, 2003. **112**(12): p. 1796-808.
32. Solinas, G., et al., *JNK1 in hematopoietically derived cells contributes to diet-induced inflammation and insulin resistance without affecting obesity.* Cell Metabolism, 2007. **6**(5): p. 386-97.
33. Brockmann, G.A. and M.R. Bevova, *Using mouse models to dissect the genetics of obesity.* Trends Genet, 2002. **18**(7): p. 367-76.
34. Martinez-Botas, J., et al., *Absence of perilipin results in leanness and reverses obesity in Lepr(db/db)* mice. Nat Genet, 2000. **26**(4): p. 474-9.
35. Surwit, R.S., et al., *Differential effects of fat and sucrose on the development of obesity and diabetes in C57BL/6J and A/J* mice. Metab Clin Exp, 1995. **44**(5): p. 645-51.
36. Wei, P., et al., *Glomerular structural and functional changes in a high-fat diet mouse model of early-stage Type 2 diabetes.* Diabetologia, 2004. **47**(9): p. 1541-9.
37. Ishimori, N., et al., *Quantitative trait loci that determine plasma lipids and obesity in C57BL/6J and 129S1/SvImJ inbred* mice. J Lipid Res, 2004. **45**(9): p. 1624-32.
38. Saltiel, A.R., *New perspectives into the molecular pathogenesis and treatment of type 2 diabetes.* Cell, 2001. **104**(4): p. 517-29.
39. Boden, G. and G.I. Shulman, *Free fatty acids in obesity and type 2 diabetes: defining their role in the development of insulin resistance and beta-cell dysfunction.* Eur J Clin Invest, 2002. **32 Suppl 3**: p. 14-23.

40. Hotamisligil, G.S., N.S. Shargill, and B.M. Spiegelman, *Adipose expression of tumor necrosis factor-alpha: direct role in obesity-linked insulin resistance.* Science, 1993. **259**(5091): p. 87-91.
41. Havel, P.J., *Control of energy homeostasis and insulin action by adipocyte hormones: leptin, acylation stimulating protein, and adiponectin.* Curr Opin Lipidol, 2002. **13**(1): p. 51-9.
42. Postic, C. and J. Girard, *The role of the lipogenic pathway in the development of hepatic steatosis.* Diabetes Metab, 2008. **34**(6 Pt 2): p. 643-8.
43. Postic, C. and J. Girard, *Contribution of de novo fatty acid synthesis to hepatic steatosis and insulin resistance: lessons from genetically engineered* mice. J Clin Invest, 2008. **118**(3): p. 829-38.
44. von Lukowicz, T., et al., *PARP1 is required for adhesion molecule expression in atherogenesis.* Cardiovascular Research, 2008. **78**(1): p. 158-66.
45. Scherer, P.E., *Adipose tissue: from lipid storage compartment to endocrine organ.* Diabetes, 2006. **55**(6): p. 1537-45.
46. Wellen, K.E. and G.S. Hotamisligil, *Inflammation, stress, and diabetes.* J Clin Invest, 2005. **115**(5): p. 1111-9.
47. Park, S.-Y., et al., *Unraveling the temporal pattern of diet-induced insulin resistance in individual organs and cardiac dysfunction in C57BL/6* mice. Diabetes, 2005. **54**(12): p. 3530-40.
48. Zick, Y., *Ser/Thr phosphorylation of IRS proteins: a molecular basis for insulin resistance.* Science's STKE, 2005. **2005**(268): p. pe4.
49. Cai, D., et al., *Local and systemic insulin resistance resulting from hepatic activation of IKK-beta and NF-kappaB.* Nat Med, 2005. **11**(2): p. 183-90.
50. Xu, A., et al., *The fat-derived hormone adiponectin alleviates alcoholic and nonalcoholic fatty liver diseases in* mice. J Clin Invest, 2003. **112**(1): p. 91-100.
51. Schäffler, A., J. Schölmerich, and C. Büchler, *Mechanisms of disease: adipocytokines and visceral adipose tissue--emerging role in nonalcoholic fatty liver disease.* Nature clinical practice Gastroenterology & hepatology, 2005. **2**(6): p. 273-80.
52. Schwabe, R.F. and D.A. Brenner, *Mechanisms of Liver Injury. I. TNF-alpha-induced liver injury: role of IKK, JNK, and ROS pathways.* Am J Physiol Gastrointest Liver Physiol, 2006. **290**(4): p. G583-9.
53. Anderson, P.J., et al., *Factor analysis of the metabolic syndrome: obesity vs insulin resistance as the central abnormality.* Int J Obes Relat Metab Disord, 2001. **25**(12): p. 1782-8.
54. Bugianesi, E., A.J. Mccullough, and G. Marchesini, *Insulin resistance: a metabolic pathway to chronic liver disease.* Hepatology, 2005. **42**(5): p. 987-1000.
55. Hickman, I.J., et al., *Effect of weight reduction on liver histology and biochemistry in patients with chronic hepatitis C.* Gut, 2002. **51**(1): p. 89-94.
56. Taniguchi, C.M., K. Ueki, and R. Kahn, *Complementary roles of IRS-1 and IRS-2 in the hepatic regulation of metabolism.* J Clin Invest, 2005. **115**(3): p. 718-27.
57. Previs, S.F., et al., *Contrasting effects of IRS-1 versus IRS-2 gene disruption on carbohydrate and lipid metabolism in vivo.* J Biol Chem, 2000. **275**(50): p. 38990-4.
58. Howell, J.J. and M. Stoffel, *Nuclear export-independent inhibition of Foxa2 by insulin.* J Biol Chem, 2009. **284**(37): p. 24816-24.

59. Brunet, A., et al., *Akt promotes cell survival by phosphorylating and inhibiting a Forkhead transcription factor.* Cell, 1999. **96**(6): p. 857-68.
60. Sakamaki, J.-i., et al., *Regulation of FOXO1-mediated transcription and cell proliferation by PARP-1.* Biochem Biophys Res Commun, 2009. **382**(3): p. 497-502.
61. Zelezniak, A., et al., *Metabolic network topology reveals transcriptional regulatory signatures of type 2 diabetes.* PLoS Comput Biol, 2010. **6**(4): p. e1000729.
62. Rodgers, J.T., et al., *Nutrient control of glucose homeostasis through a complex of PGC-1alpha and SIRT1.* Nature, 2005. **434**(7029): p. 113-8.
63. Chiang, S.-H., et al., *The protein kinase IKKepsilon regulates energy balance in obese* mice. Cell, 2009. **138**(5): p. 961-75.
64. Weir, J.B., *New methods for calculating metabolic rate with special reference to protein metabolism. 1949.* Nutrition, 1990. **6**(3): p. 213-21.

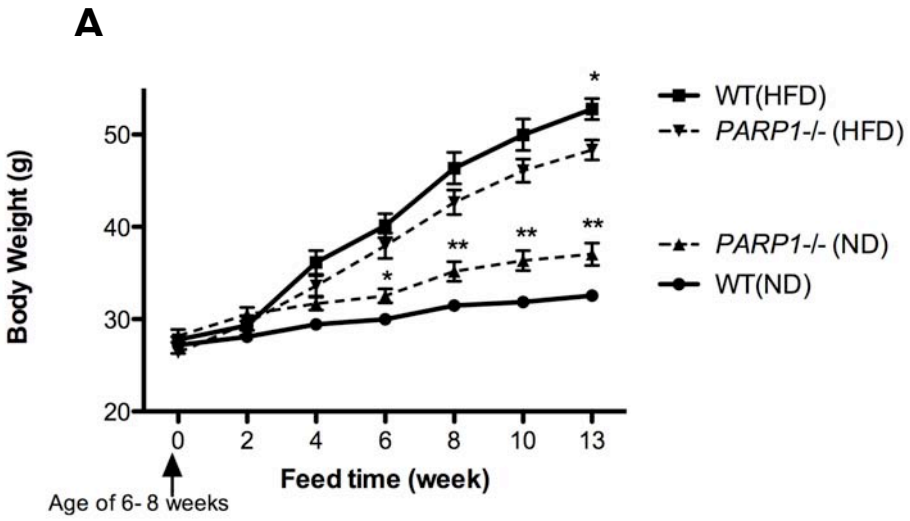

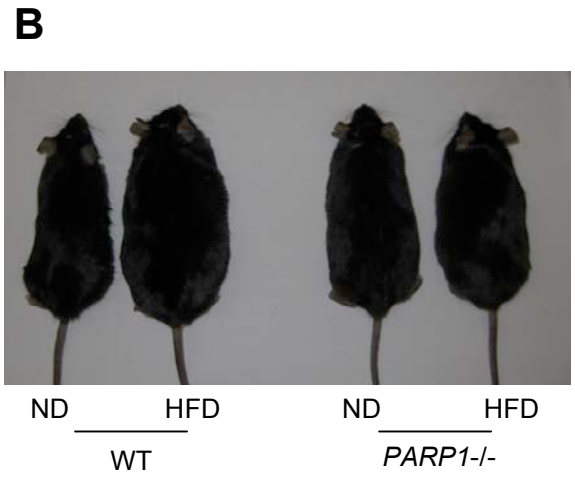

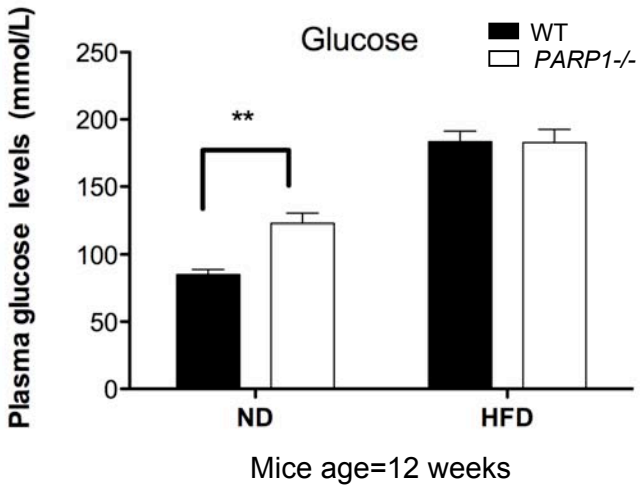

Mice age=12 weeks

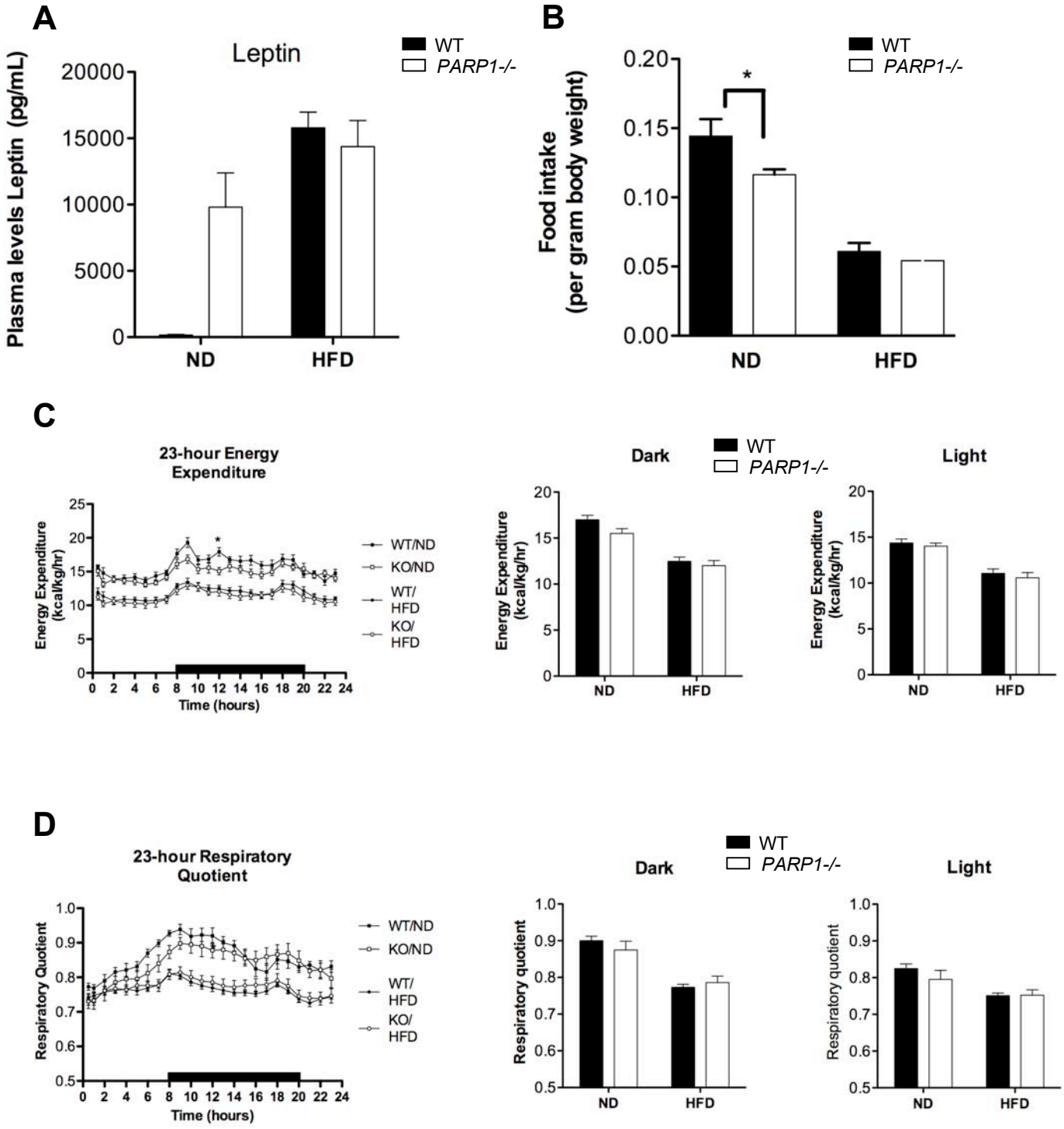
A
Leptin
WT
PARP1-/-
Plasma levels Leptin (pg/mL)
20000
15000
10000
5000
0
ND
HFD
B
WT
PARP1-/-
Food intake
(per gram body weight)
0.20
0.15
0.10
0.05
0.00
*
ND
HFD
C
23-hour Energy Expenditure
Energy Expenditure (kcal/kg/hr)
Time (hours)
WT/ND
KO/ND
WT/ HFD
KO/ HFD
Dark
Light
WT
PARP1-/-
ND
HFD
D
23-hour Respiratory Quotient
Respiratory Quotient
Time (hours)
WT/ND
KO/ND
WT/ HFD
KO/ HFD
Dark
Light
WT
PARP1-/-
Respiratory quotient
ND
HFD

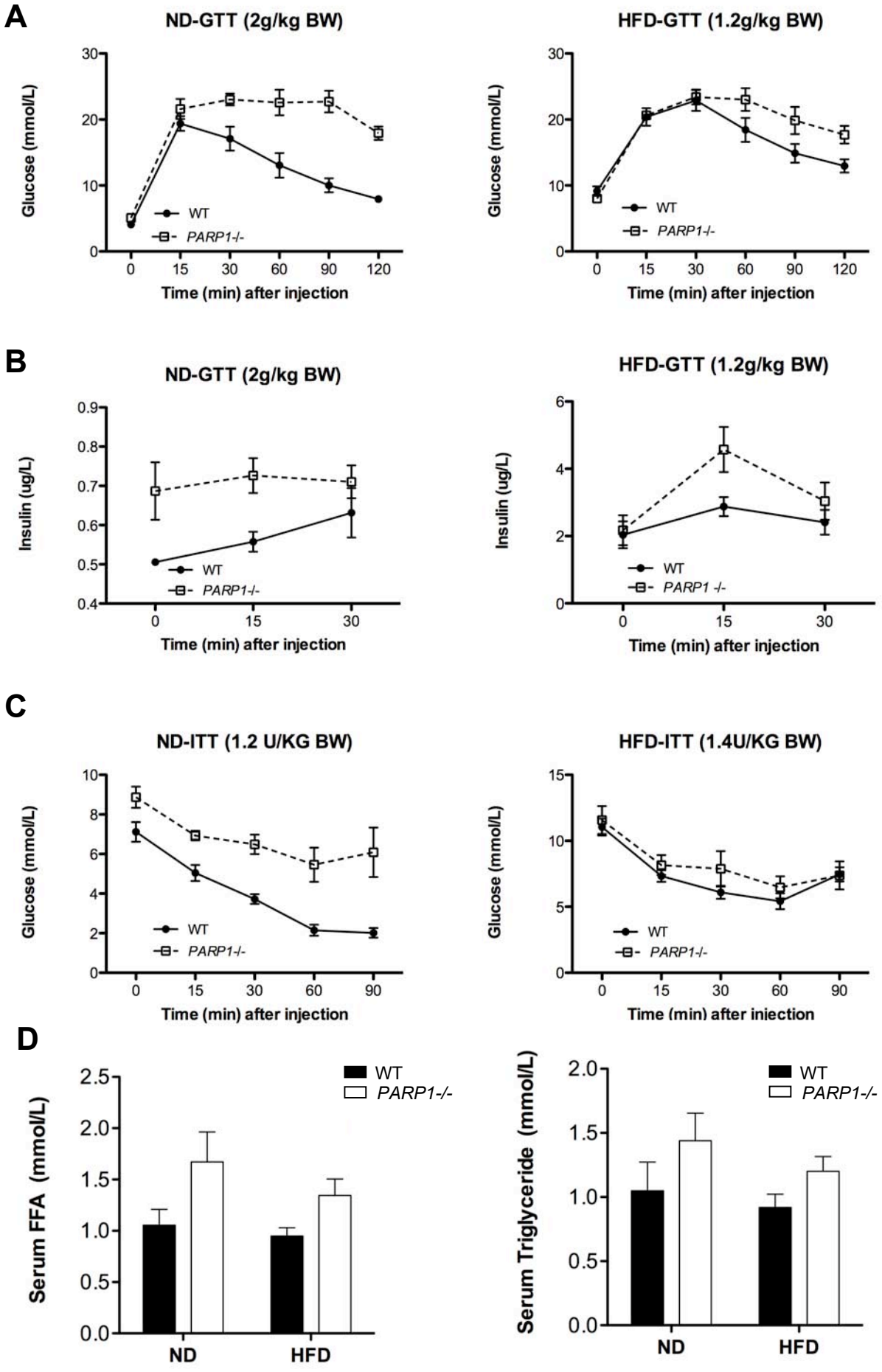
A
ND-GTT (2g/kg BW)
HFD-GTT (1.2g/kg BW)
Glucose (mmol/L)
WT
PARP1-/-
Time (min) after injection
B
ND-GTT (2g/kg BW)
HFD-GTT (1.2g/kg BW)
Insulin (ug/L)
PARP1 -/-
C
ND-ITT (1.2 U/KG BW)
HFD-ITT (1.4U/KG BW)
D
Serum FFA (mmol/L)
Serum Triglyceride (mmol/L)
ND
HFD

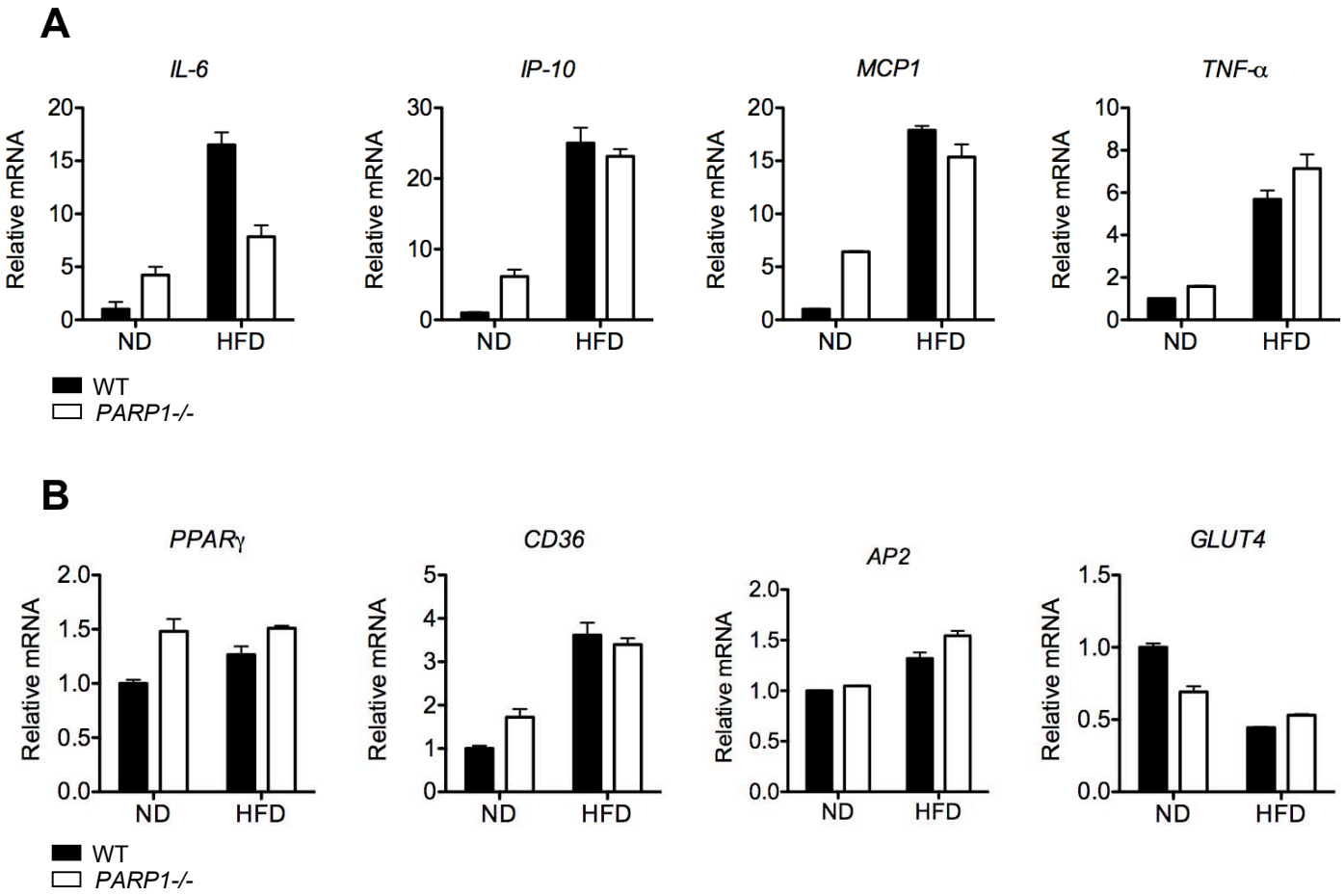
A
IL-6
IP-10
MCP1
TNF-α
Relative mRNA
ND
HFD
WT
PARP1-/-
B
PPARγ
CD36
AP2
GLUT4
Relative mRNA
ND
HFD
WT
PARP1-/-

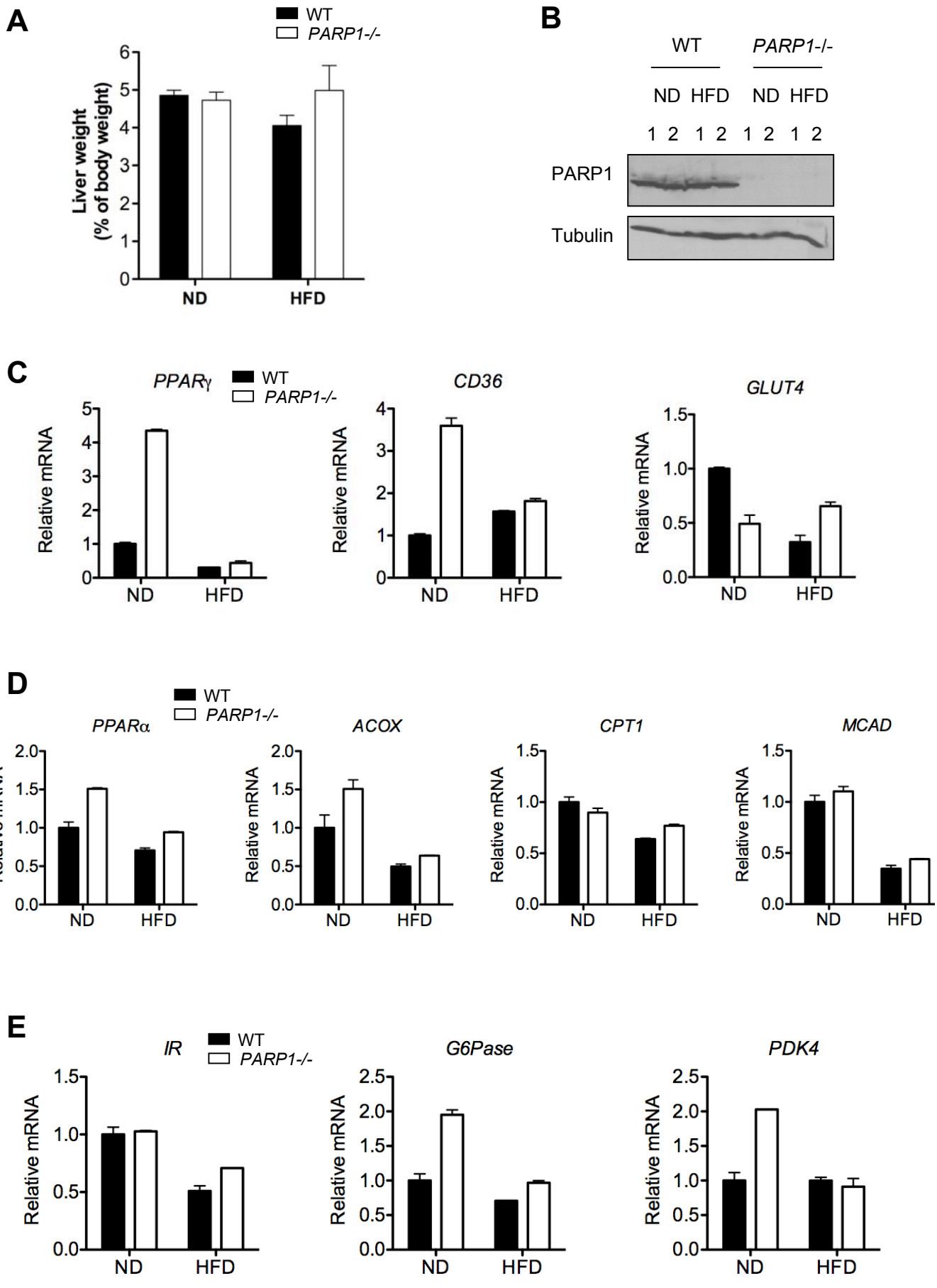
A
WT
PARP1-/-
Liver weight (% of body weight)
ND
HFD
B
WT
PARP1-/-
ND HFD ND HFD
1 2 1 2 1 2 1 2
PARP1
Tubulin
C
PPARγ
CD36
GLUT4
Relative mRNA
D
PPARα
ACOX
CPT1
MCAD
E
IR
G6Pase
PDK4

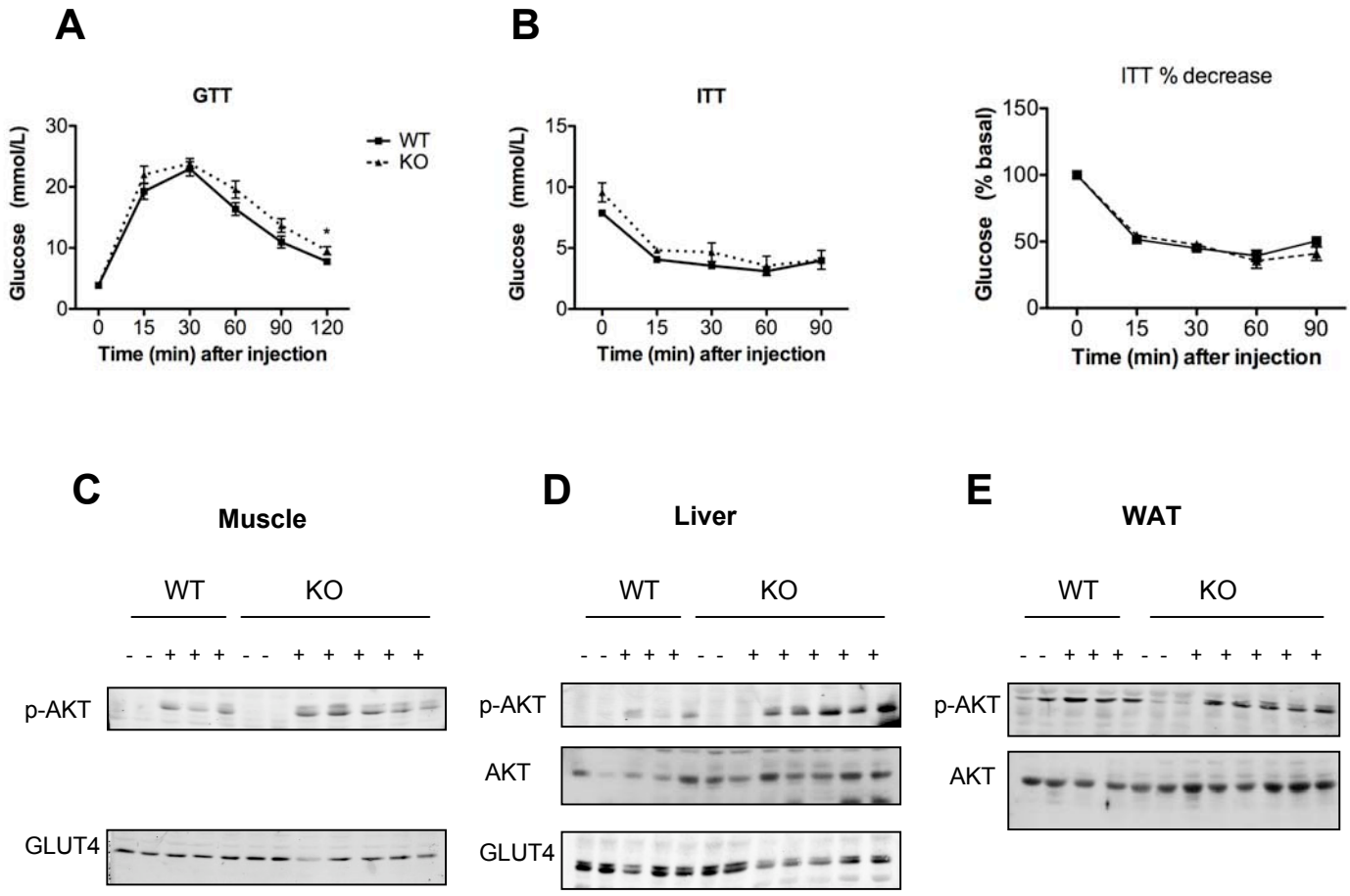
A
GTT
Glucose (mmol/L)
30
20
10
0
0 15 30 60 90 120
Time (min) after injection
WT
KO
*
B
ITT
Glucose (mmol/L)
15
10
5
0
0 15 30 60 90
Time (min) after injection
ITT % decrease
Glucose (% basal)
150
100
50
0
0 15 30 60 90
Time (min) after injection
C
Muscle
WT
KO
- - + + + - - + + + + +
p-AKT
GLUT4
D
Liver
WT
KO
- - + + + - - + + + + +
p-AKT
AKT
GLUT4
E
WAT
WT
KO
- - + + + - - + + + + +
p-AKT
AKT

SIRT2 regulates NF-κB-dependent gene expression through deacetylation of lysine 310

Karin M. Rothgiesser[1], Süheda Erener[1,2], Susanne Waibel[3],

Bernhard Lüscher[3] and Michael O. Hottiger[1]*

[1]Institute of Veterinary Biochemistry and Molecular Biology, University of Zurich

Winterthurerstrasse 190, 8057 Zurich, Switzerland

[2]Life Science Zurich Graduate School, Molecular Life Science Program, University of Zurich

[3] Institut für Biochemie und Molekularbiologie, Medical School, RWTH Aachen University, Pauwelsstrasse 30, 52074 Aachen, Germany

*Corresponding author:

Phone: +41-44-635 54 74, Fax: +41-44-635 68 40, E-mail: hottiger@vetbio.uzh.ch

Running title: SIRT2 is a NF-κB deacetylase

Summary

NF-κB regulates the expression of a large number of target genes involved in the immune and inflammatory response, apoptosis, cell proliferation, differentiation and survival. In this study, we identified SIRT2 as a novel deacetylase of p65. SIRT2 is a member of the family of sirtuins, which are NAD^+-dependent deacetylases involved in several cellular processes. SIRT2 interacts with p65 in the cytoplasm and deacetylates p65 *in vitro* and *in vivo* at lysine 310. Moreover, p65 is hyperacetylated at lysine 310 in *Sirt2*(-/-) cells after TNFα stimulation, which results in the increase in expression of a subset of p65 acetylation-dependent target genes. Together, our work provides evidence that p65 is deacetylated by SIRT2 in the cytoplasm to regulate the expression of specific NF-κB-dependent genes.

Keywords: NF-κB/ SIRT2/ acetylation/ p65/RelA/K310
Short title: Deacetylation of RelA by SIRT2

Introduction

Nuclear factor kappa B (NF-κB) belongs to a family of inducible transcription factors that modulates gene expression in response to a variety of extracellular and intracellular stimuli (Bonizzi et al., 2004; Hoffmann and Baltimore, 2006; Perkins, 2006). NF-κB plays a crucial role in the regulation of many genes involved in mammalian immune and inflammatory response, such as cytokines, cell adhesion molecules, complement factors, and a variety of immune receptors. It has additionally been implicated as an important regulator of cellular processes such as apoptosis, cell proliferation and differentiation. The mammalian NF-κB family includes five members, p65 (RelA), c-Rel, RelB, p105/p50 (NF-κB1) and p100/p52 (NF-κB2), encoded by *RELA*, *REL*, *RELB*, *NFKB1* and *NFKB2*, respectively (Hayden and Ghosh, 2008). These proteins form homo- or heterodimers. The most abundant heterodimer in the majority of cells consists of the two subunits p65 and p50.

In most unstimulated cells, NF-κB is sequestered in the cytoplasm as an inactive transcription factor complex through physical association with one of the inhibitors of NF-κB (IκB, predominantly IκBα). NF-κB induction involves the rapid activation of IKKβ- and NEMO-dependent phosphorylation and subsequent degradation of IκBs. Consequently, dissociation of IκBs from NF-κB unmasks the nuclear localization sequence (NLS) of p65, which leads to nuclear translocation and binding of NF-κB to specific κB consensus sequences in the chromatin, to regulate specific subsets of genes (Ghosh et al., 1998; Pahl, 1999). Interestingly, one consequence of NF-κB activation is the upregulation of IκBα gene expression, mediated by a κB consensus sequence within the IκBα promoter (Perez et al., 1995). Several lines of evidence suggest that newly synthesized IκBα enters the nucleus, displaces non-chromatin associated subunits of NF-κB, thereby mediating their export from the nucleus and re-establishing a cytoplasmic pool of inhibited complexes (Huang et al., 2000). Relocation of NF-κB into the cytoplasm and attenuation of NF-κB-mediated transcriptional activation therefore provides a feedback mechanism for modulating the extent and duration of inflammatory responses by cells. Nevertheless, if cells are continuously exposed to a specific stimulus, NF-κB translocates back to the nucleus after some time of the first wave of NF-κB induction to continue with transcriptional regulation of target genes (Hoffmann et al., 2002). The duration of the

NF-κB response depends at least in part on the stimulus applied and on the type of analyzed cell.

NF-κB specificity is regulated at different levels in the cell (Perkins et al., 1997). It is plausible that different stimuli induce distinct posttranslational modifications of p65, determining the outcome of p65-mediated transcriptional events. Several posttranslational modifications on p65 have been described, the most important ones being phosphorylation and acetylation (Perkins, 2006). Phosphorylation of p65 enhances its interaction with its transcriptional coactivator CBP/p300 and with components of the general transcription machinery (Zhong et al., 2002). Acetylation of p65 was reported to modulate its DNA-binding capacity, its transcriptional activity, its interaction with IκB proteins and its subcellular localization (Chen et al., 2001; Kiernan et al., 2003). We recently showed that p65 is acetylated by p300 not only at lysine 310 (K310), but also at K314 and 315, two novel acetylation sites, and that acetylation of K314 is important for late gene expression (Buerki et al., 2008; Rothgiesser et al., 2010). Microarray analysis of genetically complemented p65 knockout (-/-) cells treated with tumor necrosis factor α (TNFα) identified specific sets of genes differentially regulated by acetylation deficient mutants of p65 compared to wild type cells. Together, these results showed that site-specific p300-mediated acetylation of p65 regulate the specificity of NF-κB-dependent gene expression.

Reversible protein acetylation is an important posttranslational modification that regulates the function of histones and many other proteins (Sterner and Berger, 2000). Acetylation has a rapid turnover due to the highly dynamic equilibrium between two different groups of enzymes, histone acetyltransferases (HATs) and histone deacetylases (HDACs). The balance between these two activities is key to regulate the appropriate cellular response to signals. Mammalian HDACs are divided into four main classes based on sequence similarity and cofactor dependency (Class I-IV) (Yang and Seto, 2007). Class III HDACs, also known as sirtuins, constitute a special class of enzymes because of their requirement for NAD^+ as a cofactor in their deacetylation reaction. During the deacetylation reaction, nicotinamide (Nam) is cleaved from NAD^+ and the acetyl group of the substrate is then transferred to ADP ribose, generating the novel metabolite 2'-O-acetyl-ADP ribose (OAADPr) (Denu,

2003). The sirtuin family consists of seven members in mammals (SIRT1–7) that contain a conserved catalytic core domain comprised of approximately 275 amino acids. They regulate a variety of cellular functions, such as genome maintenance, longevity, and metabolism (Oberdoerffer and Sinclair, 2007; Westphal et al., 2007; Yamamoto et al., 2007). Up to date, all sirtuins have been described to have deacetylation activity except for SIRT4 (Taylor et al., 2008). The SIRTs exhibit differential localization from nucleus to nucleolus, and from cytoplasm to mitochondria (Sauve et al., 2006).

SIRT2 is the counterpart of yeast Hst2p, both proteins localize to the cytoplasm (Perrod et al., 2001). SIRT2 was found to bind HDAC6 and to deacetylate α-tubulin, thereby participating in the regulation of microtubule dynamics and possibly cell cycle progression (Dryden et al., 2003; North et al., 2003; Pandithage et al., 2008). Presumably, SIRT2 regulates other cellular functions, as p53, p300 and histones (H3 and H4) have been identified as substrates (Black et al., 2008; Heltweg et al., 2006; Vaquero et al., 2006). The apparent contradiction of a protein being cytoplasmically located, yet exhibiting specificity for a histone residue was resolved when SIRT2 localization was monitored during cell cycle progression. SIRT2 localized to the cytoplasm throughout the cell cycle with the exception of prophase during G2/M transition, where it translocated to the nucleus to deacetylate histone H4 at lysine 16 (H4K16) (Vaquero et al., 2006). Moreover, MEFs derived from *Sirt2*(-/-) mice showed hyperacetylation of H4K16 during mitosis (Vaquero et al., 2006). In addition, the dynamic analysis of the subcellular localization of SIRT2 revealed that this enzyme shuttles continuously between the cytoplasmic and nuclear compartments during interphase (North and Verdin, 2007).

Based on our recent findings, we extended our studies to further elucidate the molecular regulation of p65 acetylation. Here, we describe the characterization of SIRT2 as a novel deacetylase of p65. Furthermore, gene expression analysis in SIRT2-deficient MEFs indicate that SIRT2-mediated p65 deacetylation is implicated in transcriptional regulation of a subset of genes.

Results

Generation and verification of a specific antibody against acetylated p65 K310.

To further assess the functional relevance of p65 acetylation *in vivo,* we generated different antibodies raised against the acetylated K310. The selected antibody recognized specifically p65 acetylated *in vitro* and in cells by p300 at K310 (Fig. 1A and B). Furthermore, we investigated the kinetics of p65 acetylation in response to TNFα stimulation in cells. *p65*(-/-) MEFs stably complemented with p65 were stimulated for the indicated times (20 to 90 minutes). Western blot analysis of immunoprecipitated p65 from the nuclear fraction of the cells revealed that endogenous p65 predominantly translocated after 20 minutes of TNFα treatment into nucleus which correlated with its acetylation at K310 (Fig. 1C). The signal dramatically decreased after 45 minutes of stimulation and was no longer detectable after 90 minutes, which correlates with the reported cytoplasmic relocalization of p65 in MEFs after TNFα stimulation (Hoffmann et al., 2002). Together, these experiments revealed that p65 is acetylated at K310 in a TNFα-dependent manner, possibly upon translocation to the nucleus.

p65 is deacetylated by SIRT1 and SIRT2 at K310 *in vitro*.

The reversed acetylation of p65 prompted us to investigate which enzyme might be responsible for p65 deacetylation at K310. Here we focused on sirtuins. To elucidate which sirtuin can deacetylate p65 at K310, we purified (baculovirus expressed) recombinant SIRT1, 2, 6 and 7 that are known to localize either to the nucleus or to the cytoplasm (Fig. 2A). Recombinant purified p65 was acetylated *in vitro* by p300 and subsequently incubated with purified recombinant SIRT1, 2, 6 and 7, in the presence or absence of NAD^+. While SIRT2 was able to deacetylate p65 completely already after 30 minutes, as observed by western blot analysis using the anti-acK310 anbibody, SIRT1 was only able to do so after extended incubation (Fig. 2B and S1A). SIRT6 and 7 were not able to deacetylate p65 under the tested conditions.

p65 is deacetylated by SIRT2 at K310 *in vivo*.

Since SIRT1 has been previously reported to deacetylate p65 (Yeung et al., 2004), we decided to focus on SIRT2. To confirm that SIRT2 is able to deacetylate p65 also *in*

vivo, his-tagged SIRT2 and 6 or 7 (as negative controls) were overexpressed in HEK 293T cells (Fig. S1B), along with myc-tagged p65. Stimulation of transfected cells with TNFα for 30 minutes resulted in effective acetylation of p65 K310 (Fig. 2C, mock sample). Notably, overexpression of SIRT2 significantly reduced p65 acetylation at K310, while SIRT6 and SIRT7 were not able to deacetylate p65 under these conditions (Fig. 2C). Similarly overexpressing of class I HDACs HDAC1, 2 and 3 was insufficient to deacetylate K310 of p65 (Fig. S1C and D). To verify that the deacetylase activity of SIRT2 was necessary for p65 deacetylation, we overexpressed wt and a catalytically inactive mutant of SIRT2 (H187Y) together with p65 in HEK 293T cells (Fig. 2D). The enzymatic inactive SIRT2 mutant was, as expected, unable to deacetylate p65 at K310. These findings indicate that SIRT2 is capable to deacetylate K310 of p65 in cells.

TNFα stimulation does not induce nuclear translocation of SIRT2.

Next, we decided to investigate if SIRT2 translocates to the nucleus upon TNFα stimulation. Since endogenous SIRT2 could not be detected by immunofluorescence, we overexpressed HA-tagged SIRT2 in HeLa cells and stimulated the cells with TNFα for 30 or 90 minutes. Immunofluorescence studies revealed that overexpressed SIRT2 and endogenous p65 localized to the cytoplasm in untreated cells (Fig. 3A). After 30 minutes of TNFα stimulation, p65 translocated to the nucleus and relocated to the cytoplasm after 90 minutes, while SIRT2 stayed in the cytoplasm throughout the experiment, indicating that SIRT2 does not shuttle to the nucleus upon TNFα stimulation (Fig. 3A).

SIRT2 forms a complex with p65 in the cytoplasm, which is enhanced by TNFα stimulation.

To investigate whether endogenous SIRT2 and p65 would interact *in vivo*, p65 was immunoprecipitated from cytoplasmic or nuclear extracts of THP1 cells. Interestingly, SIRT2 coimmunoprecipitated with p65 in the cytoplasmic extracts under basal conditions, indicating that p65 forms a complex with SIRT2 in untreated cells (Fig. 3B). While TNFα stimulation induced p65 nuclear translocation, enhanced p65/SIRT2 complex formation was observed in the cytoplasmic fraction (Fig. 3B).

SIRT2 did not immunoprecipitate with nuclear p65, confirming that TNFα did not induce SIRT2 translocation.

SIRT2 deacetylates p65 at K310 in the cytoplasm.

To provide further evidence for the cytoplasm as the cellular compartment where SIRT2 deacetylates p65, HEK 293T cells were transfected with expression plasmids for different SIRT2 mutants containing an additional NLS or an NLS in combination with a NES deletion (NLSΔNES). While wild type SIRT2 was located exclusively in the cytoplasm, fusion of an NLS to SIRT2 slightly increased its nuclear localization (Fig. 3C). Complete nuclear localization of SIRT2 could be observed only upon additional deletion of the NES (NLSΔNES mutant). Importantly, analysis of the p65 acetylation status under these conditions revealed that the nuclear localization of SIRT2 negatively correlated with p65 deacetylation (Fig. 3D). The mutation of SIRT2 to achieve nuclear localization (SIRT2 NLSΔNES mutant) did not abolish its deacetylation activity, since it was able to efficiently deacetylate H4K16 in the nucleus (Fig. S2A and B). Collectively, these results suggest that SIRT2 interacts with and deacetylates p65 exclusively in the cytoplasm.

Hyperacetylation of p65 at K310 in *Sirt2*(-/-) cells.

To further investigate the role of SIRT2 in p65 deacetylation *in vivo*, *Sirt2*(-/-) and *Sirt2*(+/+) MEFs were stimulated with TNFα and acetylation of endogenous p65 was analyzed by western blot. The increase in acetylation of endogenous p65 at K310 upon TNFα stimulation was substantially larger in *Sirt2*(-/-) as compared to wild type MEFs (Fig. 4A). Protein levels of SIRT1 were not altered in the analyzed MEFs (Fig. 4B). Moreover, *Sirt1*(-/-) MEFs did not display hyperacetlyted p65 (Fig. S2A). Together, these results provide strong evidence that SIRT2 is the predominant enzyme involved in deacetylation of p65 at K310 after TNFα stimulation *in vivo*.

SIRT2 regulates NF-κB-dependent gene expression.

Since p65 acetylation influences NF-κB-dependent transcription, we decided to investigate whether depletion of SIRT2 affects the expression of NF-κB target genes upon TNFα stimulation *in vivo*. We analyzed the expression of *Mpa2l,* a gene

previously identified as NF-κB-dependent (Rothgiesser et al., 2010), that requires acetylation of p65 at K310 for its transcriptional activation (Fig. S2B). Gene expression analysis by real-time RT-PCR in *Sirt2*(+/+) and *Sirt2*(-/-) MEFs uncovered a dramatic increase in *Mpa2l* expression in *Sirt2*(-/-) cells compared to *Sirt2*(+/+) cells in response to TNFα (70 fold difference, Fig. 4C). The same was not observed for the control *RELA,* a gene that has neither been reported to be dependent on NF-κB nor to be a housekeeping gene (www.nf-kb.org) (Fig.4D). Moreover, knockdown of *p65* in *Sirt2*(-/-) cells reduced the induction of *Mpa2l* expression (Fig. S2C and D). Furthermore, transient knockdown of *Sirt2* with siRNA in MEFs enhanced *Mpa2l* expression as well, although not to the same extent (Fig. S2E and F). This correlated with our results showing that acetylation of p65 at K310 is required for transcriptional activation of *Mpa2l* (Fig. S2B) and that p65 is hyperacetylated in *Sirt2*(-/-) MEFs (Fig. 4A). Furthermore, these data imply that the expression of genes that are particularly dependent on K310 acetylation are strongly induced in *Sirt2*(-/-) cells, as observed for the strong *Mpa2l* induction *in vivo*.

Discussion

We have previously shown that p65 acetylation plays an important role in regulating NF-κB-dependent transcription for a subset of target genes. Here we report the identification of SIRT2 as a novel p65 deacetylase. SIRT2 deacetylates p65 *in vitro* and when overexpressed in cells after TNFα stimulation. Furthermore, endogenous p65 and SIRT2 interact in the cytoplasm of unstimulated cells. Subsequent TNFα treatment does not trigger SIRT2 translocation to the nucleus, but enhances complex formation with p65 after 30 to 60 minutes, thus indicating that it deacetylates p65 in the cytoplasm. Moreover, p65 is hyperacetylated at K310 in *Sirt2*(-/-) MEFs, which correlates with a strong increase in *Mpa2l* expression, a gene which is dependent on the acetylation of p65 at K310.

We observed that p65 was rapidly acetylated at K310 in the nucleus of MEFs upon TNFα stimulation and that the signal was drastically reduced after 45 minutes of TNFα treatment (Fig. 1C). Immunostaining and EMSA experiments have previously shown that the majority of NF-κB shuttles back to the cytoplasm between 30 to 60 minutes after TNFα stimulation in MEFs (Buerki et al., 2008; Hoffmann et al., 2002). Strikingly, the timing of p65 deacetylation at K310 correlates with its reported export to the cytoplasm, supporting the idea that p65 is deacetylated in the cytoplasm.

HDAC3 and SIRT1 have been previously described to deacetylate p65 (Chen et al., 2001; Yeung et al., 2004). However, we did not detect p65 deacetylation by overexpressed HDAC3 in HEK 293T cells. This discrepancy might be due to different experimental procedures, such as the use of HEK 293T cells instead of COS-7 cells. Deacetylation of K310 by SIRT1 was shown *in vitro* with recombinant proteins and in HEK 293T cells with overexpressed proteins, which correlates with our results but particularly the latter may be the consequence of overexpressing the proteins. Hyperacetylation of K310 upon TNFα stimulation in the *Sirt2,* but not *Sirt1*(-/-) MEFs suggests that SIRT2, but not SIRT1, is critical to deacetylate K310 of p65 in cells. Our experiments with *Sirt1*(-/-) cells are in agreement with observations where RNAi of SIRT1 did not lead to changes in NF-κB target gene expression, unless cells were treated with resveratrol (Yeung et al., 2004). These results suggest that SIRT1 and SIRT2 might function independently in p65 deacetylation and does not exclude that SIRT1 is relevant for the deacetylation of other lysines in p65. Recently, a study

showed that SIRT6 does not deacetylate p65 *in vitro* or *in vivo*, in agreement with our results (Fig. 2B and C), but deacetylates histone H3K9 to attenuate NF-κB signaling (Kawahara et al., 2009).

Gene expression analysis of *Sirt2*(-/-) MEFs revealed that transcriptional activation of *Mpa2l,* whose expression was dependent on p65 acetylation at K310 (Fig. S2A), was dramatically increased in *Sirt2*(-/-) cells compared to another gene, *RELA*, whose expression does not depend on K310 acetylation (Fig. 4D). Therefore, we propose that SIRT2 regulates the expression of a subset of NF-κB-dependent genes by deacetylating p65 at K310 in the cytoplasm upon relocation of NF-κB to this cellular compartment after the first wave of NF-κB induction. Since NF-κB is known to shuttle between nucleus and cytoplasm in 30-60 minutes periods in MEFs upon continuous TNFα stimulation (Hoffmann et al., 2002), p65 would be hyperacetylated in *Sirt2*(-/-) cells after 3 hours of TNFα treatment, which would explain the observed differential *Mpa2l* gene regulation.

Despite the identification of p65 acetylation, the exact mechanism by which p65 K310 acetylation regulates the expression remains to be further elucidated. Huang *et al.* reported that double bromodomain of Brd4 binds to acetylated K310, which enhances transcriptional activation of NF-κB and the expression of a subset of NF-κB inflammatory genes in an acetylated K310-dependent manner (Huang et al., 2008).

Our data suggest that in unstimulated cells, SIRT2 exists in a complex with p65. Upon TNFα stimulation, p65 translocates to the nucleus, while SIRT2 stays in the cytoplasm. Co-activator p300 binds to nuclear p65 and acetylates it at K310, 314 and 315 to fine tune gene expression. Once the NF-κB response is terminated, p65 shuttles back to the cytoplasm, where SIRT2 deacetylates p65 at K310, thereby resetting the whole NF-κB response. Any p65 that would afterwards translocate to the nucleus again during continuous TNFα stimulation would have to be freshly acetylated by p300 to modulate gene expression, thereby allowing a tight control of NF-κB-dependent transcription.

Together, our results identify SIRT2 as a novel deacetylase of NF-κB and an important regulator of TNFα-induced NF-κB-dependent gene expression.

Materials and methods

Tissue culture

Complemented *p65*(-/-) NIH 3T3 mouse embryonic fibroblasts (MEFs) stably expressing p65 wild type or the acetylation-deficient mutants were previously described in (Buerki et al., 2008). They were maintained in DMEM supplemented with 10% FCS, 100 units/ml penicillin/streptomycin (Gibco) and non-essential amino acids (Gibco). *Sirt2*(-/-) and (+/+) MEFs were a generous gift from A. Vaquero. Those cells were originally generated in the lab of F. Alt (Vaquero et al., 2006). *Sirt1*(-/-) and (+/+) MEFs were kindly provided by F. Alt (Cheng et al., 2003). *Sirt1*(-/-) , *Sirt1*(+/+), *Sirt2*(-/-) and *Sirt2*(+/+) MEFs were kept in DMEM supplemented with 15% FCS, 100 units/ml penicillin/streptomycin (Gibco), non-essential amino acids (Gibco), β-mercaptoethanol (Gibco) and Na-Pyruvate (Gibco). HEK 293T and HeLa cells were maintained in DMEM supplemented with 10% FCS and 100 units/ml penicillin/streptomycin. THP1 cells were maintained in RPMI medium containing 10% FCS, 100 units/ml penicillin/streptomycin (Gibco), non-essential amino acids (Gibco), β-mercaptoethanol (Gibco) and Na-Pyruvate (Gibco).

Plasmids

Plasmids for the mammalian expression of human p65 wild type and mutants K310R, K314/315R and KTR were described elsewhere (Buerki et al., 2008). Mammalian expression plasmids of human SIRT1, 2, 6 and 7 in the pcDNA-DEST40-V5/HIS background were kindly provided by I. Horikama (Michishita et al., 2005). The enzymatic inactive mutant was generated by site-directed mutagenesis of H187 to Y with pcDNA-DEST40-SIRT2 as template. The introduced mutation was verified by DNA sequencing. Plasmids for the expression of HA-tagged SIRT2 and HA vector control were described elsewhere (Pandithage et al., 2008). The GW-pHA-SIRT2-NLS vector was created by cloning the sequence 5'-GATCCCCAAAGAAGAAGCGAAAGGTAC into GW-pHA-SIRT2. Site-directed mutagenesis was performed to change the SIRT2 K4 and K12 to alanines, creating the GW-pHA-SIRT2-NLSΔNES vector. The introduced sequence and mutations were verified by DNA sequencing.

Reagents and antibodies

Human tumor necrosis alpha (TNFα), Trichostatin A (TSA), Nicotinamide (Nam) and acetyl-Coenzyme A (acetyl Co-A) were purchased from Sigma. Recombinant mouse TNFα was either purchased from Sigma or generated in our laboratory. Sodium fluorid (NaF) and beta-glycerophosphate were obtained from Fluka. The acetyl-specific antibodies for p65 anti-acetyl K310 (ab19870) was generated by Abcam. The following antibodies were purchased from Santa Cruz Biotechnologies: anti-p65 (sc-372), anti-p300 (sc-585) and anti-SIRT2 (sc-20966 and sc-28298). The anti-SIRT1 antibody was from Millipore (07-131). The anti-myc antibodies were either purchased from Roche (11-667-149-001) or purified from hybridoma cells. The anti-tubulin antibody was purchased from Sigma (T 6199), the anti-his was from Qiagen (34670) and the anti-HA was from Covance (MMS-101P).

Generation of recombinant proteins

The recombinant proteins were expressed by baculovirus in Sf21 cells using either the FastBac or the BacPAK systems (Clontech). His-tagged proteins were purified over Ni^{2+}-beads (ProBond, Invitrogen) and GST-tagged proteins over L-Glutathione beads (Sigma).

***In vitro* acetylation assay**

1 μg of recombinant p65 wild type or the acetylation-deficient mutants were incubated with 500 ng recombinant p300 in HAT buffer (50 mM Tris HCl pH8, 100 mM NaCl, 10% glycerol, 1mM PMSF, 1mM DTT, 1 μg/ml bepstatin, 1 μg/ml leupeptin, 1 μg/ml pepstatin and 1 mM sodium butyrate) with or without addition of 150 μM acetyl-CoA. After 1 hour at 30°C, samples were resolved on SDS-PAGE and analyzed by western blot.

***In vitro* deacetylation assay**

500 ng recombinant p65 wild type was *in vitro* acetylated as described previously and then immunoprecipitated. The beads-bound p65 was incubated with 14 pmol of each recombinant SIRT in 100 μl deacetylation buffer (50 mM Tris HCl pH9, 4 mM $MgCl_2$, 0.2 mM DTT, 1 μg/ml bepstatin, 1 μg/ml leupeptin and 1 μg/ml pepstatin)

supplemented or not with 1 mM NAD^+ for 30 minutes or 2 hours with constant agitation. Proteins were subsequently resolved in SDS-PAGE and analyzed by western blot. Purified recombinant SIRTs were additionally resolved on SDS-PAGE and stained with coomassie blue.

Acetylation and deacetylation assays in cells

HEK 293T cells were transfected with expression plasmids for p300 and either myc-tagged p65 wild type, the acetylation-deficient mutants or an empty vector, using the calcium phosphate precipitation method. After 23 hours, cells were treated with 10 ng/ml human TNFα for 30 minutes. Then, whole cell extracts were prepared and 40 μg protein was analyzed by SDS-PAGE and western blot. For the deacetylation assay in cells, 0.1 pmol expression plasmid encoding the different sirtuins (wild type or mutants) or empty vector were additionally co-transfected in HEK 293T cells.

Immunostaining

Transfected HEK 293T cells or HeLa cells were stimulated with 10 ng/ml human TNFα for 30 minutes. They were fixed with 4% paraformaldehyde and then permeabilized with 0.2% TritonX-100. Blocking solution (2% BSA and 0.1% TritonX-100 in PBS) was added for 1 hour before the slides were incubated with anti-HA and anti-p65 antibodies (1:250 each in blocking solution), followed by incubation with FITC-labeled anti-mouse and Cy3-labeled anti-rabbit antibodies (1:250 each in blocking solution, Jackson Immunology). The slides were washed, covered with Vectashield mounting solution (Vector laboratories) and visualized using a Leica SP 5 confocal microscope.

Nuclear and cytoplasmic extract preparation and immunoprecipitation

THP1 cells were stimulated with 10 ng/ml TNFα for the indicated time periods, harvested, washed once with PBS, and washed three times in buffer A (10 mM HEPES KOH pH7.9, 1.5mM $MgCl_2$, 10 mM KCl, 1μg/ml pepstatin, 1μg/ml bestatin, 1μg/ml leupeptin, 2mM PMSF, 5mM DTT). Cells were lysed with A+ buffer (Buffer A+ 0.05 % NP-40) and centrifuged for 5 minutes at 5000 rpm. Supernatant corresponding to cytoplasm was saved and kept on ice till the nuclear fraction was

ready. Pellet was washed three times with buffer A and subsequently resuspended in three volumes of Buffer C (20 mM HEPES KOH pH7.9, 0.42 M NaCl 1.5 mM $MgCl_2$, 25% v/v glycerol, 1μg/ml pepstatin, 1μg/ml bestatin, 1μg/ml leupeptin, 2 mM PMSF, 5 mM DTT) and incubated for 15`at 4°C on rotating wheels. Lysate was centrifuged for 10 minutes at 4°C at 14000 rpm and the supernatant corresponding to nuclear extract was seperated for immunoprecipitation.150 μg nuclear extracts or 450 μg cytoplasmic extracts were mixed with IP buffer (20mM HEPES KOH pH 7.9, 2.5mM $MgCl_2$, 0.1/ NP-40, 50mM NaCl, 1μg/ml pepstatin, 1μg/ml bestatin, 1μg/ml leupeptin, 2mM PMSF) in a final of 120mM NaCl concentration, 2.5 % of the mix was saved for the input analysis. p65 antibody was added and incubated for 2 hours at 4°C on a roller. At the end of the incubation, prewashed protein G beads were added to the mix for another 2 hours. Finally, beads were washed three times with IP buffer containing 120 mM NaCl. Beads and the inputs were added Laemmli buffer, boiled and resolved on SDS-PAGE and subjected to western blot using different antibodies.

Gene expression by real-time RT-PCR

Complemented MEFs were starved overnight before treatment with 30 ng/ml recombinant TNFα for different time points. *Sirt2*(+/+) and *Sirt2*(-/-) MEFs were starved for 6 hours and then stimulated with 30 ng/ml recombinant TNFα for 3 hours or left unstimulated. Total RNA was isolated from at least two biological samples at different days with the 'Total RNA isolation mini kit' (Agilent Technologies). RNA was subsequently retro-transcribed using the 'High-capacity cDNA reverse transcription kit' (Applied Biosystems). Real-time PCR was performed using the Rotor-Gene 3000 (Corbett Life Science, now Qiagen) and TaqMan assays from Applied Biosystems for *Mpa2l, Mmp13, Rps6* and *CanX* genes. The last two genes were used as internal controls to normalize for RNA input. In addition, gene expression of *Mpa2l, Mmp13, RELA* and *Rps12* (as internal control) was assessed with SYBR Green using the following primers: Mpa2l_forward (GATGCTGAAGAAGCTAATGAAGG ATC), Mpa2l_reverse (CCTTGATGACATCTCTCAGTTGCTG), Mmp13_forward (GGACAAGCAGTTCCAAAGGCTACA) and Mmp13_reverse (GTCTTCATCGCCTG GACCATAAAG). RNA from at least two biological

replicates per sample was measured and analyzed with REST (Pfaffl et al., 2002). Each experiment was run three independent times, the mean value and ± SD was calculated and blotted into graphs.

Transient Transfections

MEF cells were seeded on 6-well tissue culture plates and next day transfected with 30 pmol siRNA oligos (Qiagen) with 4 µl Lipofectamine RNAimax reagent (Invitrogen) according to manufacturer`s protocol for two days.

Acknowledgements

We thank F. Alt, A. Vaquero, K. Chua and I. Horikama for providing useful tools. We are also grateful to all the members of the Institute of Veterinary Biochemistry and Molecular Biology (University of Zurich, Switzerland) for helpful advice and discussions. This work was supported by the IZKF Aachen (to B.L.) and in part by Swiss National Science Foundation Grant 31-109315 and 31-122421 (to K.R. and S.E.) and the Kanton of Zurich (to M.O.H.).

Author contributions:

KR and SE performed experiments; SW generated useful tools; KR analyzed gene expression data and drafted the manuscript; BL and MOH designed and supervised the study. KR, SE and MOH wrote the manuscript.

References

Black, J. C., Mosley, A., Kitada, T., Washburn, M. and Carey, M. (2008). The SIRT2 deacetylase regulates autoacetylation of p300. *Mol Cell* **32**, 449-55.

Bonizzi, G., Bebien, M., Otero, D. C., Johnson-Vroom, K. E., Cao, Y., Vu, D., Jegga, A. G., Aronow, B. J., Ghosh, G., Rickert, R. C. et al. (2004). Activation of IKKalpha target genes depends on recognition of specific kappaB binding sites by RelB:p52 dimers. *EMBO J* **23**, 4202-10.

Buerki, C., Rothgiesser, K. M., Valovka, T., Owen, H. R., Rehrauer, H., Fey, M., Lane, W. S. and Hottiger, M. O. (2008). Functional relevance of novel p300-mediated lysine 314 and 315 acetylation of RelA/p65. *Nucleic Acids Res* **36**, 1665-80.

Chen, L., Fischle, W., Verdin, E. and Greene, W. C. (2001). Duration of nuclear NF-kappaB action regulated by reversible acetylation. *Science* **293**, 1653-7.

Cheng, H. L., Mostoslavsky, R., Saito, S., Manis, J. P., Gu, Y., Patel, P., Bronson, R., Appella, E., Alt, F. W. and Chua, K. F. (2003). Developmental defects and p53 hyperacetylation in Sir2 homolog (SIRT1)-deficient mice. *Proc Natl Acad Sci U S A* **100**, 10794-9.

Denu, J. M. (2003). Linking chromatin function with metabolic networks: Sir2 family of NAD(+)-dependent deacetylases. *Trends Biochem Sci* **28**, 41-8.

Dryden, S. C., Nahhas, F. A., Nowak, J. E., Goustin, A. S. and Tainsky, M. A. (2003). Role for human SIRT2 NAD-dependent deacetylase activity in control of mitotic exit in the cell cycle. *Mol Cell Biol* **23**, 3173-85.

Ghosh, S., May, M. J. and Kopp, E. B. (1998). NF-kappa B and Rel proteins: evolutionarily conserved mediators of immune responses. *Annu Rev Immunol* **16**, 225-60.

Hayden, M. S. and Ghosh, S. (2008). Shared principles in NF-kappaB signaling. *Cell* **132**, 344-62.

Heltweg, B., Gatbonton, T., Schuler, A. D., Posakony, J., Li, H., Goehle, S., Kollipara, R., Depinho, R. A., Gu, Y., Simon, J. A. et al. (2006). Antitumor activity of a small-molecule inhibitor of human silent information regulator 2 enzymes. *Cancer Res* **66**, 4368-77.

Hoffmann, A. and Baltimore, D. (2006). Circuitry of nuclear factor kappaB signaling. *Immunol Rev* **210**, 171-86.

Hoffmann, A., Levchenko, A., Scott, M. L. and Baltimore, D. (2002). The IkappaB-NF-kappaB signaling module: temporal control and selective gene activation. *Science* **298**, 1241-5.

Huang, B., Yang, X., Zhou, M. M., Ozato, K. and Chen, L. F. (2008). Brd4 Coactivates Transcriptional Activation of NF-{kappa}B Via Specific Binding to Acetylated RelA. *Mol Cell Biol*.

Huang, T. T., Kudo, N., Yoshida, M. and Miyamoto, S. (2000). A nuclear export signal in the N-terminal regulatory domain of IkappaBalpha controls cytoplasmic localization of inactive NF-kappaB/IkappaBalpha complexes. *Proc Natl Acad Sci U S A* **97**, 1014-9.

Kawahara, T. L., Michishita, E., Adler, A. S., Damian, M., Berber, E., Lin, M., McCord, R. A., Ongaigui, K. C., Boxer, L. D., Chang, H. Y. et al. (2009). SIRT6 links histone H3 lysine 9 deacetylation to NF-kappaB-dependent gene expression and organismal life span. *Cell* **136**, 62-74.

Kiernan, R., Bres, V., Ng, R. W., Coudart, M. P., El Messaoudi, S., Sardet, C., Jin, D. Y., Emiliani, S. and Benkirane, M. (2003). Post-activation turn-off of NF-kappa B-dependent transcription is regulated by acetylation of p65. *J Biol Chem* **278**, 2758-66.

Michishita, E., Park, J. Y., Burneskis, J. M., Barrett, J. C. and Horikawa, I. (2005). Evolutionarily conserved and nonconserved cellular localizations and functions of human SIRT proteins. *Mol Biol Cell* **16**, 4623-35.

North, B. J., Marshall, B. L., Borra, M. T., Denu, J. M. and Verdin, E. (2003). The human Sir2 ortholog, SIRT2, is an NAD+-dependent tubulin deacetylase. *Mol Cell* **11**, 437-44.

North, B. J. and Verdin, E. (2007). Interphase nucleo-cytoplasmic shuttling and localization of SIRT2 during mitosis. *PLoS One* **2**, e784.

Oberdoerffer, P. and Sinclair, D. A. (2007). The role of nuclear architecture in genomic instability and ageing. *Nat Rev Mol Cell Biol* **8**, 692-702.

Pahl, H. L. (1999). Activators and target genes of Rel/NF-kappaB transcription factors. *Oncogene* **18**, 6853-66.

Pandithage, R., Lilischkis, R., Harting, K., Wolf, A., Jedamzik, B., Luscher-Firzlaff, J., Vervoorts, J., Lasonder, E., Kremmer, E., Knoll, B. et al. (2008). The regulation of SIRT2 function by cyclin-dependent kinases affects cell motility. *J Cell Biol* **180**, 915-29.

Perez, P., Lira, S. A. and Bravo, R. (1995). Overexpression of RelA in transgenic mouse thymocytes: specific increase in levels of the inhibitor protein I kappa B alpha. *Mol Cell Biol* **15**, 3523-30.

Perkins, N. D. (2006). Post-translational modifications regulating the activity and function of the nuclear factor kappa B pathway. *Oncogene* **25**, 6717-30.

Perkins, N. D., Felzien, L. K., Betts, J. C., Leung, K., Beach, D. H. and Nabel, G. J. (1997). Regulation of NF-kappaB by cyclin-dependent kinases associated with the p300 coactivator. *Science* **275**, 523-7.

Perrod, S., Cockell, M. M., Laroche, T., Renauld, H., Ducrest, A. L., Bonnard, C. and Gasser, S. M. (2001). A cytosolic NAD-dependent deacetylase, Hst2p, can modulate nucleolar and telomeric silencing in yeast. *EMBO J* **20**, 197-209.

Pfaffl, M. W., Horgan, G. W. and Dempfle, L. (2002). Relative expression software tool (REST) for group-wise comparison and statistical analysis of relative expression results in real-time PCR. *Nucleic Acids Res* **30**, e36.

Rothgiesser, K. M., Fey, M. and Hottiger, M. O. (2010). Acetylation of p65 at lysine 314 is important for late NF-kappaB-dependent gene expression. *BMC Genomics* **11**, 22.

Sauve, A. A., Wolberger, C., Schramm, V. L. and Boeke, J. D. (2006). The biochemistry of sirtuins. *Annu Rev Biochem* **75**, 435-65.

Sterner, D. E. and Berger, S. L. (2000). Acetylation of histones and transcription-related factors. *Microbiol Mol Biol Rev* **64**, 435-59.

Taylor, D. M., Maxwell, M. M., Luthi-Carter, R. and Kazantsev, A. G. (2008). Biological and potential therapeutic roles of sirtuin deacetylases. *Cell Mol Life Sci* **65**, 4000-18.

Vaquero, A., Scher, M. B., Lee, D. H., Sutton, A., Cheng, H. L., Alt, F. W., Serrano, L., Sternglanz, R. and Reinberg, D. (2006). SirT2 is a histone deacetylase with preference for histone H4 Lys 16 during mitosis. *Genes Dev* **20**, 1256-61.

Westphal, C. H., Dipp, M. A. and Guarente, L. (2007). A therapeutic role for sirtuins in diseases of aging? *Trends Biochem Sci* **32**, 555-60.

Yamamoto, H., Schoonjans, K. and Auwerx, J. (2007). Sirtuin functions in health and disease. *Mol Endocrinol* **21**, 1745-55.
Yang, X. J. and Seto, E. (2007). HATs and HDACs: from structure, function and regulation to novel strategies for therapy and prevention. *Oncogene* **26**, 5310-8.
Yeung, F., Hoberg, J. E., Ramsey, C. S., Keller, M. D., Jones, D. R., Frye, R. A. and Mayo, M. W. (2004). Modulation of NF-kappaB-dependent transcription and cell survival by the SIRT1 deacetylase. *EMBO J* **23**, 2369-80.
Zhong, H., May, M. J., Jimi, E. and Ghosh, S. (2002). The phosphorylation status of nuclear NF-kappa B determines its association with CBP/p300 or HDAC-1. *Mol Cell* **9**, 625-36.

Figure legends

Figure 1. Kinetics of p65 K310 acetylation upon TNFα stimulation. (**A-B)** Characterization of specific antibody against p65 acetylated at K310. **(A)** Purified recombinant p65 wild type and the acetylation-deficient mutants were incubated with recombinant p300 in the presence (+) or absence (-) of acetyl CoA. Proteins were resolved on SDS-PAGE and analyzed by western blot using the indicated antibodies. **(B)** HEK 293T cells were transfected with p65 wild type or mutants, with (+) or without (-) p300 co-transfection. Acetylation of p65 at specific K310 was assessed by western blot using the specific antibody. **(C)** Endogenous p65 is rapidly and possibly transiently acetylated in the nucleus upon TNFα stimulation *in vivo*. Wild type complemented MEFs were treated with TNFα for the indicated time periods. p65 was immunoprecipitated from nuclear extracts and analyzed by western blot using anti-acetyl K310 antibody. PARP1 from 5% input was used as nuclear loading control.

Figure 2. SIRT2 deacetylates p65 at K310.

(A) Expression and purification of hist-tagged SIRT1, SIRT2, SIRT6 or SIRT7 from insect cells. **(B)** *In vitro* acetylated p65 wild type was incubated for 30 minutes with recombinant sirtuins in the presence (+) or absence (-) of NAD^+. Deacetylation was confirmed by Western blot analysis using the acK310 specific antibody. **(C)** Overexpressed SIRT2 deacetylate p65 in HEK 293T cells. HEK 293T cells were transfected with the expression plasmids for the indicated his-tagged SIRTs along with p300 and myc-tagged p65. Whole cell extracts were prepared after 30 minutes of TNFα stimulation and analysed by western blot. **(D)** Deacetylase activity of SIRT2 is required for p65 deacetylation in cells. SIRT2 wild type or the enzymatic inactive mutant was overexpressed in HEK 293T cells together with p300 and myc-tagged p65. The acetylation status of p65 after 30 minutes of TNFα stimulation was assessed with the indicated antibody.

Figure 3. SIRT2 deacetylates p65 in the cytoplasm.

(A) p65 translocates to the nucleus in response to TNFα stimulation, while SIRT2 stays in the cytoplasm. HeLa cells were transfected with HA-tagged SIRT2 and

stimulated with TNFα for the indicated time points, followed by immunofluorescence detection of p65 and HA-SIRT2. Dapi staining shows the nucleus. Subcellular localization of p65 and HA-SIRT2 was analysed with a confocal microscope. **(B)** p65 interacts with SIRT2 in the cytoplasm. THP1 cells were stimulated with TNFα for the indicated time points. p65 was immunoprecipitated from nuclear and cytoplasmic extracts and analyzed by western blot using indicated antibodies. Levels of PARP1 as nuclear control are shown. **(C)** HEK 293T cells were transfected with HA-tagged SIRT2 wild type, NLS mutant or NLSΔNES mutant. After 30 minutes of TNFα stimulation, cells were fixed and immunostained with anti-HA antibody to display cellular localization of SIRT2 wild type and mutant proteins, assessed with a confocal microscope. **(D)** Strongly reduced decatylation of p65 acK310 upon overexpression of nuclear SIRT2 mutant. The same constructs as in (C) were overexpressed in HEK 293T cells along with p65 wild type and p300, followed by 30 minutes of TNFα stimulation, whole cell extracts preparation and western blot analysis with the indicated antibodies.

Figure 4. Lack of SIRT2 increases TNFα-induced NF-κB-dependent transcriptional activation.

(A) Endogenous p65 is hyperacetylated in *Sirt2*(-/-) cells. MEFs from the indicated genotypes were pre-treated with the HDAC inhibitors (HDACi) TSA and Nam for 30 minutes and then stimulated with TNFα for 1 hour before preparing whole cell extracts. Extracts were analyzed by western blot using anti-acK310 antibody. The membrane was reprobed for p65, and tubulin was used as loading control. * indicates a non-specific band. (**B**) Western blot analyses for endogenous SIRT1 and SIRT2 in *Sirt2*(-/-) cells. Tubulin was used as loading control. Gene induction of *Mpa2l* **(C)** and *RELA* **(D)** in *Sirt2*(+/+) and *Sirt2*(-/-) MEFs after 3 hours of TNFα stimulation, as measured by real-time RT-PCR. At least two biological replicates were analyzed. Shown are the means ± SD of three independent runs.

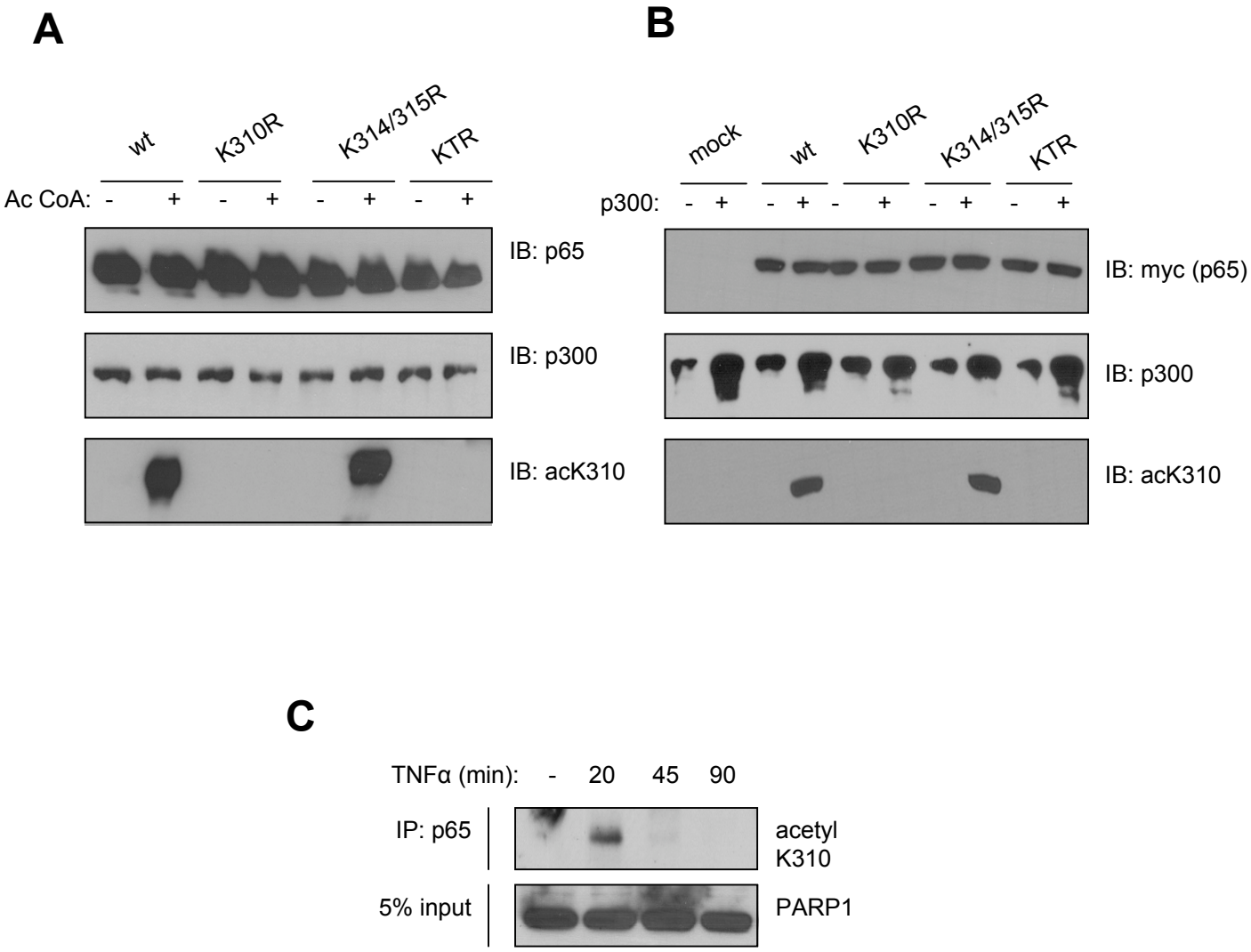
A
wt
K310R
K314/315R
KTR
Ac CoA: - + - + - + - +
IB: p65
IB: p300
IB: acK310
B
mock
wt
K310R
K314/315R
KTR
p300: - + - + - + - + - +
IB: myc (p65)
IB: p300
IB: acK310
C
TNFα (min): - 20 45 90
IP: p65
acetyl K310
5% input
PARP1

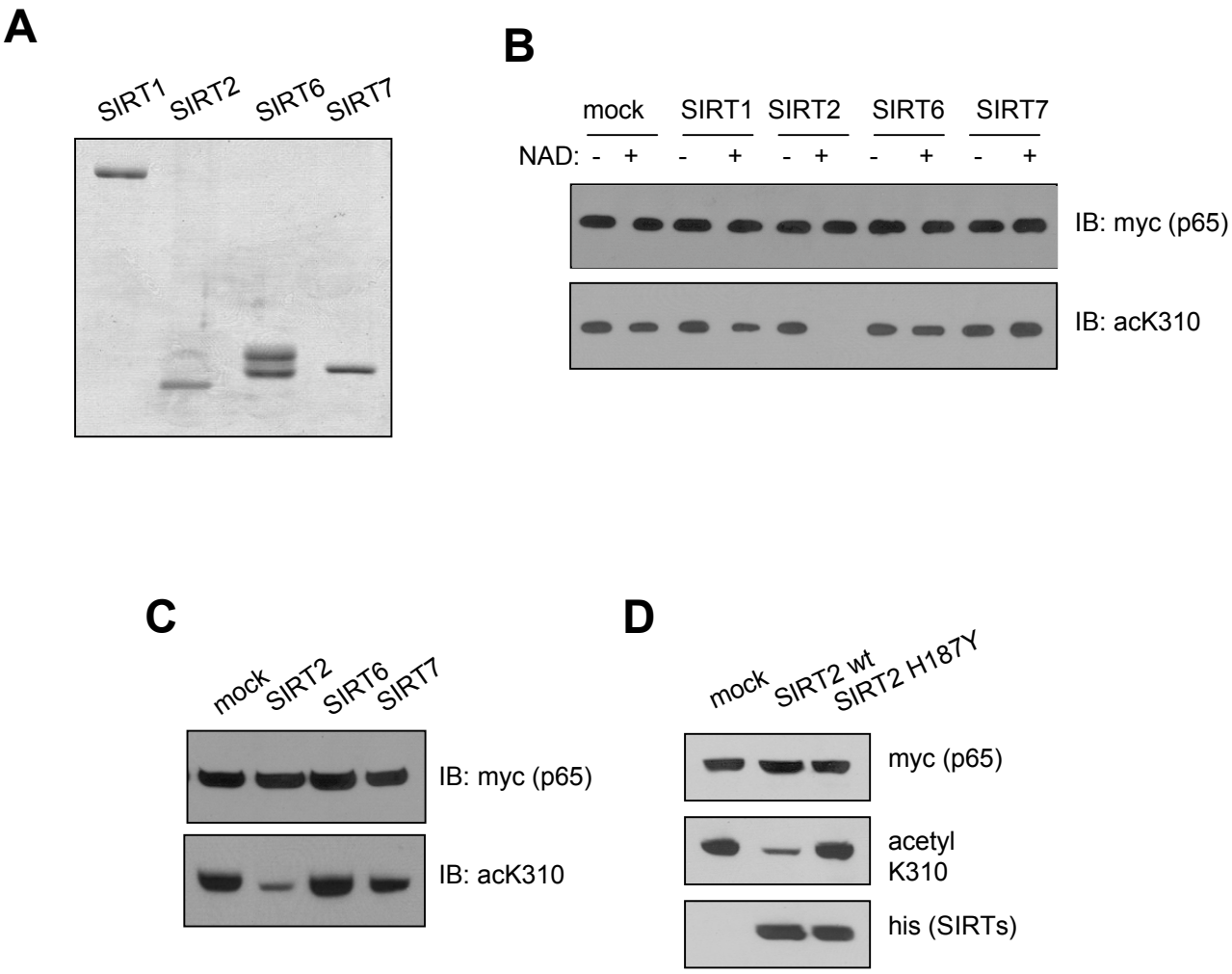
A
SIRT1
SIRT2
SIRT6
SIRT7
B
mock
SIRT1
SIRT2
SIRT6
SIRT7
NAD: - + - + - + - + - +
IB: myc (p65)
IB: acK310
C
mock
SIRT2
SIRT6
SIRT7
IB: myc (p65)
IB: acK310
D
mock
SIRT2 wt
SIRT2 H187Y
myc (p65)
acetyl K310
his (SIRTs)

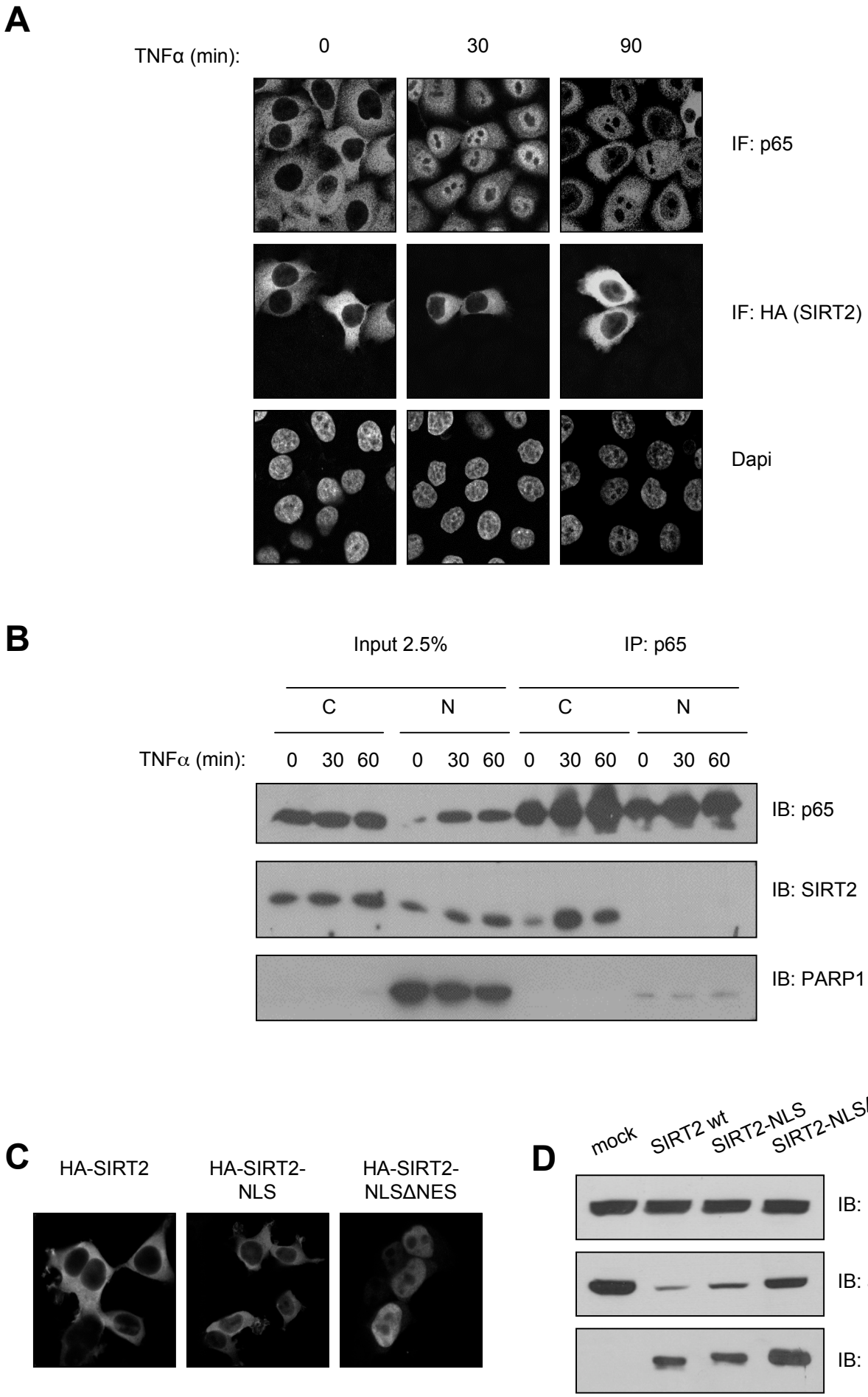
A
TNFα (min):
0
30
90
IF: p65
IF: HA (SIRT2)
Dapi
B
Input 2.5%
IP: p65
C
N
C
N
TNFα (min):
0 30 60 0 30 60 0 30 60 0 30 60
IB: p65
IB: SIRT2
IB: PARP1
C
HA-SIRT2
HA-SIRT2-NLS
HA-SIRT2-NLSΔNES
D
mock
SIRT2 wt
SIRT2-NLS
SIRT2-NLSΔNES
IB: myc (p65)
IB: acK310
IB: HA (SIRT2)

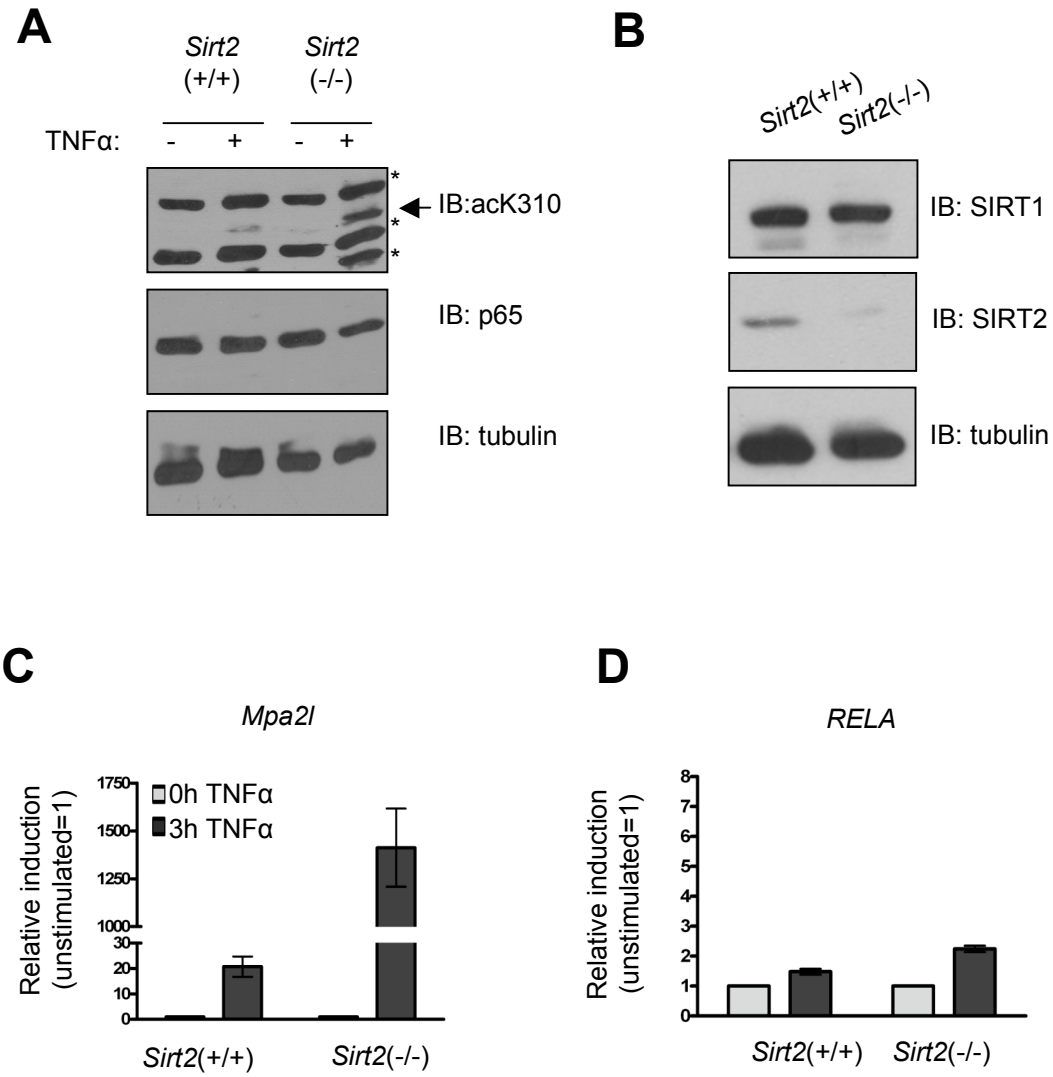
A
Sirt2 (+/+)
Sirt2 (-/-)
TNFα: - + - +
IB:acK310
IB: p65
IB: tubulin
B
Sirt2(+/+)
Sirt2(-/-)
IB: SIRT1
IB: SIRT2
IB: tubulin
C
Mpa2l
Relative induction (unstimulated=1)
0h TNFα
3h TNFα
Sirt2(+/+)
Sirt2(-/-)
D
RELA
Relative induction (unstimulated=1)
Sirt2(+/+)
Sirt2(-/-)

Figure S1.

(A) *In vitro* acetylated p65 wild type was incubated for 120 minutes with recombinant sirtuins in the presence (+) or absence (-) of NAD^+. Deacetylation was confirmed by Western blot analysis using the anti-acK310 specific antibody. **(B)** HEK 293T cells were transfected with the expression plasmids for the indicated his-tagged SIRTs. Whole cell extracts were prepared after 30 minutes of TNFα stimulation and analysed by western blot. **(C)** HEK 293T cells were transfected with the expression plasmids for the indicated myc-tagged HDACs. Whole cell extracts were prepared after 30 minutes of TNFα stimulation and analysed by western blot. **(D)** The indicated HDACs were overexpressed in HEK 293T cells together with p300 and myc-tagged p65. The acetylation status of p65 after 30 minutes of TNFα stimulation was assessed with the indicated antibody.

Figure S2.

(A) HeLa, transient transfection, stained as indicated. Pictures were taken with a confocal microscope. **(B)** HeLa cells were transfected with expression vectors encoding the indicated proteins. The transfected cells were selected and the acetylation of different sites on H4 analyzed by Western blotting. The different antibodies were used on parallel blots.

Figure S3.

(A) *Sirt1(+/+)* and *Sirt1*(-/-) MEFs were pre-treated with the HDAC inhibitors (HDACi) TSA and Nam for 30 minutes and then stimulated with TNFα for 1 hour before preparing whole cell extracts. Extracts were analyzed by western blot using anti-acK310 antibody. The membrane was reprobed for p65, and tubulin was used as loading control. * indicates a non-specific band. **(B)** Gene induction of *Mpa2l* in *p65*(-/-) in a TNFα-dependent manner, as measured by real-time RT-PCR, from the following complemented cell lines: wild type (green), K310R (orange) and pTV (black). Samples were normalized to *Rps6* and *CanX* expression levels, and expressed as fold increase relative to wild type unstimulated. Two biological replicates were included. Shown are the means ± SD of three independent runs. **(C)** TNFα-dependent *Mpa2l* activation is p65-dependent. Knock-down of p65 in *Sirt2*(-/-) cells. p65 levels

were assessed by western blot analysis; and **(D)** *Sirt2(-/-)* MEFs were transiently transfected with the indicated siRNA oligos and stimulated with TNFα for 3 hours. *Mpa2l* gene induction was measured by real-time RT-PCR. **(E)** Knock-down of *Sirt2* increases gene induction of NF-κB target genes. **(F)** *p65*(-/-) MEFs stably complemented with wt p65 were transiently transfected with the indicated siRNA oligos, stimulated with TNFα for 3 hours and gene induction of *Mpa2l* was analyzed by real-time RT-PCR.

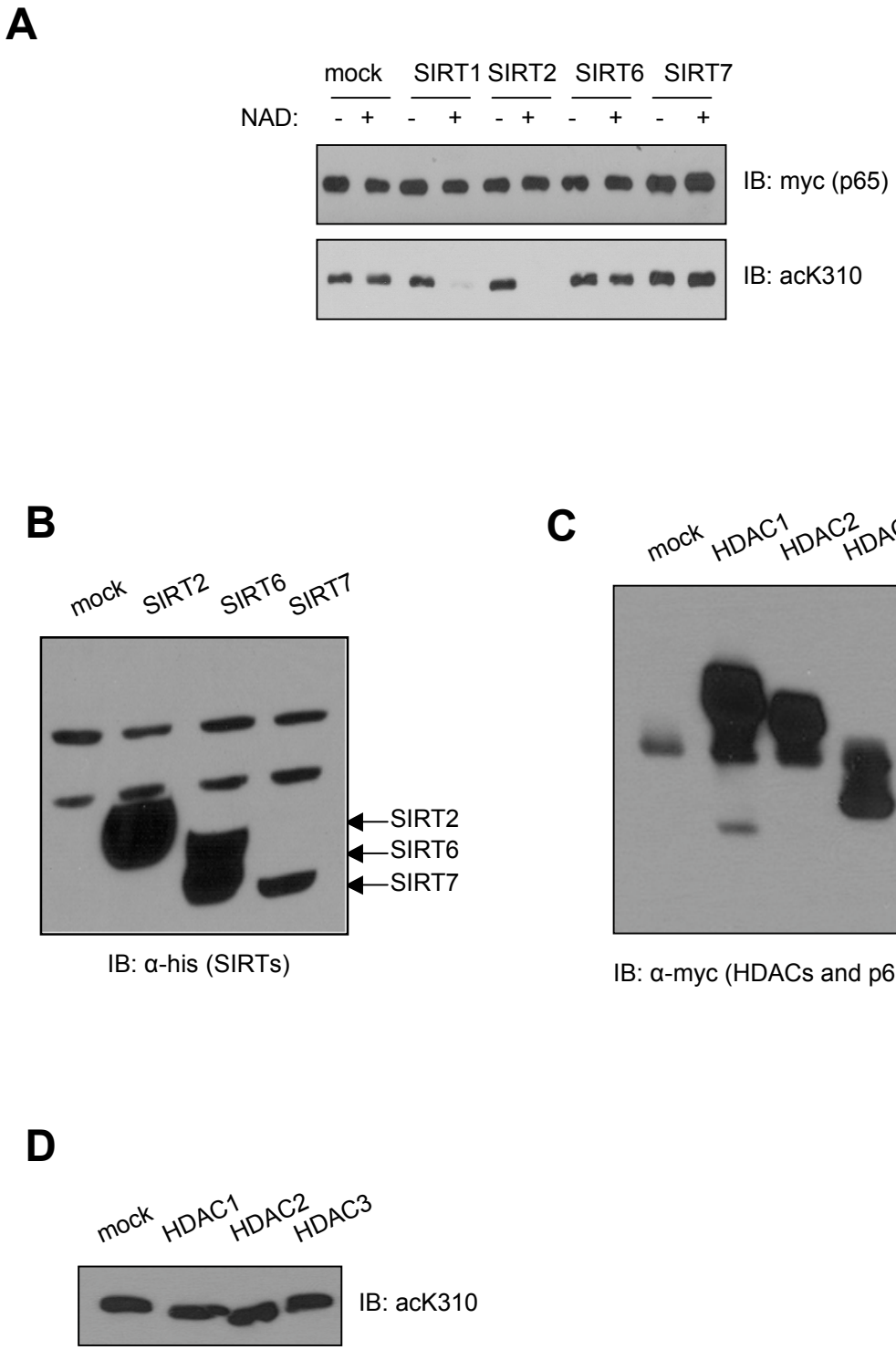
A
mock
SIRT1
SIRT2
SIRT6
SIRT7
NAD: - + - + - + - + - +
IB: myc (p65)
IB: acK310
B
mock
SIRT2
SIRT6
SIRT7
SIRT2
SIRT6
SIRT7
IB: α-his (SIRTs)
C
mock
HDAC1
HDAC2
HDAC3
HDAC1
HDAC2
p65
HDAC3
IB: α-myc (HDACs and p65)
D
mock
HDAC1
HDAC2
HDAC3
IB: acK310

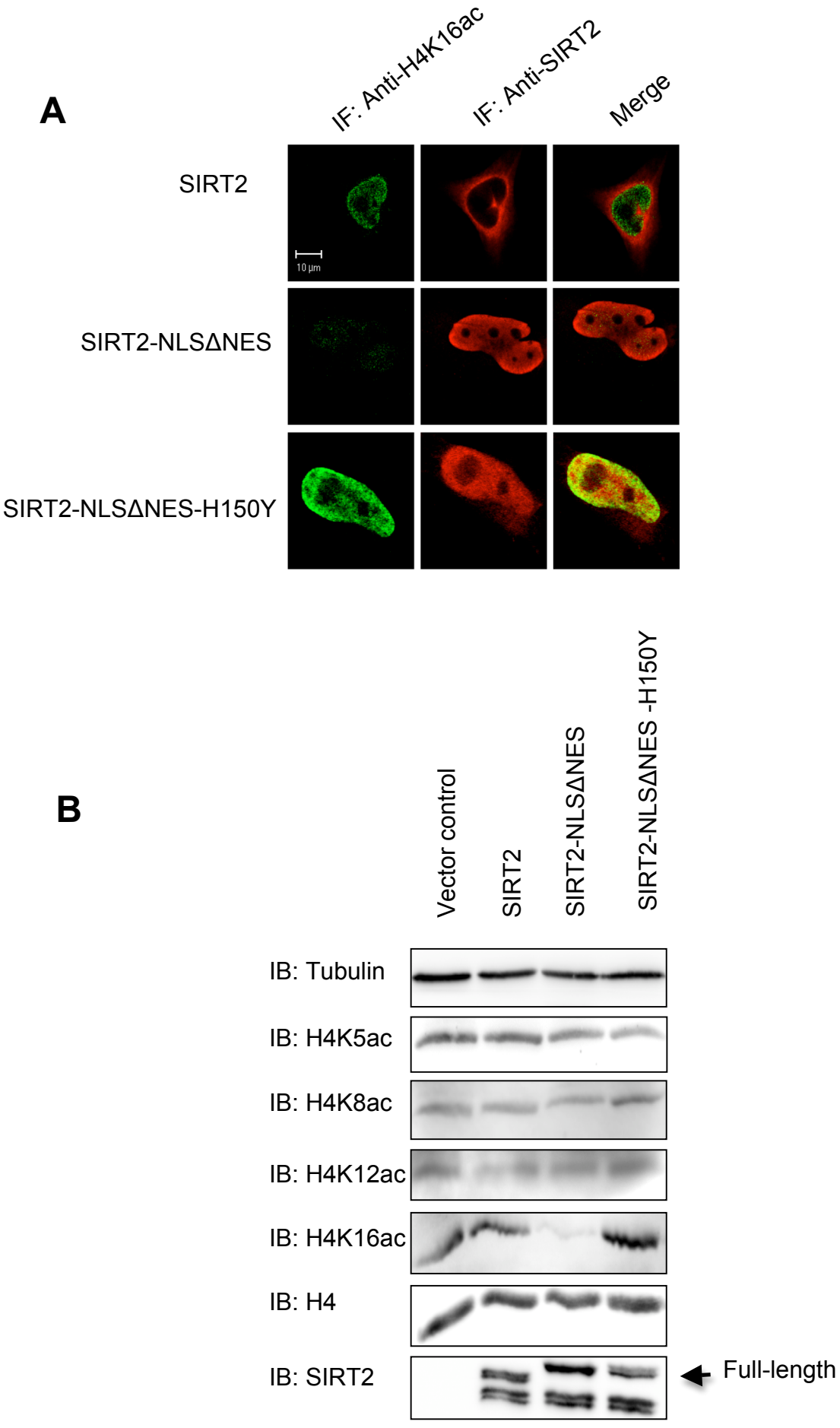
A
IF: Anti-H4K16ac
IF: Anti-SIRT2
Merge
SIRT2
SIRT2-NLSΔNES
SIRT2-NLSΔNES-H150Y
10 µm
B
Vector control
SIRT2
SIRT2-NLSΔNES
SIRT2-NLSΔNES -H150Y
IB: Tubulin
IB: H4K5ac
IB: H4K8ac
IB: H4K12ac
IB: H4K16ac
IB: H4
IB: SIRT2
Full-length

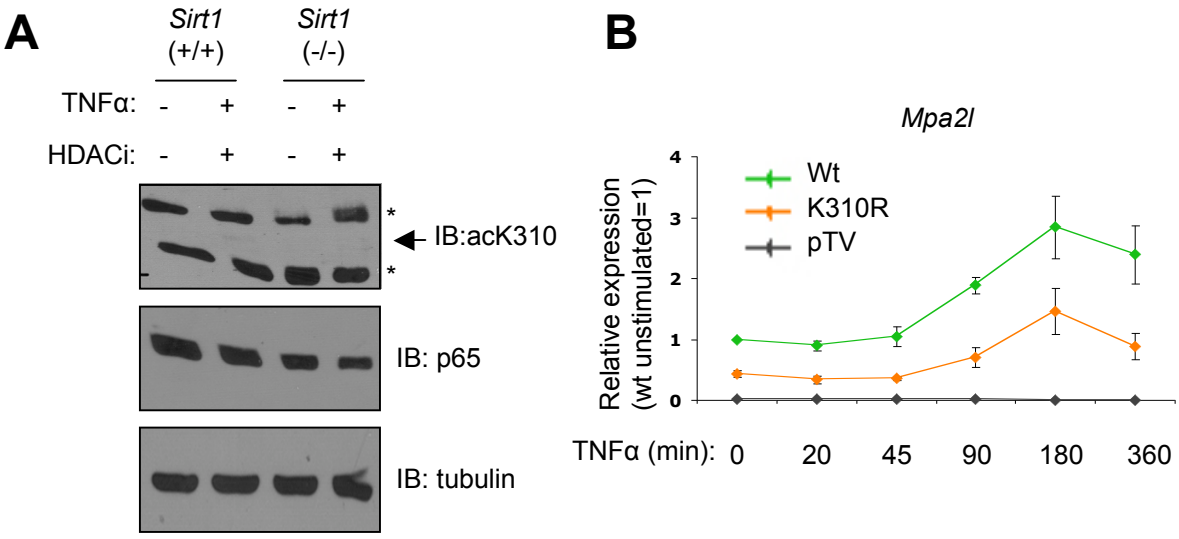
A
Sirt1 (+/+)
Sirt1 (-/-)
TNFα: - + - +
HDACi: - + - +
IB:acK310
IB: p65
IB: tubulin
B
Mpa2l
Relative expression (wt unstimulated=1)
Wt
K310R
pTV
TNFα (min): 0 20 45 90 180 360

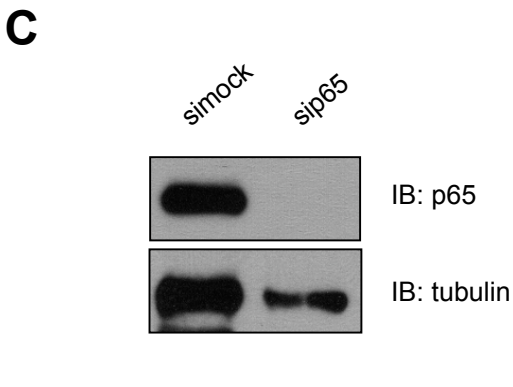
C
simock
sip65
IB: p65
IB: tubulin
D
Mpa2l
% response to TNFα (simock=100%)
simock
sip65

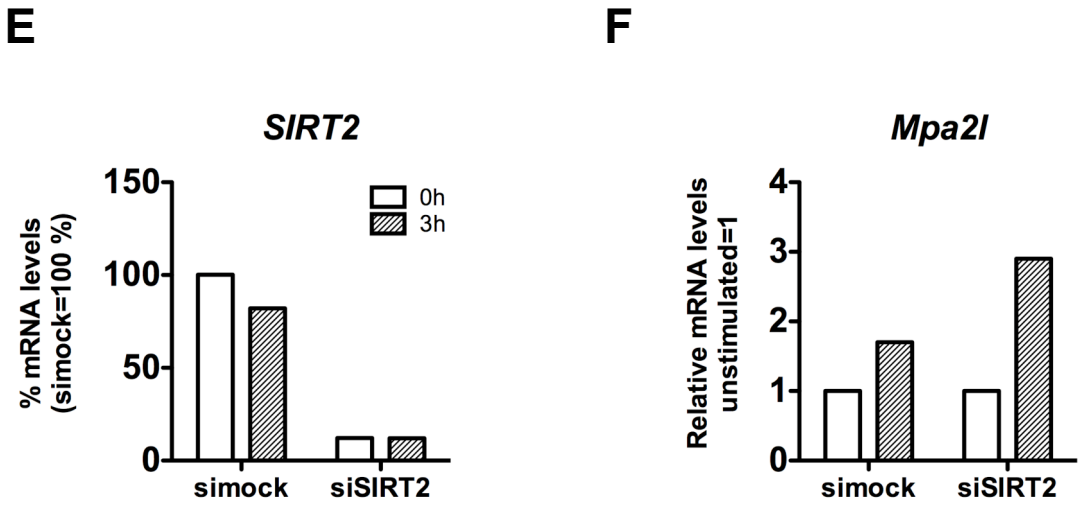
E
SIRT2
% mRNA levels (simock=100 %)
0h
3h
simock
siSIRT2
F
Mpa2l
Relative mRNA levels unstimulated=1
simock
siSIRT2

Poly(ADP-Ribose) Polymerase 1 Promotes Tumor Cell Survival by Coactivating Hypoxia-Inducible Factor-1–Dependent Gene Expression

Michael Elser,[1] Lubor Borsig,[2] Paul O. Hassa,[4] Suheda Erener,[1] Simon Messner,[1] Taras Valovka,[1] Stephan Keller,[3] Max Gassmann,[3] and Michael O. Hottiger[1]

[1]Institute of Veterinary Biochemistry and Molecular Biology, [2]Zurich Center for Integrative Human Physiology (ZIHP) and Institute of Physiology, and [3]Zurich Center for Integrative Human Physiology (ZIHP) and Institute of Veterinary Physiology, University of Zurich, Zurich, Switzerland; and [4]Gene Expression Unit, European Molecular Biology Laboratory (EMBL), Heidelberg, Germany

Abstract

Hypoxia-inducible factor 1 (HIF-1) is the key transcription factor regulating hypoxia-dependent gene expression. Lack of oxygen stabilizes HIF-1, which in turn modulates the gene expression pattern to adapt cells to the hypoxic environment. Activation of HIF-1 is also detected in most solid tumors and supports tumor growth through the expression of target genes that are involved in processes like cell proliferation, energy metabolism, and oxygen delivery. Poly(ADP-ribose) polymerase 1 (PARP1) is a chromatin-associated protein, which was shown to regulate transcription. Here we report that chronic myelogenous leukemia cells expressing small interfering RNA against PARP1, which were injected into wild-type mice expressing PARP1, showed tumor growth with increased levels of necrosis, limited vascularization, and reduced expression of GLUT-1. Of note, PARP1-deficient cells showed a reduced HIF-1 transcriptional activation that was dependent on PARP1 enzymatic activity. PARP1 neither influenced binding of HIF-1 to its hypoxic response element nor changed HIF-1α protein levels in hypoxic cells. However, PARP1 formed a complex with HIF-1α through direct protein interaction and coactivated HIF-1α–dependent gene expression. These findings provide convincing evidence that wild-type mice expressing PARP1 cannot compensate for the loss of PARP1 in tumor cells and strengthen the importance of the role of PARP1 as a transcriptional coactivator of HIF-1–dependent gene expression during tumor progression. (Mol Cancer Res 2008;6(2):282–90)

Received 8/10/07; revised 9/28/07; accepted 10/29/07.

Grant support: Swiss National Science Foundation grants 31-109315.05 and 31-112216 and the Kanton of Zurich (P.O. Hassa, M. Gassmann, and M.O. Hottiger).

The costs of publication of this article were defrayed in part by the payment of page charges. This article must therefore be hereby marked *advertisement* in accordance with 18 U.S.C. Section 1734 solely to indicate this fact.

Note: Supplementary data for this article are available at Molecular Cancer Research Online (http://mcr.aacrjournals.org/).

Requests for reprints: Michael O. Hottiger, Institute of Veterinary Biochemistry and Molecular Biology, University of Zurich, Winterthurerstrasse 190, 8057 Zurich, Switzerland. Phone: 41-44-635-54-74; Fax: 41-44-635-68-40. E-mail: hottiger@vetbio.uzh.ch

doi:10.1158/1541-7786.MCR-07-0377

Introduction

In solid tumors, rapid cell proliferation is associated with areas of hypoxia. Intratumoral hypoxia induces neoangiogenesis, which is an essential switch from tumorigenesis to tumor progression (1). Oxygen limitation regulates vascularization, glucose metabolism, cell survival, and tumor spread. The hypoxic response critically depends on the transcription factor hypoxia-inducible factor-1 (HIF-1; ref. 2). HIF-1α was found to be overexpressed in more than 70% of human cancers and their metastases (3). The effect of HIF-1 on tumor growth is complex and involves the activation of several adaptive pathways and results in the induction of target genes (4). In solid tumors, immunohistochemistry often shows larger fronts of HIF nuclear expression delineating areas of necrosis (5). Induction of HIF is therefore believed to be supportive, if not causative, in cancer (6-8). In tumor xenograft and orthotopic mouse models, manipulation of the levels of either HIF-1α or HIF-2α has shown a causal link between HIF expression and tumor progression (4). HIF signaling has emerged as an important hypoxia-driven response allowing tumor cells to survive, expand, and invade. As a result, tumor hypoxia or HIF expression is strongly associated with a diminished therapeutic response and malignant progression (9).

HIF induction is a multistep process, which is tightly regulated *in vivo* (10, 11). HIF-1 is composed of two polypeptides: HIF-1α and HIF-1β (12). Two additional HIF-α members, the closely related HIF-2α (13) and more distantly related HIF-3α (14), were recently identified. HIF-1 activity is regulated at the posttranscriptional level by protein degradation of HIF-1α subunits after oxygen-dependent hydroxylation of specific proline residues (15). During hypoxia, the prolyl hydroxylases are inactive and HIF-1α is not complexed with the ubiquitin E3 ligase complex containing von Hippel Lindau, thereby allowing for the formation of active HIF-1 complexes (2, 5, 12). Transactivation involves dimerization of the two HIF-1 subunits, which bind to an enhancer element, called hypoxia response element, in target genes. Among the most studied promoters with regard to the recruitment of HIF-1 are those of the *EPO*, *GLUT-1*, and *CA9* [carbonic anhydrase IX (*CAIX*)] genes (16-18). The presence of hypoxia response element sites is necessary, but not sufficient, to direct gene expression in response to hypoxia, suggesting that HIF-1 must interact with other transcription factors or cofactors bound

around these sites (19). The assembly of a higher-order HIF-1 transcription complex is an important stage in HIF-1–dependent transcription, involving multiple coactivator/cofactor-HIF-1-DNA interactions. Two key coactivators of HIF-1 are the histone acetyltransferases p300 and its homologue, the cyclic AMP-responsive element binding protein–binding protein, which can directly associate with the COOH-terminal transactivation domain of HIF-1α. HIF-1α also interacts with other coactivators such as SRC-1 and TIF1 (20).

Poly(ADP-ribose) polymerase 1 (PARP1) is a nuclear chromatin-associated protein and belongs to a large family of enzymes that can synthesize polymers of ADP-ribose units by using β-NAD^+ as substrate (21). Several studies showed that $PARP1^{-/-}$ mice were protected against myocardial infarction, streptozotocin-induced diabetes, lipopolysaccharide-induced septic shock, zymosan-induced vascular failure, a nonseptic model of multiple organ dysfunction, as well as collagen-induced arthritis (21). We recently presented evidence that PARP1 can act as a coactivator of nuclear factor κB *in vivo* (22).

In a 12-*O*-tetradecanoylphorbol-13-acetate–induced skin cancer model, PARP1 was suggested to be important for tumor induction (23). The importance and contribution of PARP1 for tumor progression in tumor cells is still not clear. Here we present evidence that tumors derived from chronic myelogenous leukemia cell line K562 lacking PARP1 but grown in wild-type mice expressing PARP1 show a significant increase in necrotic areas, reduced vascularization, and reduced expression of *GLUT-1*, a HIF-1–dependent gene. HIF-1–dependent gene expression was also reduced in K562 cells expressing siRNA against PARP1 (siPARP1) or primary $PARP1^{-/-}$ mouse lung fibroblasts (MLF). PARP1 interacted directly with HIF-1α, providing convincing evidence that PARP1 acts mechanically as a transcriptional cofactor of HIF-1α transcriptional activation. Interestingly, HIF-1–dependent gene expression was dependent on the enzymatic activity of PARP1. Taken together, our results show that PARP1 and its enzymatic activity are important for tumor progression, possibly leading to new therapeutic approaches for the treatment of human tumors.

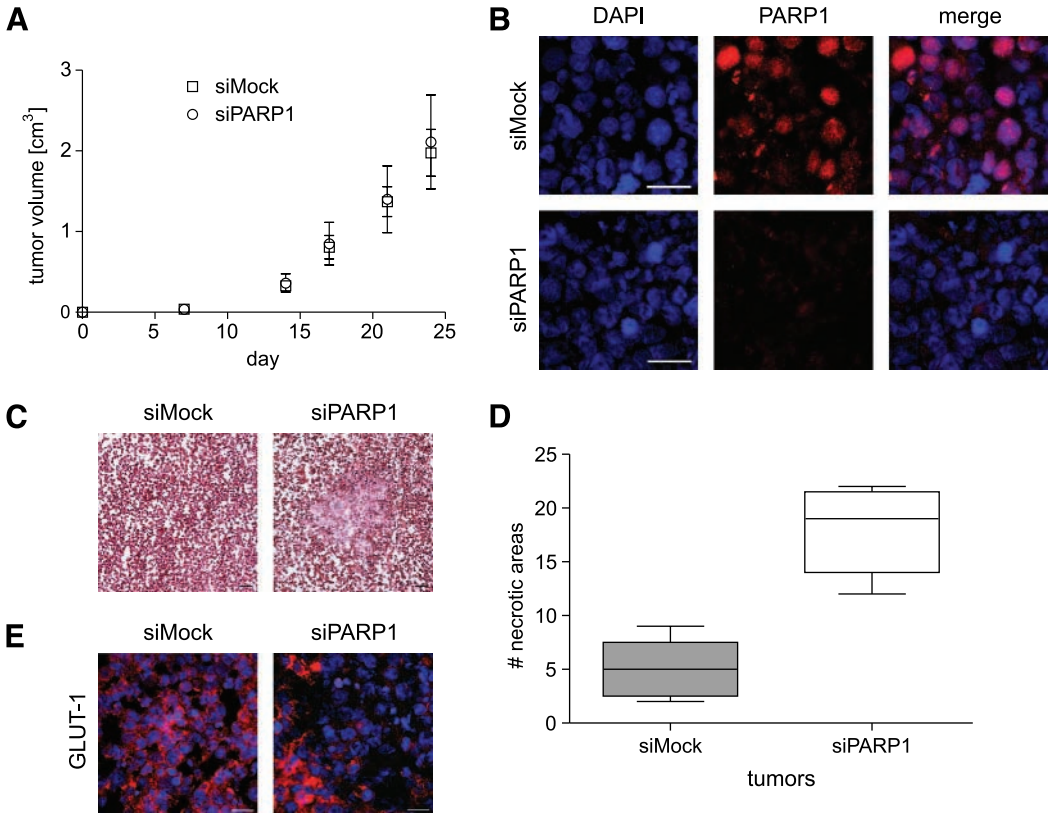

FIGURE 1. The down-regulation of PARP1 enhances tumor cell death but does not affect tumor growth. Chronic myeloid leukemia cell line K562 was subcutaneously injected in athymic nude mice. Cells with down-regulated *PARP1* gene by transduction of siPARP1 were compared with cells transfected with siMock. **A.** Tumor growth curves for siMock (□) and siPARP1 (○) injected mouse groups (four mice and eight implantation sites for each group). Bars, SE. **B.** Staining of tumor sections with anti-PARP1 antibody confirmed the sustained down-regulation of PARP1 in tumor cells after subcutaneous growth in mice. PARP1 staining (*red*), nuclear staining [4′,6-diamidino-2-phenylindole (DAPI; *blue*)], and merged image (*merge*) indicated presence of PARP1 in the nuclei of wild-type (*wt*) tumors. **C.** Representative pictures of tumors stained by H&E indicating an enhanced presence of necrotic tumor areas in siPARP1 tumors. **D.** Quantification of necrotic lesions. All tumors were sequentially sectioned and areas from three different depths of tumor were H&E stained and evaluated. Number of necrotic lesions in each tumor type is presented in a group of mice ($P < 0.001$). **E.** Staining of tumor sections with anti–glucose-transporter (GLUT-1) antibody (*red*) and 4′,6-diamidino-2-phenylindole (*blue*) reveals down-regulation of GLUT-1 expression in siPARP1 tumors.

Results

Down-Regulation of PARP1 Induces Areas of Necrosis in Tumors

To test the role of PARP1 in tumor progression, we stably transduced cell line K562 with a construct expressing siPARP1 or the corresponding mock control using a scrambled sequence (siMock). Down-regulation of PARP1 was analyzed by immunoblot of cell lysates (see Supplementary Fig. S1A). The established siMock and siPARP1 cells were subcutaneously injected in both flanks of athymic nude mice. First signs of tumor formation appeared as early as 1 week postinjection for both cell groups. The formation of tumors was obvious 2 weeks after implantation. Tumor growth was similar in both mouse groups, irrespective of PARP1 down-regulation (Fig. 1A). To confirm that PARP1 was still down-regulated in these tumors, we stained the sections with anti-PARP1 antibody (Fig. 1B). Whereas siMock tumors were positive for PARP1, no signal was visible in siPARP1 tumors. Histologic evaluation of tumors from siPARP1 cells showed larger areas of necrosis (areas with no nuclear-blue staining) compared with their controls (Fig. 1C). Quantification of necrotic areas revealed that the incidence (number of lesions) and size of lesions were increased in tumors expressing siPARP1 (12-22 lesions per tumor in siPARP1 tumors versus 2-9 lesions in siMock tumors; Fig. 1D and data not shown). The areas of cell death with histologic necrotic features were further analyzed by detection of glucose transporter GLUT-1, which is known to be up-regulated in the hypoxic areas of tumors (24). Whereas siMock tumors showed almost homogenous presence of GLUT-1, large areas without GLUT-1 staining were observed in siPARP1 tumors (Fig. 1E). Immunohistochemical analysis with the endothelial marker CD31 revealed a significantly decreased blood vessel density in the siPARP1 tumors (Fig. 2). The reduced vascularization corresponded well with the increased number of necrotic areas observed in siPARP1 tumors, indicating limited blood supply. Repeated experiments with mouse colon carcinoma cell line MC38 injected in a syngeneic mouse model (C57BL/J6) provided the same pattern of enhanced necrosis in the absence of PARP1 (data not shown). These data indicate that the constitutive down-regulation of PARP1 by siRNA did not affect tumor growth within the limits allowed by animal protocol, but caused larger areas of cell death, which in turn could affect tumor progression. Together with the reduced levels of GLUT-1 in siPARP1 tumors, those results suggested the involvement of PARP1 in HIF-dependent gene expression.

HIF-Dependent Gene Expression Is Impaired in siPARP1-Expressing K562 Cells

To test whether PARP1 influences HIF-dependent gene expression, siMock- and siPARP1-expressing K562 cells were treated with ciclopirox olamine (25), a hypoxiamimetic drug, and the expression of HIF-dependent genes was assessed by transient transfection of a reporter gene under the control of hypoxia response element (Fig. 3A). The experiments revealed that ciclopirox olamine–induced expression levels of the reporter gene were dependent on HIF and severely reduced in siPARP1-expressing K562 cells. Transfection of siPARP1-expressing K562 cells with a nondegradable PARP1 restored the observed HIF-1–dependent gene expression (Fig. 3A), confirming that PARP1 is required for HIF-1–dependent gene expression.

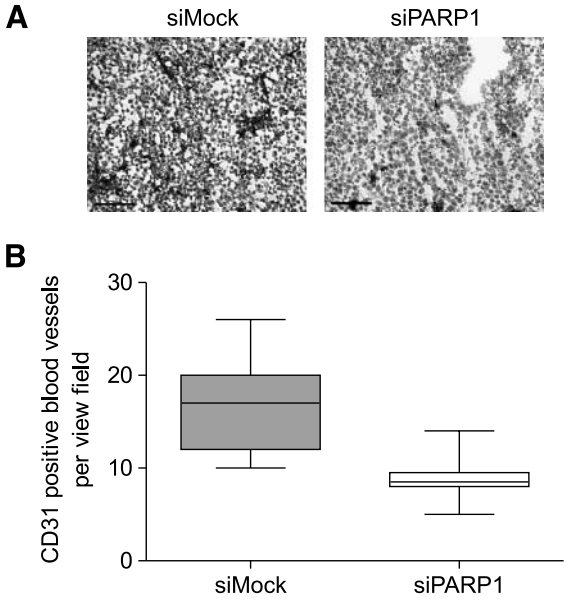

FIGURE 2. Reduced vascularization of K562 tumors is associated with the down-regulation of PARP1. **A.** Tumor vasculature was evaluated by immunohistochemical staining with CD31 antibody. Representative pictures show a higher number of blood vessels in siMock tumors compared with scarcely vascularized siPARP1 tumors. Bar, 100 μm. **B.** Vascular density based on CD31 staining is quantified for both tumors. The decreased number of blood vessels in siPARP1 tumors was found statistically significant by Student's *t* test ($P < 0.01$).

HIF-Dependent Gene Expression Is Impaired in Primary PARP1−/− MLF

To further investigate the contribution of PARP1 in HIF-dependent gene expression, primary $PARP1^{+/+}$ and $PARP1^{-/-}$ MLF were exposed to different concentrations of ciclopirox olamine or hypoxia as indicated, and the expression of HIF-dependent genes was assessed by reporter gene analysis as described above (Fig. 3B and C). Ciclopirox olamine–induced expression of the reporter gene was again severely reduced in $PARP1^{-/-}$ cells when compared with wild-type MLF (Fig. 3B). The experiments under hypoxic conditions (1% O_2) confirmed that PARP1 is important for HIF-1–dependent gene expression (Fig. 3C).

The Enzymatic Activity of PARP1 Is Required for Full HIF-Dependent Transcription

To explore whether the enzymatic activity was important for HIF-dependent gene expression, cells were treated with the PARP inhibitor DAM-TIQ-A. Efficacy of the inhibitor was tested in K562 cells treated with H_2O_2. DAM-TIQ-A was shown to efficiently suppress the H_2O_2-induced formation of poly(ADP-ribose) (Supplementary Fig. S1B). siMock- and siPARP1-expressing K562 cells were then treated with DAM-TIQ-A and subsequently incubated under hypoxic conditions (1% O_2). RNA levels of HIF-1 target gene *CAIX* were

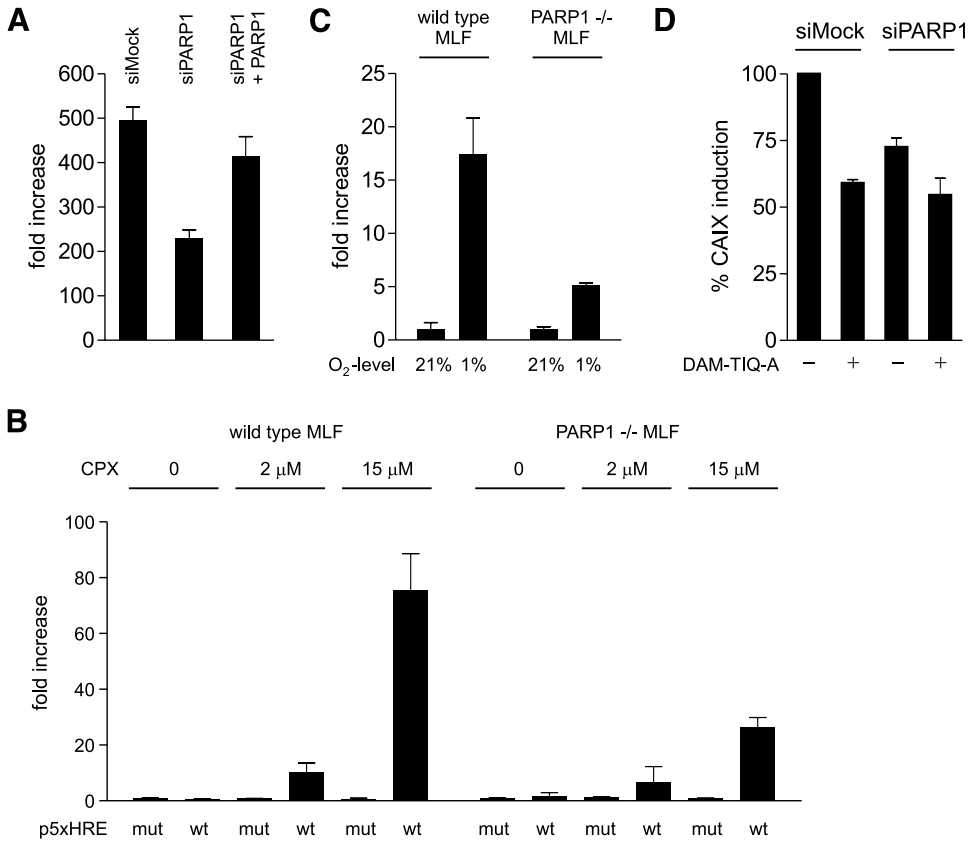

FIGURE 3. PARP1 is required for HIF-1–dependent gene expression. **A.** Transient reporter assay in cell lines K562 siMock, siPARP1, and siPARP1 complemented with wild-type PARP1. Cells were transfected with either the hypoxia reporter (*Epo*) or the mutated control (*mut*) and treated with 15 μmol/L ciclopirox olamine (*CPX*) for 10 h. Cells were harvested and hypoxia-dependent gene expression was determined. The depicted fold increase is calculated as the ratio of normalized luciferase activity of the Epo reporter over the mut reporter. Bars, range of two replicates. **B.** $PARP1^{+/+}$ and $PARP1^{-/-}$ MLF were transfected with either the hypoxia reporter or the mutated control and treated with the indicated amount of ciclopirox olamine for 12 h. Cells were harvested and hypoxia-dependent gene expression was determined. The depicted fold increase is determined by normalization of the relative luciferase activity of the reporter plasmids to that of an internal control (RSV-βGal). The ratios for untreated mutant reporter in both cell lines were arbitrarily set to 1. Bars, range of two replicates. **C.** Cells were prepared as in **B** but kept in either normoxic (21%) or hypoxic (1%) condition for 9 h after transfection. The depicted fold increase is calculated as the ratio of normalized luciferase activity of the Epo reporter over the mut reporter. Bars, SD of three replicates. **D.** Quantitative reverse transcription-PCR analysis of CAIX expression. siMock- and siPARP1-expressing K562 were treated with DAM-TIQ-A as indicated and incubated in normoxic (21% O_2) or hypoxic (1% O_2) conditions. Induction is defined as the ratio of hypoxic over normoxic CAIX levels. The induction of untreated siMock cells was arbitrarily set to 100%. Bars, SD of four replicates.

measured by quantitative real-time PCR (Fig. 3D). Inhibition of PARP1 in siMock cells also resulted in a reduction comparable to the level obtained by knockdown of PARP1. Treatment of siPARP1-expressing cells with inhibitor did not further reduce *CAIX* expression levels.

Normal HIF-1 Signaling in PARP1-Deficient Cells

To investigate the molecular mechanism of PARP1 regulation of HIF-1–dependent gene expression, we analyzed whether the activation of the HIF-1 signaling pathway is overall affected in PARP1-deficient cells on stimulation with ciclopirox olamine or hypoxia. Immunoblot analysis of nuclear extracts from siMock- and siPARP1-expressing K562 revealed that HIF-1α was induced to equal levels after stimulation with ciclopirox olamine (Fig. 4A). Additionally, these experiments showed that there is equivalent nuclear stabilization of HIF-1α in the tested cells. Repeated experiment with $PARP1^{+/+}$ and $PARP1^{-/-}$ MLF provided the same conclusions (data not shown). DNA binding activity of HIF-1 on naked templates was tested by electrophoretic mobility shift assay studies with MLF extracts and DNA oligonucleotides corresponding to the hypoxia response element sites of the erythropoietin *EPO* promoter. PARP1 deficiency did not influence HIF-1 binding to the template (Fig. 4B). Addition of an anti–HIF-1α antibody induced a supershift, confirming that HIF-1 was indeed present in the observed complex (Fig. 4C).

PARP1 Forms a Complex with HIF-1 and Binds Directly to HIF-1 In vitro

HIF-1 and p300/cyclic AMP-responsive element binding protein–binding protein were shown to form a ternary complex and to function synergistically to enhance the activity of nuclear receptors (26). Thus, PARP1 might also synergistically coactivate HIF-1–mediated transactivation. To directly test whether PARP1 physically interacts with HIF-1, we immunoprecipitated PARP1 from HeLa whole-cell extracts after

stimulation with ciclopirox olamine and tested for the presence of HIF-1α by immunoblot analysis. HIF-1α formed a complex with PARP1 (Fig. 5A), which was not mediated by DNA because the presence of ethidium bromide did not affect complex formation (data not shown). To further confirm a direct protein-protein interaction, we bound recombinant purified full-length glutathione *S*-transferase (GST)-PARP1 to glutathione beads followed by incubation with *in vitro* translated HIF-1α subunit, and bound proteins were resolved by SDS-PAGE. PARP1 bound directly to the HIF-1α subunit (Fig. 5B). Similar binding was observed for HIF-2α but not for HIF-3α, HIF-1β, or HIF-2β subunits (Supplementary Fig. S1C and data not shown).

Expression of PARP1 Increases HIF-1α–Dependent Transactivation in PARP1$^{-/-}$ Cells

To further investigate the functional relevance of the PARP1-HIF-1α interaction, primary PARP1$^{+/+}$ and PARP1$^{-/-}$ MLF were transfected with an expression plasmid for HIF-1α, and the expression of HIF-1α–dependent genes was assessed by reporter gene analysis as described above (Fig. 3). Transcriptional activation by HIF-1α expression was again severely reduced in PARP1$^{-/-}$ cells when compared with wild-type MLF (Fig. 5C). The same experiment using a plasmid with a mutated promoter confirmed that the observed gene expression is indeed HIF-1α specific. Assuming that the reduced luciferase levels in PARP1$^{-/-}$ MLF (Figs. 3 and 5C) are indeed due to the absence of PARP1, one expects that complementation of PARP1$^{-/-}$ cells with the wild-type *PARP1* gene restores HIF-1–dependent gene expression. HIF-dependent reporter plasmids (wild-type and mutant) were therefore cotransfected in PARP1$^{-/-}$ MLF with expression vectors for HIF-1α and PARP1. Overexpression of PARP1 or HIF-1α alone could not, or modestly, activate HIF-dependent gene expression; however, coexpression of HIF-1α with PARP1 synergistically activated HIF-1α–dependent transcriptional activation (Fig. 5D). In the same set of experiments, we did not observe transcriptional coactivation of HIF-2α by PARP1, suggesting that HIF-2α might be regulated differentially by PARP1. The regained ability of PARP1$^{-/-}$ MLF to activate genes in a HIF-1α–dependent manner on reintroduction of PARP1 provides convincing functional evidence that PARP1 acts as a classic transcriptional coactivator of HIF-1–dependent gene expression.

Discussion

HIF-1–regulated genes have been implicated in the promotion of tumor progression and metastasis by enhancing angiogenesis, cell proliferation, and the resistance to apoptotic cell death (27). In this study, we find that PARP1 is a regulator of HIF-1–dependent xenograft tumor progression. Mechanistically, we identified PARP1 as a transcriptional coactivator of HIF-1–induced gene expression and we determined a novel process of HIF-1 regulation under hypoxia that acts through PARP1 by regulating target gene expression of critical HIF-1 genes such as *GLUT-1, CAIX, EPO*, and *VEGF*.

The knockout strategy has revealed an important role of PARP1 in cell death after myocardial or brain ischemia-reperfusion injury (28, 29). Significant protection against oxidant-induced tissue damage can also be achieved with

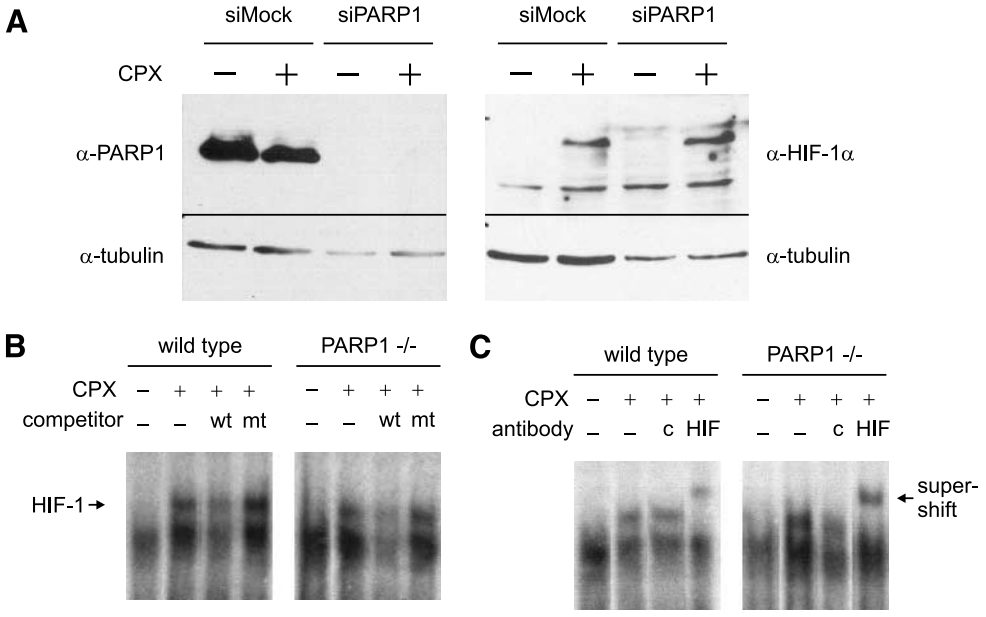

FIGURE 4. HIF-1 stabilization and DNA binding activity are not affected in PARP1$^{-/-}$ cells. **A.** K562 siMock and siPARP1 cell lines were treated with 15 μmol/L ciclopirox olamine for 14 h. Nuclear proteins were then extracted and resolved by SDS-PAGE followed by immunoblot analysis with anti-PARP1 and anti–HIF-1α antibodies. Anti-tubulin was used as a loading control. **B.** Autoradiographs of electrophoretic mobility shift assay for ^{32}P-labeled oligonucleotides containing a HIF-1 binding site. Nuclear extracts of PARP1$^{+/+}$ and PARP1$^{-/-}$ MLF treated with 10 μmol/L ciclopirox olamine for 6 h were used in the assay. Competition for binding was done with unlabeled wild-type and binding mutant oligonucleotides. **C.** Confirmation of HIF-1 binding was effected by adding anti–HIF-1α (*HIF*) or control IgG (*c*) antibodies for a supershift.

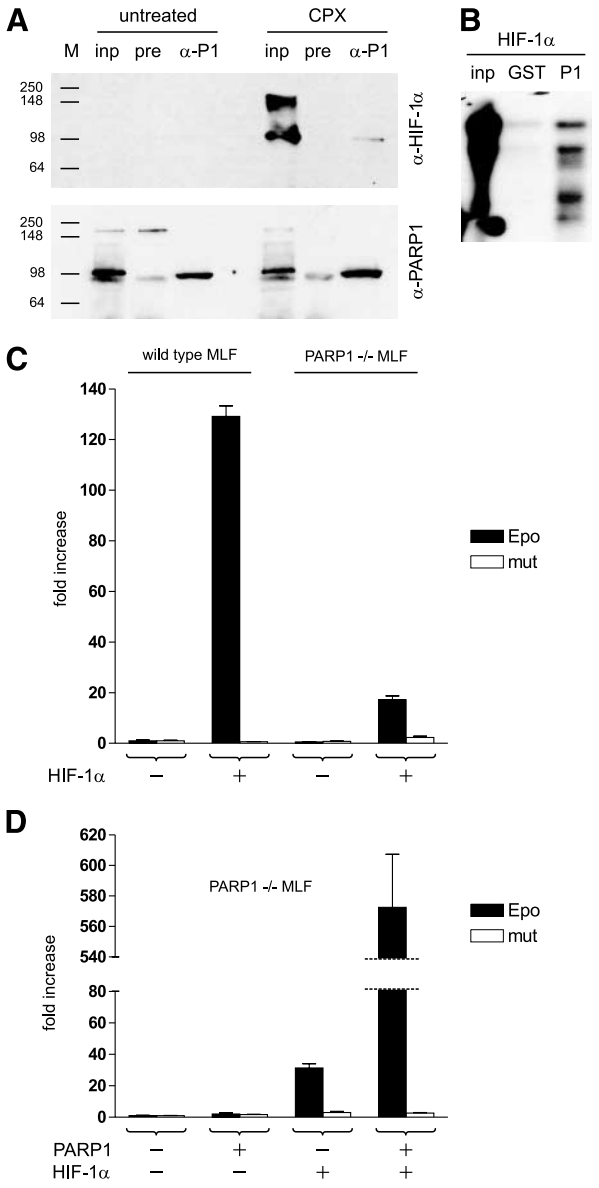

FIGURE 5. PARP1 directly interacts with HIF-1α and synergistically activates HIF-1α–dependent gene expression. **A.** Immunoprecipitation of HIF-1α with anti-PARP1 antibody serum (*α-P1*) and preimmune serum (*pre*) as a control. Total extracts of HeLa cells treated with 15 μmol/L ciclopirox olamine for 16 h were used. Input lane (*inp*) was loaded with 10% the amount of extract used for the immunoprecipitation. The sizes of protein marker bands (*M*) are indicated in kilodaltons. **B.** Autoradiography of *in vitro* translated HIF-1α pulled down with GST-PARP1 (*P1*) or GST alone (*GST*). Input lane was loaded with 1% the amount of translation product used for the pull-down. **C** and **D.** PARP1$^{-/-}$ MLF were transfected for 24 h by polyethylenimine with either the hypoxia reporter or the mutated control together with PARP1 or HIF-1α, as indicated. Cells were harvested and hypoxia-dependent gene expression was determined. The depicted fold increase is determined by normalization of the relative luciferase activity of the reporter plasmids to the protein concentration of each sample. The ratios for untreated mutant reporter in both cell lines were arbitrarily set to 1. Bars, SD of three replicates.

pharmacologic PARP1 inhibitors (30). The most obvious explanation for this observation is that on reperfusion, oxygen-derived free radicals, NO, and peroxynitrite induce DNA breaks, which in turn overactivate PARP1 (31). This excessive activation leads to intracellular NAD and ATP depletion resulting in mitochondrial free radical generation and necrosis (32, 33). Whether these observed effects are due to anoxia or reduced nutritional supply or both (e.g., ischemia) is currently not clear. In our tumor model, we found PARP1 to promote cell survival rather than cell death. The observed increase in necrotic areas in tumors grown from PARP1-deficient cells was also accompanied by a decrease in vascularization of tumors. These findings are in agreement with earlier observation that inhibition of PARP1 decreases angiogenesis in an *in vitro* model (34). We therefore propose that insufficient oxygen and nutrient supply due to impaired HIF-1 activation is the cause for the increased necrosis during tumor progression, independent of radical oxygen species formation. Experiments by Tong et al. (35) provided evidence that in a p53$^{-/-}$ background, PARP1 is important as cofactor for suppression of tumorigenesis in certain tissues. Conde et al. (36) reported that injection of ras-transformed PARP1$^{-/-}$ p53$^{-/-}$ cells failed to generate any visible tumor. We did not observe an influence of PARP1 protein on tumor latency and cell proliferation using K562 or MC38 cells (data not shown). This could be due to the fact that both cell lines are expressing functional p53. Furthermore, our results indicate that in a p53-proficient background, PARP1 acts as promoter of tumor survival as shown by the increase of necrosis in tumors formed by siPARP1-expressing K562 and MC38 cells. Obviously, the tissue expressing PARP1 around the tumors was not able to overcome the lack of PARP1 in the tumor cells.

Our gene expression studies suggest a transcriptional coactivator role for PARP1 in HIF-1–dependent gene expression because in the absence of PARP1, impaired expression of HIF-1–dependent genes was found when mouse fibroblasts and K562 cells were exposed to ciclopirox olamine or hypoxia. Interestingly, the protein levels of HIF-1 were not reduced in treated cells, indicating that the signaling pathway and turnover rate of HIF-1 per se were not affected. Moreover, the DNA binding activity of HIF-1 assayed *in vitro* on naked nonchromatinized templates was not impaired in nuclear extracts from PARP1$^{-/-}$ fibroblasts, suggesting that HIF-1 does not require PARP1 for binding to its hypoxia response element.

Complementation experiments of PARP1$^{-/-}$ cells with a PARP1 expression plasmid confirmed that PARP1 is required when HIF-dependent gene expression is activated by HIF-1α overexpression. We detected endogenous PARP1 in a complex with HIF-1. Moreover, PARP1 directly bound to the HIF-1α subunit *in vitro*. Together these observations implicate that PARP1 is playing a critical and central role downstream of the HIF signaling pathway and strengthens the involvement of PARP1 as transcriptional coactivator. It is of great interest to elucidate the relationship of PARP1 to other HIF-1–associated coactivators with regard to their relative contribution to HIF-1–dependent gene activation, in relation to different promoters and stimuli. Chromatin immunoprecipitation experiments could be used to study the presence of PARP1 at promoters of HIF-1–dependent genes. Unfortunately, such experiments are made difficult by the lack of suitable antibodies and the high affinity of PARP1 for DNA strand breaks in general.

The requirement of PARP1 enzymatic activity for HIF-1–dependent transcription is shown by experiments including PARP inhibitors. As such, expression of CAIX was reduced in the presence of the PARP inhibitor DAM-TIQ-A. Thus, for at least a subset of PARP1-dependent HIF-1 target genes, the enzymatic activity of PARP1 is necessary for full activation. Whether only PARP1 is poly(ADP-ribosylated) or also other factors, such as histones or even HIF-1α, has to be further elucidated. Two groups recently reported that lack of homologous recombination by BRCA1 and BRCA2 dysfunction sensitized tumor cells to the inhibition of PARP enzymatic activity (37, 38). Others provided evidence that the enzymatic activity of PARP1 can also be induced by D-myo-inositol-1,4,5-triphosphate in a DNA damage–independent mechanism (39). Whether the observed effect of PARP inhibitor is due to the PARP1 activation induced by damaged DNA or other stimuli has to be further investigated. PARP inhibitors were also reported to possess free radical scavenging properties (40). Because hypoxia could potentially induce local oxidative stress, it is tempting to speculate that PARP inhibitors with antioxidative potency contribute indirectly and nonspecifically to decreased HIF-1–dependent transcriptional activity by reduction of free radicals. We cannot exclude that the observed effects are due to the off-targeting activity of PARP inhibitors (41, 42). The residual activation of gene expression in the presence of PARP inhibitor might be explained by a process that is independent from PARP1. The small observed difference between siRNA knockdown and pharmacologic inhibition, on the other hand, could be due to incomplete knockdown of PARP1 or the contribution of other PARP family members.

Martin-Oliva et al. recently provided evidence that the number of 7,12-dimethylbenz(*a*)anthracene– and 12-*O*-tetradecanoylphorbol-13-acetate–induced skin tumors is reduced in mice treated with PARP inhibitor, suggesting that PARP1 is important for tumor initiation. They suggested that the transcriptional activity of HIF-1 was compromised by PARP inhibition or, in immortalized PARP1-deficient cells, on stimulation with 12-*O*-tetradecanoylphorbol-13-acetate or desferoxamine (an iron chelator and activator of HIF; ref. 23). In contrast, our studies provide evidence that PARP1 is important for the progression of tumors formed by transformed cell lines and that wild-type mice expressing PARP1 cannot compensate for the loss of PARP1 in cancer cells. One possible explanation for the observed discrepancies is the differences in examined tumor types. Furthermore, our studies with primary PARP1$^{-/-}$ MLF and siPARP1-expressing cells under hypoxic conditions or treated with a hypoxiamimetic drug revealed that HIF-1 signaling (HIF-1 protein stability and DNA binding) per se is not affected by PARP1.

By integrating our data with previous findings, we propose a model by which HIF-1 regulation under hypoxic conditions occurs additionally through PARP1 as transcriptional coactivator. The presence of PARP1 stimulates HIF-1–dependent gene expression and thus allows induction of genes involved in neoangiogenesis and cell survival. From a therapeutic point of view, inhibition of PARP1 enzymatic activity could be an effective target in conditions of tissue ischemia because tumors lacking PARP1 show increased necrosis on ischemic insult. Thus, well-tolerated PARP1 inhibitors that are known to inhibit PARP1 enzymatic activity (38) could be beneficial in the treatment of HIF-1–dependent tumor progression.

Materials and Methods

Reagents and Antibodies

Ciclopirox olamine was purchased from Sigma and dissolved in methanol before diluting to final concentration in supplemented media. Radiochemicals were obtained from Amersham Biosciences. The anti-PARP1 antibody is described in ref. 43, and the anti–HIF-1α antibody in ref. 44. Antimouse IgG was purchased from Santa Cruz Biotechnology. Anti–GLUT-1 antibody was purchased from Abcam, Inc. Anti-PAR antibody was a kind gift of Guy Poirier.

Mouse Strains and Experiments

All animal procedures were done in accordance with the regulations of the Cantonal Veterinary Authority of Zurich in accordance with the Swiss laws on animal protection.

For the tumor growth studies, athymic nude mice (HsdCpb:NMRI-Foxn1^{nu}) were obtained from Harlan Laboratories. Eight-week-old females were injected subcutaneously with 8×10^6 K562 chronic myelogenous leukemia cells, which were either stably transfected with siRNA against PARP1 (siPARP1 tumors) or transfected with mock siRNA (siMock tumors). Tumor growth was checked regularly and mice were terminated when the size of tumor was reaching approved limits.

Histology

Dissected tumors were macroscopically evaluated, cut in half, and frozen in embedding medium (Tissue-Tek O.C.T. compound, Sakura, USA, Inc.). Paraformaldehyde-fixed cryosections (8 μm) were blocked in 0.5% bovine serum albumin and incubated with either polyclonal rabbit anti-PARP1 or rabbit anti-GLUT-1 (Abcam) antibody for 1 h at room temperature. Tumors were further incubated with Cy3-conjugated goat anti-rabbit antibodies (Jackson ImmunoResearch) followed by nuclear staining with 4′,6-diamidino-2-phenylindole and mounting in Prolong medium (Invitrogen). Formalin-fixed cryosections were stained with H&E and evaluated for the presence of necrosis. The quantification of necrosis was done on the whole area of each tumor in several sections. Blood vessels were stained with CD31 antibody (Becton Dickinson). Specific binding was detected with the Vectrastain ABC Kit with the AEC substrate (Vector Laboratories) followed by hematoxylin counterstaining.

Generation of siRNA Cell Lines

Generation of viruses and transduction of cells were previously described (45). After several rounds of selection, expression level of PARP1 was screened by immunoblot analysis.

Cell Culture, Transient Transfection, and Nuclear Extracts

Mouse PARP1$^{+/+}$ or PARP1$^{-/-}$ MLF cells were isolated from 129S/EV-PARP1$^{+/+}$ and 129S/EV-PARP1$^{-/-}$ mice, both described in ref. 46. Only cell passages 2 to 10 were used for experiments. MLF and HeLa cell lines were grown in DMEM Glutamax-I (Invitrogen) containing 4.5 g/L glucose. K562 cells

were grown in RPMI (Invitrogen). All media were supplemented with 10% FCS (Invitrogen), 50 units/mL penicillin, 50 μg/mL streptomycin (Sigma), and α-naphthylacetic acid (Invitrogen). Cells were grown in 5% CO_2 at 37°C in a humidified incubator. MLF and HeLa cells were transfected with polyethylenimine or calcium phosphate, and K562 cells with DEAE-dextran, as previously described. Because of differences in transfection efficiencies, an expression plasmid of β-galactosidase (pph-RSV-nt-β-gal; ref. 47) was cotransfected as a transfection efficiency control, and luciferase activities were normalized based on β-galactosidase activity. In case of K562 and MLF, normalization was done with total protein amount measured by Bradford assay. Luciferase activity was measured as described in ref. 48. Nuclear extracts of HeLa and K562 cells were produced as described in ref. 49.

Quantitative Real-time PCR

Total RNA of cells was extracted with the RNA Isolation Mini Kit (Agilent) following the manufacturer's protocol. RNA was then reverse transcribed with the High Capacity cDNA Reverse Transcription Kit (Applied Biosystems). Quantitative PCR was done on a Rotor-Gene 3000 machine (Corbett Research) with TaqMan probes (Applied Biosystems) against two endogenous controls (ribosomal proteins P0 and S14) and against CAIX. Quantitation was done using the Rotor-Gene software version 6.1 (Corbett Research) and the built-in two-standard curve method.

Plasmids

The reporter plasmid p5xHREwt was created by cloning one oligonucleotide containing a HIF-1 binding site from the VEGF promoter (5′-AGCTTGATATCGGATCCGCATACGTGGGCTCCAACAGGTCCTCTTCCCTCCCAGTCACTGACTAACCCT-3′; binding site underlined) and two oligonucleotides containing two binding sites from the EPO promoter (5′-AGCTTGGATCCGGCCCTACGTGCTGCCTCGCATGGGCCCTACGTGCTGCCTCGCATGGCCC-3′; binding sites underlined) into the multiple cloning site of pGL3-Basic (Promega). For p5xHREmut, the oligonucleotides were the same except for the binding sites that were changed to 5′-TAAAAGGG-3′ and 5′-TAAAAGCT-3′, respectively. Expression vectors CMV-HIF-1α, CMV-HIF-2α, and CMV-HIF-3α used for *in vitro* transcription were constructed by PCR amplification of the open reading frame of I.M.A.G.E. cDNA clones #3842146, #6305604, and #6250259, respectively. PCR products were then ligated into pphCMV-T7-km-3 described in ref. 50.

shRNA coding sequences (available on request) were cloned into pSUPER vector by using *Bgl*II and *Hin*dIII cloning sites. *Bam*HI/*Sal*I fragment containing HI promoter upstream of shRNA coding sequence was subcloned into pRDI292 vector (51). The envelope plasmid pMD.G and the packaging plasmid pCMV-ΔR8.91 have previously been described (45).

In vitro *Transcription/Translation and GST Pull-Down Assays*

GST and GST-PARP1 were expressed in *Escherichia coli*. *In vitro* transcription/translation reactions were carried out with the TNT T7 Quick Coupled Transcription/Translation System (Promega) according to the manufacturer's protocol. GST pull-down assays were done with bacterial extracts, glutathione-Sepharose beads (Amersham Pharmacia Biotech), and the radiolabeled product in the presence of 80 mmol/L NaCl as described in ref. 52.

Immunoprecipitation and Immunoblot

For immunoprecipitation, 1 mg of HeLa nuclear extract was incubated with anti-PARP1 serum or preimmune serum in immunoprecipitation buffer containing 80 mmol/L NaCl and Protein A-Sepharose beads (Amersham Biosciences). Beads were then extensively washed in the presence of 100 mmol/L NaCl and 0.05% NP40, followed by SDS-PAGE and immunoblot analysis according to the manufacturer's protocol (enhanced chemiluminescence; Pierce).

Electrophoretic Mobility Shift Assay

The electrophoretic mobility shift assay was done as described in ref. 53. Briefly, the oligonucleotides 5′-GCCCTACGTGCTGCCT-3′ and 5′-GCCCTAAAAGCTGCCT-3′ were annealed to their antisense counterparts, labeled with ^{32}P by T4 PNK, and purified in Microspin G-25 columns (Amersham Biosciences). The radiolabeled oligonucleotides were then added to 10 μg of HeLa nuclear extract. After 20 min, samples were loaded and separated on a 4% native acrylamide gel. The gels were then dried for autoradiography. For competition, HeLa nuclear extracts were preincubated for 5 min with unlabeled competitor oligonucleotides for a final ratio of 25:1 of unlabeled over labeled oligonucleotide. For supershift, nuclear extracts were preincubated for 20 min with anti–HIF-1α or with an unrelated antimouse IgG antibody.

Acknowledgments

We thank Dr. Z. Q. Wang (Fritz-Lipmann-Institut, Jena, Germany) for the 129S/EV-PARP1$^{+/+}$ and 129S/EV-PARP1$^{-/-}$ breeding pairs of mice, Dr. D. Trono (EPFL, Lausanne, Switzerland) for retroviral constructs, Dr. R.H. Wenger (University of Zurich, Zurich, Switzerland) for technical advice, Dr. G.G. Poirier (Université Laval, Sainte-Foy, Québec, Canada) for antibodies, and the members of the Institute of Veterinary Biochemistry and Molecular Biology (University of Zurich, Switzerland) for their helpful advice and comments.

References

1. Hanahan D, Folkman J. Patterns and emerging mechanisms of the angiogenic switch during tumorigenesis. Cell 1996;86:353–64.

2. Fandrey J, Gorr TA, Gassmann M. Regulating cellular oxygen sensing by hydroxylation. Cardiovasc Res 2006;71:642–51.

3. Paul SA, Simons JW, Mabjeesh NJ. HIF at the crossroads between ischemia and carcinogenesis. J Cell Physiol 2004;200:20–30.

4. Semenza GL. Targeting HIF-1 for cancer therapy. Nat Rev Cancer 2003;3:721–32.

5. Pouyssegur J, Dayan F, Mazure NM. Hypoxia signalling in cancer and approaches to enforce tumour regression. Nature 2006;441:437–43.

6. Ohh M, Park CW, Ivan M, et al. Ubiquitination of hypoxia-inducible factor requires direct binding to the β-domain of the von Hippel-Lindau protein. Nat Cell Biol 2000;2:423–7.

7. Hopfl G, Wenger RH, Ziegler U, et al. Rescue of hypoxia-inducible factor-1α-deficient tumor growth by wild-type cells is independent of vascular endothelial growth factor. Cancer Res 2002;62:2962–70.

8. Ryan HE, Poloni M, McNulty W, et al. Hypoxia-inducible factor-1α is a positive factor in solid tumor growth. Cancer Res 2000;60:4010–5.

9. Vaupel P. The role of hypoxia-induced factors in tumor progression. Oncologist 2004;9 Suppl 5:10–7.

10. Brahimi-Horn C, Mazure N, Pouyssegur J. Signalling via the hypoxia-inducible factor-1α requires multiple posttranslational modifications. Cell Signal 2005;17:1–9.

11. Hopfl G, Ogunshola O, Gassmann M. HIFs and tumors-causes and consequences. Am J Physiol Regul Integr Comp Physiol 2004;286:R608–23.

12. Wang GL, Semenza GL. Purification and characterization of hypoxia-inducible factor 1. J Biol Chem 1995;270:1230–7.

13. Tian H, McKnight SL, Russell DW. Endothelial PAS domain protein 1 (EPAS1), a transcription factor selectively expressed in endothelial cells. Genes Dev 1997;11:72–82.

14. Makino Y, Cao R, Svensson K, et al. Inhibitory PAS domain protein is a negative regulator of hypoxia-inducible gene expression. Nature 2001;414:550–4.

15. Berra E, Ginouves A, Pouyssegur J. The hypoxia-inducible-factor hydroxylases bring fresh air into hypoxia signalling. EMBO Rep 2006;7:41–5.

16. Semenza GL, Wang GL. A nuclear factor induced by hypoxia via *de novo* protein synthesis binds to the human erythropoietin gene enhancer at a site required for transcriptional activation. Mol Cell Biol 1992;12:5447–54.

17. Ebert BL, Firth JD, Ratcliffe PJ. Hypoxia and mitochondrial inhibitors regulate expression of glucose transporter-1 via distinct *cis*-acting sequences. J Biol Chem 1995;270:29083–9.

18. Wykoff CC, Beasley NJ, Watson PH, et al. Hypoxia-inducible expression of tumor-associated carbonic anhydrases. Cancer Res 2000;60:7075–83.

19. Camenisch G, Stroka DM, Gassmann M, Wenger RH. Attenuation of HIF-1 DNA-binding activity limits hypoxia-inducible endothelin-1 expression. Pflugers Arch 2001;443:240–9.

20. Semenza GL. HIF-1 and mechanisms of hypoxia sensing. Curr Opin Cell Biol 2001;13:167–71.

21. Hassa PO, Hottiger MO. The functional role of poly(ADP-ribose)polymerase 1 as novel coactivator of NF-κB in inflammatory disorders. Cell Mol Life Sci 2002;59:1534–53.

22. Hassa PO, Haenni SS, Buerki C, et al. Acetylation of poly(ADP-ribose) polymerase-1 by p300/CREB-binding protein regulates coactivation of NF-κB-dependent transcription. J Biol Chem 2005;280:40450–64.

23. Martin-Oliva D, Aguilar-Quesada R, O'Valle F, et al. Inhibition of poly(ADP-ribose) polymerase modulates tumor-related gene expression, including hypoxia-inducible factor-1 activation, during skin carcinogenesis. Cancer Res 2006;66:5744–56.

24. Airley R, Loncaster J, Davidson S, et al. Glucose transporter glut-1 expression correlates with tumor hypoxia and predicts metastasis-free survival in advanced carcinoma of the cervix. Clin Cancer Res 2001;7:928–34.

25. Wanner RM, Spielmann P, Stroka DM, et al. Epolones induce erythropoietin expression via hypoxia-inducible factor-1α activation. Blood 2000;96:1558–65.

26. Ema M, Hirota K, Mimura J, et al. Molecular mechanisms of transcription activation by HLF and HIF1α in response to hypoxia: their stabilization and redox signal-induced interaction with CBP/p300. EMBO J 1999;18:1905–14.

27. Liu L, Simon MC. Regulation of transcription and translation by hypoxia. Cancer Biol Ther 2004;3:492–7.

28. Thiemermann C, Bowes J, Myint FP, Vane JR. Inhibition of the activity of poly(ADP ribose) synthetase reduces ischemia-reperfusion injury in the heart and skeletal muscle. Proc Natl Acad Sci U S A 1997;94:679–83.

29. Eliasson MJ, Sampei K, Mandir AS, et al. Poly(ADP-ribose) polymerase gene disruption renders mice resistant to cerebral ischemia. Nat Med 1997;3:1089–95.

30. Szabo C, Dawson VL. Role of poly(ADP-ribose) synthetase in inflammation and ischaemia-reperfusion. Trends Pharmacol Sci 1998;19:287–98.

31. Berger NA. Poly(ADP-ribose) in the cellular response to DNA damage. Radiat Res 1985;101:4–15.

32. Ha HC, Snyder SH. Poly(ADP-ribose) polymerase is a mediator of necrotic cell death by ATP depletion. Proc Natl Acad Sci U S A 1999;96:13978–82.

33. Pieper AA, Verma A, Zhang J, Snyder SH. Poly (ADP-ribose) polymerase, nitric oxide and cell death. Trends Pharmacol Sci 1999;20:171–81.

34. Rajesh M, Mukhopadhyay P, Godlewski G, et al. Poly(ADP-ribose)polymerase inhibition decreases angiogenesis. Biochem Biophys Res Commun 2006;350:1056–62.

35. Tong WM, Hande MP, Lansdorp PM, Wang ZQ. DNA strand break-sensing molecule poly(ADP-Ribose) polymerase cooperates with p53 in telomere function, chromosome stability, and tumor suppression. Mol Cell Biol 2001;21:4046–54.

36. Conde C, Mark M, Oliver FJ, Huber A, de Murcia G, Menissier-de Murcia J. Loss of poly(ADP-ribose) polymerase-1 causes increased tumour latency in p53-deficient mice. EMBO J 2001;20:3535–43.

37. Bryant HE, Schultz N, Thomas HD, et al. Specific killing of BRCA2-deficient tumours with inhibitors of poly(ADP-ribose) polymerase. Nature 2005;434:913–7.

38. Farmer H, McCabe N, Lord CJ, et al. Targeting the DNA repair defect in BRCA mutant cells as a therapeutic strategy. Nature 2005;434:917–21.

39. Homburg S, Visochek L, Moran N, et al. A fast signal-induced activation of Poly(ADP-ribose) polymerase: a novel downstream target of phospholipase c. J Cell Biol 2000;150:293–307.

40. Czapski GA, Cakala M, Kopczuk D, Strosznajder JB. Effect of poly(ADP-ribose) polymerase inhibitors on oxidative stress evoked hydroxyl radical level and macromolecules oxidation in cell free system of rat brain cortex. Neurosci Lett 2004;356:45–8.

41. Hassa PO, Haenni SS, Elser M, Hottiger MO. Nuclear ADP-ribosylation reactions in mammalian cells: where are we today and where are we going? Microbiol Mol Biol Rev 2006;70:789–829.

42. Veres B, Gallyas F, Jr., Varbiro G, et al. Decrease of the inflammatory response and induction of the Akt/protein kinase B pathway by poly-(ADP-ribose) polymerase 1 inhibitor in endotoxin-induced septic shock. Biochem Pharmacol 2003;65:1373–82.

43. Petrilli V, Herceg Z, Hassa PO, et al. Noncleavable poly(ADP-ribose) polymerase-1 regulates the inflammation response in mice. J Clin Invest 2004;114:1072–81.

44. Wenger RH, Kvietikova I, Rolfs A, Camenisch G, Gassmann M. Oxygen-regulated erythropoietin gene expression is dependent on a CpG methylation-free hypoxia-inducible factor-1 DNA-binding site. Eur J Biochem 1998;253:771–7.

45. Zufferey R, Nagy D, Mandel RJ, Naldini L, Trono D. Multiply attenuated lentiviral vector achieves efficient gene delivery *in vivo*. Nat Biotechnol 1997;15:871–5.

46. Wang ZQ, Stingl L, Morrison C, et al. PARP is important for genomic stability but dispensable in apoptosis. Genes Dev 1997;11:2347–58.

47. Hassa PO, Covic M, Hasan S, Imhof R, Hottiger MO. The enzymatic and DNA binding activity of PARP-1 are not required for NF-κB coactivator function. J Biol Chem 2001;276:45588–97.

48. Hassa PO, Hottiger MO. A role of poly(ADP-ribose) polymerase in NF-κB transcriptional activation. Biol Chem 1999;380:953–9.

49. Perkins ND, Agranoff AB, Pascal E, Nabel GJ. An interaction between the DNA-binding domains of RelA(p65) and Sp1 mediates human immunodeficiency virus gene activation. Mol Cell Biol 1994;14:6570–83.

50. Hassa PO, Buerki C, Lombardi C, Imhof R, Hottiger MO. Transcriptional coactivation of nuclear factor-κB-dependent gene expression by p300 is regulated by poly(ADP)-ribose polymerase-1. J Biol Chem 2003;278:45145–53.

51. Bridge AJ, Pebernard S, Ducraux A, Nicoulaz AL, Iggo R. Induction of an interferon response by RNAi vectors in mammalian cells. Nat Genet 2003;34:263–4.

52. Hottiger MO, Felzien LK, Nabel GJ. Modulation of cytokine-induced HIV gene expression by competitive binding of transcription factors to the coactivator p300. EMBO J 1998;17:3124–34.

53. Donovan CE, Mark DA, He HZ, et al. NF-κB/Rel transcription factors: c-Rel promotes airway hyperresponsiveness and allergic pulmonary inflammation. J Immunol 1999;163:6827–33.